Three-Dimensional Finite Element Stress Analysis of Post-Core Restored Endodontically Treated Teeth

BY

GUANG-QUAN SONG

A Thesis
Submitted to the Faculty of Graduate Studies
In Partial Fulfillment of the Requirements
For the Degree of

MASTER OF SCIENCE

*****

Department of Mechanical & Industrial Engineering

The University of Manitoba

Winnipeg, Manitoba

THE UNIVERSITY OF MANITOBA
FACULTY OF GRADUATE STUDIES
*****
COPYRIGHT PERMISSION PAGE

THREE-DIMENSIONAL FINITE ELEMENT STRESS ANALYSIS OF POST-CORE REINFORCED ENDODONTICALLY TREATED TEETH

BY

GUANG-QUAN SONG

A Thesis/Practicum submitted to the Faculty of Graduates Studies of The University of Manitoba in partial fulfillment of the requirements of the degree Of

Master of Science

Abstract

Determination of the stress distributions in post-core restored endodontically treated teeth is challenging due to the fact that the post and core systems, the root and its canal, and the bony structures supporting the root have small dimensions and are structurally complex. In this research, a 3D finite element model was developed to evaluate the stress distributions in a post-core restored endodontically treated maxillary incisor under various static loads. The physical model includes dentin, PDL, bone, post, core, gutta percha and crown. All materials are assumed to be homogenous, isotropic, and linear elastic. The effects of various factors on the stress distributions are investigated through simulations. These factors include post materials, post and core combinations, ferrule heights, post and dentin gaps at the coronal entrance of the canal, and canal diameters.

It has been found that the horizontal loading is the most dangerous, which causes the highest stresses in dentin and posts, followed by the oblique loading and the vertical loading. The above listed factors, such as post materials, post and core combinations, ferrule heights, post and dentin gaps at the coronal entrance of the canal, and canal diameters, do not change the stress distributions and magnitudes significantly under horizontal and oblique loading. However, the stresses are sensitive to the above factors under the vertical loading, and it has been found that the stress distributions in both dentin and the post are the most uniform without stress concentrations when the elastic modules of the post and the core are similar to that of dentin. Regarding the effects of the gaps at the cervical region on the stress distributions in dentin, the high stresses at the

apical portion of the root and the bottom of the gaps decrease as the increase of the depth of the gap under vertical loading. Overall, the sharp angle and notch of the gap at the coronal entrance of the canal should be avoided in tooth restoration since they can cause stress concentrations. On the effects of the ferrule heights, the changes of the stress distributions in dentin and the post are insignificant except that higher ferrule shows lower stresses at the top of the ferrule. Regarding the effects of the diameters of the posts, the results show that although the posts with large diameters support more loads, they cause high stress concentrations at the apical portion of the root, which is not desirable.

Acknowledgement

I would like to express my sincere thanks to my advisors for their support, insight, and guidance in the preparation of this thesis, Dr. Christine Q. Wu, Dr. Peter.T. Williams, and Dr. Lawrence.W. Stockton. I would also like to thank the other member of my examine committee, Dr. J.R. Cahoon and Dr. Nipon Rattanawangcharoen for reading the thesis.

I would also like to extend my thanks to the other professors whose timely suggestions saved much time and effort in the preparation of this work. Thank my wife, Li, for her love and care. A special word of thanks to my parents for their never ending support and encouragement during my studies.

Table of Contents

List of Tables

List of Figures

List of Graphs

Chapter 1 Introduction

1.1 General

Post and core systems are commonly used for the restoration of endodontically treated teeth when the teeth have suffered coronal damage. Loosening of the post and core or fracture of remaining dentin root are most frequent problems observed. According to Gher *et al.* (1987)'s clinical survey, among 100 fractured teeth, 92 teeth had been previously restored. Williams *et al.* (1987) indicated that the failure of restored teeth was related to the design of posts and cores. The analysis of the stress distribution found in endodontically treated teeth that have been restored with a post and core will contribute to our understanding of the causes of the high incidence of failure in these teeth and may result in the design of post and core restorations with improved clinical performance.

During the last three decades, much literature about the stress analysis of the post-core restored endodontically treated teeth has been published. The publications on the effects of the posts on stress distributions are controversial. Some researchers promoted the use of posts by claiming that they served to reinforce the teeth. Other researchers reported that the placement of a post could create stresses that lead to root fracture during functions. The study of stress analysis on this subject is incomplete. Much work remains to be done in this area.

1.2 Literature survey

Endodontic treatments are usually recommended when the pulp tissue is diseased or

injured. According to the Canadian Academy of Endodontics (CAE, 1998), the procedure of an endodontical treatment includes several steps. The infected tissues inside the tooth are first removed to prevent periapical spread of the infection. Once the root canal space is cleaned, a material called gutta percha is placed to fill and seal the canal. A post-core system is commonly used to restore the tooth. On the top of the core, a crown is placed.

Many post-core systems are available. Posts are divided into two types: active posts and passive posts (Ho *et al.,* 2002). In the case of the active engagement, the post mechanically engages to the wall of the canal through the use of the threads. However, in the case of passive engagement, there is no mechanical bonding and the post relies mainly on cement to hold it in the canal. For example, the Para Post Plus is a parallel-sided and passive post, the Para Post XT is a combination of the active and passive post, and the Flexi Post and the Flexi-Flange are active posts (Stockton *et al.,* 2000).

Insertion of a post into a prepared root canal presents a difficult challenge to restorative dentists. During mastication, the stresses developed in dentin often reach values that can cause the dislodgement of the post and the fracture of the tooth. A fractured tooth often can not be restored and must be extracted. The dental procedures required to replace the lost tooth are usually very expensive and provide a less satisfactory result than the post and core restored tooth they are replacing. The analysis of the stress distributions of endodontically treated teeth with post and core reinforcements will facilitate the design of post and core configurations that are less likely to cause tooth fracture.

Evaluations of the stress distributions of post-core restored endodontically treated teeth are very complicated. The restored tooth consists of several different materials: a crown, core, post, cement and gutta percha, and several types of tissue such as periodontal ligament (PDL), bone, and dentin. The respective material properties are significantly different. The post-core system, the root and canal, the PDL and the supporting bone have small dimensions and are structurally complex. The direction and the magnitude of the load are complicated. Post design, thickness of the remaining dentin, and the height of the dentin ferrule affect the stress distributions of the restoration.

Several methods have been used to analyze the effects of the post-core system on the stress distributions in dentin. Experimental methods and the finite element method are commonly used. Experimental methods include tensile test, shear loading test, and photoelastic analysis. Photoelasticity is based on the property of some transparent materials to exhibit colorful patterns when viewed with polarized light. In the two dimensional (2D) method, models are fabricated using a transparent plastic sheet. The three dimensional (3D) photoelastic stress analysis is not often reported because the experiment is very expensive and difficult to conduct. The finite element method has been used for more than two decades for stress analysis of teeth. Some 2D finite element models such as plane stress, plane strain, and axi-symmetric models simplified the analysis. However, 2D finite element models are regarded as inadequate since the tooth structure and the loading forces are not two-dimensional. A 3D finite element method is a more accurate way to analyze the stresses in a tooth (Ho *et al*., 1994; Toparli *et al*., 2000; Ko *et al*., 1992; Rubin *et al*., 1983).

1.2.1 Experimental methods

The retentions of the Integra Post and Para Post were compared by Hew *et al.* (2001) using the tensile test. The Integra Post is a parallel-sided post, made of titanium alloy. Twenty extracted single-rooted human teeth free of restorations and defects in the roots were selected. The root canals were endodontically prepared. The prepared samples were placed in a retentive device, and mounted in a testing machine. The maximum tensile force (N) tolerated by the post before being dislodged was recorded. The results showed that the Integra Post did not produce any advantages in retention of the post in the root when compared to the Para Post.

The effects of the post length and the diameter on the retention were studied by Nergiz *et al.* (2002) using the tensile test. In the study, ninety prefabricated tapered titanium posts with retentive heads were used. Posts were of different diameters (0.5mm, 0.9mm, and 1.1mm) and different lengths (9, 12, 15mm). Through the combination of the post length and the diameter, nine groups each having 10 specimens were formed. 90 newly extracted single-rooted human teeth without micro-fracture were endodontically treated. All the canals were roughened with a diamond-coated drill. Posts were placed and cemented to the prepared canal spaces. A tensile force-measuring instrument was used to apply force along the long axis of the post. The force required to dislodge each post was then recorded. It was found that the retention of the posts is affected proportionally by the post length as well as the diameter. The retention increases more with the increase in the post length than with the increase in the post diameter. They believed that the post surface configuration was an important factor in post and core retention.

Post-core shear bond strengths of Para Post Plus, Para Post XT, Flexi Post, and Flexi Flange post were studied by Stockton *et al.* (2000) using the 45-degree shear loading test. The Para Post Plus is a parallel-sided, passive design. The Para Post XT is a combination active/passive design. The Flexi Post and the Flexi Flange are active post designs. Forty human maxillary incisors were selected and assigned to four groups of 10 teeth. One of four different post types was assigned to each group. The shear strengths were determined by applying an increasing load 1 mm apical of the incisal edge and at 45-degree to the longitudinal axis of the root until failure occurred. The load at failure as well as the site of failure was recorded. The results showed that the shear strength of the Para Post is significantly higher than those with other posts.

In addition to the above experimental studies, the method of photoelasticity has also been used widely. The photoelasticity method is based on the property of double refraction. In the 2D photoelasticity method, the specimens under investigation are fabricated using a transparent plastic sheet that possesses the property of the double refraction. When the specimen is stressed in a polariscope and examined in white light, color patterns known as the fringes can be observed (Mahler and Peyton, 1955). The fringe patterns can be evaluated to determine the stress distributions in the specimen. Each fringe order can be considered as a gradient of the differences in the principle stresses of the model. Fringes can be highly concentrated, such as at the apex in some retention posts, where the stress gradient is so high that distinguishing the various fringe orders can be difficult. When the fringe orders are concentrated, it indicates that the stress varies greatly from one area to

another (Caputo and Standlee, 1987).

Stress distributions caused by the insertion of posts were analyzed by Ho *et al.,* (2002) using the photoelasticity method. Four types of endodontic posts, used in their work, were the Carbon Fiber Post, Para Post Plus, Flexi Post, and Para Post XT. The carbon Fiber Post and the Para Post Plus are passively engaging posts while the Flexi Post and the Para Post XT are actively engaging posts. Photoelastic models were prepared with a PSM-5 photoelastic sheet. The shape was simplified to a 2D half-ellipse. Results indicated that the passively engaging posts exert no installation stresses while the actively engaging posts result in high installation stresses. The high stresses from the two groups of actively engaging posts indicated that installation stresses were likely caused by mechanical bonding between the endodontic post and the canal wall. Features of endodontic posts, such as the threads and the increased diameter, increased stress during installation of the posts.

The stress distributions surrounding endodontic posts were studied by Burns *et al.* (1990) using the photoelasticity method. Test blocks of photoelastic material were prepared with simulated endodontic canals. Posts of different designs, diameters and lengths were cemented in the test blocks. Using a circular polariscope, the fringes were photographed when each specimen was loaded. The load used were 0N, a 135N compressive load, and either 90N or 135N oblique load applied at 26 degree. The results showed that the Para Post and the Para Post Plus produce similar evenly-distributed stress patterns. The Flexi Post produced asymmetric stress patterns with stress concentrations at each thread. After

cementation and during compressive loading, the Flexi Posts caused significantly higher shoulder stresses and substantially greater stresses along the coronal surface than those with the Para Posts and the Para Post Plus Posts. They also found that the apical stress distributions were similar for the Flexi Posts, Para Posts, and Para Post Plus Posts during compressive loading.

Research using three dimensional photoelastic stress analysis was rarely reported in literature. In one of them, (Loney *et al*. 1990), a silicone mold was first made from the master tooth. A duplicate master tooth was cast in photoelastic resin and a canal was prepared in it using a drill. The photoelastic model was then examined under a polariscope to ensure that the thermal stress had not developed during milling procedures. A post and core restoration was then cemented in place. The assembled model was heated while a load was applied obliquely. An oven was subsequently used to cure the model, where the stress pattern was frozen in the model. The photoleastic model was then sectioned, and the stress pattern in each section was observed. The three dimensional photoelastic stress analysis is more realistic than the two dimensional one, because it can achieve the full geometric fidelity and the full 3D stresses. However, 3D photoelastic tests are more expensive and difficult to conduct as compared with the 2D tests. Furthermore, the material properties of the photoelastic materials are not the same as those of the teeth. As Loney *et al.,* (1990) had admitted, the bone and PDL were imperfectly modeled because photoelastic resin is not same as that of bone and PDL. Variations in the material properties could have affected the magnitude of stresses observed in bone.

In summary, experimental methods have provided direct results related to the failure mechanisms of the restored teeth. However, it is very challenging to use the experimental methods to evaluate the stresses quantitatively. The shapes of teeth are irregular and load conditions are various. The cost of experimental equipment is very high, and although the procedure of analysis is sophisticated, the qualitative results are extremely coarse. In contrast, the FEA method provides a very refined quantitative analysis. Even though the photoelastic analysis provides visual evidence of stress patterns within the model, the material property of the photoelastic model is not the same as that of the structure being simulated. The difficulty in modeling objects of more than one material is a significant disadvantage (Cailleteau *et al.* 1992).

1.2.2 Finite element method

The finite element method is a numerical method for solving the differential equations. The geometric model of the structure is built and subdivided into small elements. In each of the elements, element equations are formed according to the relationship between the displacement and loading. The equations are assembled together to form the global finite element equations. The global equations are then solved using a computer. With the finite element method, the parameters of the geometry of the structure, post design, material properties, and the magnitude and direction of the load can be changed easily in simulations, which is a significant advantage over experimental methods.

The finite element method includes the 2D finite element method and the 3D finite element method. The 2D stress analyses are the first successful examples of the application of the

finite element method (Zienkiewicz, 1971). The 2D finite element analysis includes plane stress, plane strain, and axi-symmetric finite element analysis. In the case of plane stress, the stress perpendicular to the plane of interests is zero. The corresponding strain is not zero. In the case of plane strain, the stress in a direction perpendicular to the plane of interests is not zero. The strain in the corresponding direction is zero. Axi-symmetric stress analysis is related to the studies of the stress distributions in bodies of revolution under axi-symmetric loading. Although 2D approximation offers affordable and economic models, the stress results are exaggerated (Toparli *et al.* (1999); Joshi *et al.* (2001)). The 3D finite element analysis provides more realistic and accurate results.

1.2.2.1 Two Dimensional Finite Element Analysis

Ko *et al.* (1992) studied the roles of post in reducing dentin stress in endodontically treated teeth using the 2D finite element method. The geometry of the midlabiolingual section of the human maxillary incisor was adopted from Wheeler (1984). Two plane strain models were built, one with a post and another one without a post. All parts were treated as homogeneous, isotropic, and linear elastic materials. The material properties were adopted from the literature. The cement layer between the post and dentin was treated as part of dentin because of its low thickness and the similarity in elastic modulus between dentin and cement. Three types of loading forces were applied to the models horizontally, vertically, and obliquely. Von-Mises's equivalent stresses were calculated. It was found that when the tooth without a post was subjected to the oblique loading, the equivalent stress was concentrated on the coronal and middle thirds of the root. When a post was present, the peak stress in dentin was reduced 30% while the post was stressed significantly.

Under the horizontal loading, the stress distribution in dentin when no post was present was similar to oblique loading except that the lingual side had the higher stress. All peak stresses in dentin were also reduced substantially in the presence of the post. Under the vertical loading, the stresses were concentrated at the cervical dentin and at the crown. When a post was present, dentin stresses were concentrated around the apex of the post and were reduced drastically in other parts of the dentin.

The stresses along the inner canal wall of a maxillary central incisor were studied by Cailleteau *et al*. (1992) using the plane stress finite element method. Four 2D finite element models were developed to evaluate the stress distributions in an intact incisor, an endodontically treated incisor, and an endodontically treated crown-restored incisor, and a cylindrical post and crown-restored incisor. All models were created using the triangular and the quadrilateral isoparametric elements. The crown was present to act primarily as a point of the load application and to transmit the load to the root structure. Each model was statically loaded with 1N of force perpendicular to the lingual surface. The maximum tensile, compressive, and shear stresses were calculated using a general-purpose finite element program. Results indicated that the stress patterns within the root were changed as a result of the post insertion. Post placements did not result in a uniform distribution of stress along the canal wall.

The stress distribution in a maxillary central incisor caused by different post designs and load directions was investigated by Yang *et al.* (2001) using the 2D finite element method. A 2D finite element model of a maxillary central incisor was constructed. The triangular

shaped elements were used. Four types of post designs of different diameters, lengths, and shapes were created. The force of 98N was applied on the crown vertically, horizontally and obliquely. The results showed that the lateral force produces high stress concentration along the cortical bone. Stresses generated in the bone and PDL were influenced more by the loading direction than the design of the posts.

The effect of different post designs on the stresses in mandibular first molar teeth were studied by Ersoz (2000) using the 2D finite element method. A 2D finite element model was developed where the quadrilateral elements were used. The anatomic form and dimensions, the elastic modulus, and Poisson's ratios were entered into the model. Self-threading posts with two different post materials were included in the model. Two types of post materials were stainless steel and titanium. The results showed that both types of posts exhibited high internal stress in mandibular first molar teeth. It was observed that the post placement caused a diffused stress along the root. With the stainless steel post, the highest value of stress of 100MPa was recorded at the apical portion of the prepared canal. The stress distribution with the titanium self-threading post was quite similar to that for the stainless steel post. Although the stress distributions were quite similar, the highest stress caused by the titanium post was found to be 60MPa, which was significantly lower than the one with the stainless steel post.

Axi-symmetric models are appealing for stress analysis of axi-symmetric structures. In an axi-symmetric model, the elements are represented by 2D elements, but a 3D structure is implied. When compared with the conventional 2D analysis of an equivalent model,

axi-symmetric analysis is believed to improve the accuracy of the results. When compared to 3D models, axi-symmetric models greatly reduce the modeling and analysis time required. The effects of the post diameter and length on the stress distributions in the mandibles were investigated by Holmes *et al.* (1996) using the axi-symmetric finite element method. Various post dimensions were tested. A model of a block section of the mandible was developed using the commercial software ANSYS. The model was meshed into 906 eight-node axi-symmetric finite elements with 2664 nodes. Each element was assigned unique elastic properties to represent the materials modeled. For each case a load of 100N was applied to the cuspal tip from the facial direction at a 45 degree angle to the long axis of the tooth. Shear, compressive, and tensile stresses were computed. It was found that the distributions of the tensile and compressive stresses were approximately the same for all cases. The study predicted the greatest compressive and tensile stresses occur in dentin at the coronal third of the root. The distribution of tensile and compressive stresses was not affected with variation in the dimensions of the posts. Even though the axi-symmetric finite element method simplified the modeling, axi-symmetric models have limitations for analyzing complex structures, which do not possess symmetry around axis.

Although numerical results can be easily obtained in 2D modeling, it has some significant shortcomings. Human teeth are neither planer nor symmetrical. They are highly irregular in shape. They cannot be represented in a 2D space. The distributions of various materials properties are not two-dimensional. The loading on teeth is neither in a plane nor symmetric. The assumption that the loading is symmetrical would be expected to produce errors. The 3D finite element method is required in order to overcome that limitations of

the 2D modeling.

1.2.2.2 Three Dimensional Finite Element Analysis

A 3D finite element model was developed by Rubin *et al.* (1983) to analyze the stress distribution in a representative human right first mandibular molar. A computer program called WHEEL was used. The program allowed the calculation of stresses, strains, and deformations in an arbitrarily shaped 3D finite element model representing a structure under static loading. The tooth dimensions used in this study were taken from the literature. The PDL and the cementum layer were not considered because of their low thickness. The tooth materials were assumed to be homogeneous, isotropic and linear elastic. The model consisted of 336 elements and 520 nodes. Their results were compared with Atmaram and Mohammed's work (1981), where a 2D finite element model was used to treat a two-dimensional buccolingual section of a molar tooth. They found that the maximum longitudinal stresses in the enamel were quite similar to those obtained by Atmaram and Mohammed (1981) with similar loading. The lateral stresses in the enamel and all the stresses in the dentin are considerably lower in the 3D model than those in the 2D model. They concluded that the overall stresses in the tooth are actually lower than those predicted by the 2D model.

Darendeliler *et al.* (1992) built a 3D finite element model to determine the stress distribution in a maxillary central incisor. The geometry of the tooth was taken from Wheeler's study (1984). The tooth was considered to be composed of enamel and dentin since the thickness of PDL and cementum were very small. The effect of pulp on stress

distribution was neglected. The tooth material was assumed to be isotropic, homogenous, and elastic. The bone supporting the root was assumed to be rigid and an external load of 450N was applied on the incisal margin of the tooth. The angle between the direction of the force and the tooth's vertical axis was 26^{o}, which represented the angle at the first contact of tooth during biting. Their 3D finite element model was divided into 12 parts along the longitudinal axis. Each part was then divided into smaller prismatic elements having the same height, which were equal to the thickness of each part. 204 prismatic elements were obtained. Each element consisted of eight nodes at which elements were connected. For each element, the force-displacement relations were written in terms of nodal variables (displacements) to obtain the element stiffness matrices. The element stiffness matrices were assembled to obtain the global stiffness matrix. Based on the initial and boundary conditions, the displacements at the nodes were found for the given load. The values and directions of the principle stresses were calculated from the nodal displacements using the stress-strain and strain-displacement relations. Their results showed that the stresses were the highest around the cervical line and at the incisal margin. The high stresses were attributed to the termination of enamel at the cervical line, and the thin structure of enamel at the incisal margin where the distributed load is applied. The compressive stresses were comparatively larger than the tensile and shear stress values in both enamel and dentine.

Huysmans and Van der Varst (1993) developed a 3D finite element model and validated the model for pre-failure and failure modes by comparing the computational results with the laboratory observations. The model represented a laboratory setup of direct post and core restored premolars. Only half of a specimen was modeled. The materials included root,

post, core, and loading cap. The cement layer was not considered. The applied load was half the mean quasi-static failure load, 470N for amalgam and 459N for composite. The load was applied on the loading cap, from the palatal side at an angle of 45^{o} to the longitudinal axis of the specimen. The mesh consisted of eight-node, isoparametric brick elements. The interface between the loading cap and the core was modeled without bonding, using 96 gap elements to distribute load applied to the loading cap. The interfaces between the post and the core, and between the post and the dentin were modeled as perfectly bonded. The analysis concentrated on the stresses within the core as it was the region of failure in vitro. Four model variations were (1) interface between core material and tooth perfectly bonded, and (2) interface between core material and tooth without bonding. Von Mises and Drucker-Prager equivalent stress were calculated. It was found that Von Mises and Drucker-Prager equivalent stresses were very alike qualitatively. In the composite core material with bonded core, equivalent stresses reached a peak value along the apical surface of the core.

Joshi *et al.* (2001) evaluated the mechanical performance of endodontically treated teeth using the 3D finite element method. 3D brick and tetrahedral elements were used to generate the tooth model. The master model consisted of dentin, gutta percha, endodontic post, core, crown, PDL, and bone. Four master models were generated with different post designs, which were cast post and core, solid parallel-sided post, hollow parallel-sided post, and the post with new design. The new post has an anti-rotation element in the cervical third. The cast post and core models had a core material of base metal alloy. All other models had a core made of composite resin. The dimensions of the teeth were adopted from

Wheeler (1981). The vertical, horizontal, and oblique loads of 100N were applied on each model. Von Mises stresses were determined. Observations of the deformed posts indicate a cantilever beam bending action. Among the post designs studied, the cast post showed the lowest stresses with the most favorable distribution, while the hollow post showed the highest stress concentration. Among the materials studied, stainless steel posts showed the highest stress followed by titanium, ceramic, and FRC posts. It was concluded that the posts fabricated from conventional materials did not reinforce teeth. Rather they caused stress concentration that may make endodontically treated teeth susceptible to fracture. They also concluded that FRC post bonded to the dentin have the best potential to reinforce teeth and that the ideal post material should have stiffness properties close to that of dentin.

Seven 3D finite element models were developed by Pierrisnard *et al.* (2002) to compare how the mechanical parameters of different degrees of coronal tissue loss and restoration with different materials affected the restoration. The two level of coronal dentin loss were: (1) total loss of the coronal dentin (absence of a ferrule) and (2) partial loss of the coronal dentin with 2-mm surviving dentin walls (presence of a ferrule). Two post materials were nickel chromium and carbon fiber. Four different simulations were conducted: (1) NiCr cast post and core, (2) NiCr post and composite core combination, (3) carbon fiber post and composite core combination, and (4) composite restoration without a post. The posts were cylindrical with a cone-shaped tip. A crown covered each of the models. The crown received a 30-degree oblique occlusal load at 100N. Regardless of the model, the greatest stress was observed in the cervical region. The analysis confirmed that the reconstructed tooth was subject to the most stress in the cervical region. In the cervical region, the

stresses were higher than those reported when the post had a high elasticity modulus. The role of the post in providing reinforcement was demonstrated. The absence of peripheral ferrule, especially when the post was metallic (with a high Young's modulus), was found to be the most significant contributory factor in increasing the risk of fracture regardless of the type of core material.

These studies show that 3D finite element models give better results than 2D finite element models. Thus, in our study, the 3D finite element mode will be developed to analysis the stress distributions of the post-core restored endodontically treated teeth.

1.3 Objectives

The objective of this study was two-fold: (i) to develop a 3D finite element model to evaluate the stress distributions in a post-core restored endodontically treated maxillary incisor, and (ii) to conduct various simulations to investigate the effects of various parameters on stress distributions. The goal was to gain an in-depth understanding of the mechanical performance of the post-core restored endodontically treated teeth.

Various 3D finite element simulation models were developed to analyze the stress distribution in a post-core restored endodontically treated maxillary centre incisor. The physical model includes dentin, PDL, bone, post, core, gutta percha and crown. Components are perfectly bonded. All materials are assumed to be homogenous, isotropic, and linear elastic. Their properties are taken from the related literature. Vertical, horizontal, and oblique forces of 100N are applied on the crown respectively. The boundary of the

model is the bone surrounding the tooth root. This boundary is assumed to be fixed. Geometrical models, which are built using Pro/Engineer, are meshed into elements. The commercial finite element analysis package named ANSYS is used for calculations and post processing. 3D tetrahedral elements are used. Von Mises equivalent stresses in dentin, posts, cores and crowns are calculated. The effects of various factors on the stress distributions are investigated. These factors include post materials, post and core combinations, ferrule heights, post and dentin contacts at the dentin coronal surface, and thickness of dentin.

1.4 Scope

The goal of this work is to develop a 3D finite element model that will facilitate an in-depth understanding of the mechanical performance of the post-core restored endodontically treated teeth. Chapter one reviews the recent literature and this provides theories and methods for this study. Effects of the properties of the post materials and other restorative materials are also reviewed. Chapter two presents the development of the 3D finite element model of the maxillary central incisor. Some discussions are included on model validations. Chapter three presents the simulation results. Chapter four is the discussion and conclusion. The structure of the analysis procedure is described in Appendix A. An example of a command input file demonstrates the procedure of analysis.

Chapter 2 Methodology

2.1 General Procedure

In this study, a 3D finite element model is developed to analyze the stress distribution in a post-core restored endodontically treated maxillary central incisor. The geometric models are first developed using a commercial package — Pro/Engineer (Parametric Technologies Corporation). Pro/Engineer is a parametric solid-modeling system. The advantages of using Pro/Engineer are the capabilities to build smooth curves and generate accurate geometries. The generation of the finite element model, calculation of the stress distributions and post processing are carried out using ANSYS 6.0 University High version (ANSYS, Inc.). ANSYS is a general-purpose finite element analysis tool with the ability to analyze a wide range of problems from a simple, linear, static analysis to a complicated, nonlinear, transient dynamic analysis. In this work, 3D tetrahedral elements are used to generate the tooth finite element model. Von Mises equivalent stresses in dentin, posts, cores and crowns are determined. The results are plotted in a graphic form. A PC-compatible computer with a Windows 98 operating system is used.

2.2 Description of the model

In this work, the physical model of a post-core restored endodontically treated tooth includes seven components: the bone supporting the tooth, PDL, dentin, post, core,

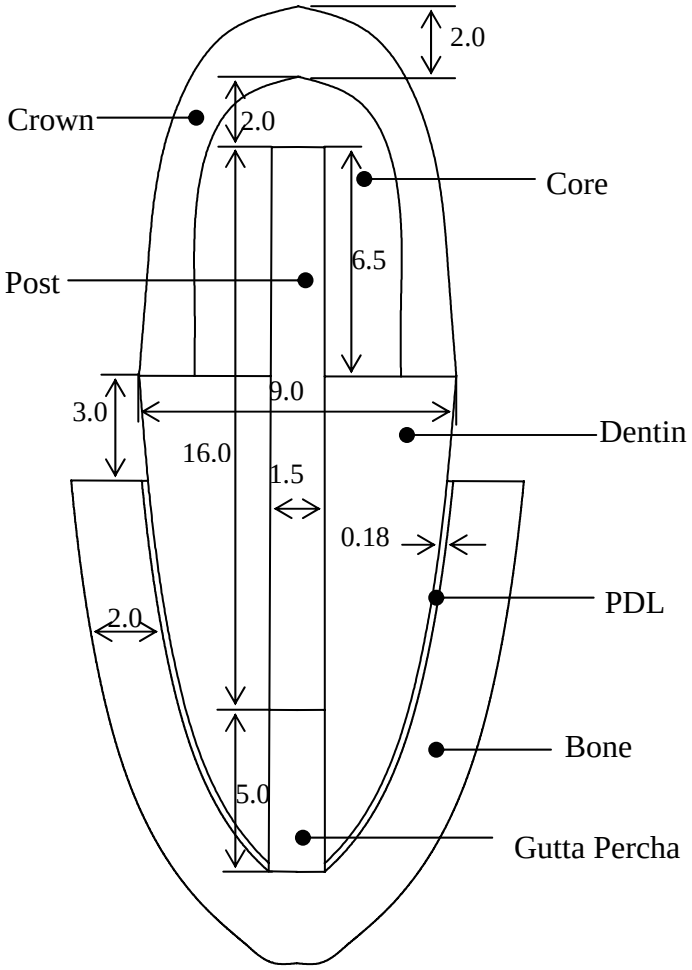

Figure 2.1 Dimension of the restored maxillary central incisor (mm). The total length of the tooth is 25mm. The length of tooth root is 14.5 mm.

crown, and gutta percha. The geometry and the dimensions of the physical model are shown in Figure 2.1. To simplify the development of the FEA model, some assumptions have been made regarding the material properties of each part and its geometry.

- The geometry of the post and core restored incisor is simplified in that all components are modeled to be axi-symmetric along the vertical centerline.
- Since any cement (luting agent) layer between any of the restorative materials, or between these materials and tooth structure is very thin, the cement layer is regarded as part of dentin.
- Since the layer of cementum covering the surface of the root is very thin, the cementum layer is regarded as part of the dentin.
- No gap exists between the components, and all components are assumed to be perfectly bonded.
- The outside surface of the bone is fixed, which allows zero displacement.
- A force with a magnitude of 100N is applied on the surface of the crown at three different locations and in three different directions.
- Pre-stress due to the endodontic treatment is neglected.

2.3 Material Properties

The material of each component included in the finite element model of a post-core restored endodontically treated tooth is assumed to be homogeneous, isotropic and linear

elastic. Stainless steel, titanium, ceramic and FRC are the most frequently used materials for posts. The elastic modulus and Poisson's ratio are listed in the Table 2.1.

Table 2.1 Material properties of components

No.	Material	Young's Modulus (GPa)	Poisson's ratio
1	Dentin	18.60	0.30
2	Periodontal Ligament	68.9×10^{-3}	0.40
3	Cortical Bone	13.70	0.30
4	Gutta Percha	0.96×10^{-3}	0.40
5	Composite Resin of the Core	16.60	0.24
6	Stainless Steel Post	200.00	0.30
7	Titanium Post	120.00	0.30
8	Ceramic Post	69.00	0.28
9	Fiber Reinforced Composite (FRC) Post	15.00	0.28

2.4 Development of model

Geometric models were built using Pro/Engineer. Finite element models were formed using Ansys. Von Mises equivalent stresses were calculated, and results were ploted.

2.4.1 Development of Geometric models with Pro/Engineer

The length of dentin is 14.5mm. The diameter at the coronal surface is 9mm as shown in Figure 2.1. It is assumed to be axi-symmetric along the vertical centerline as shown in Figure 2.2(a). The dentin component is connected to post, core, crown, PDL, and gutta percha. Gutta percha is derived from the secretions of the rubber tree. During placement,

the gutta percha is heated so that it flows under mild pressure. It fills the previously prepared root canal and seals the canal apex. In our model, the canal is axi-symmetric along the longitudinal axis as shown in Figure 2.2(b). After endodontic treatment, the canal is filled with gutta percha. When a post is placed, all the gutta percha except a 5mm length near the apex is removed (Fig 2.1). In our model the diameter of the gutta percha is 1.5 mm. The thickness of PDL is 0.18 mm. Two parallel curves form the profile of the PDL. The profile is revolved to generate the solid model, which is shown in Figure 2.2(c). The thickness of supporting bone is 2mm, which is shown is Figure 2.2(d). The post length is 16mm, and the post diameter is 1.5mm. The post length in the root is 9.5mm and the post length above coronal surface is 6.5mm as shown in Figure 2.1. The geometric model of the post is shown in Figure 2.2(e). The height of the core is 14.5 mm. The diameter of core at the bottom is 6 mm. The solid core component is shown in Figure 2.2(f). The length of the crown is 10.5 mm. The diameter of crown is 9 mm. The thickness of the crown at the top is 2.0mm, and the thickness at the bottom edge is 1.5mm as shown in Figure 2.1. The geometric model of the crown is shown in Figure 2.2(g).

2.4.2 Assembly

After the geometric models are generated, they are imported into ANSYS and assembled to create the finite element model. In the finite element analysis, assembly means that the nodes of the neighboring components are connected with each other on the common neighboring surfaces. After the assembly (shown in Figure 2.3), the components are

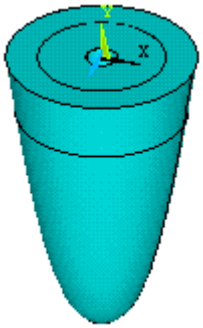

(a) Dentin

(b) Gutta Percha

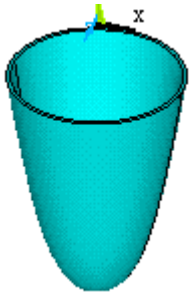

(c) PDL

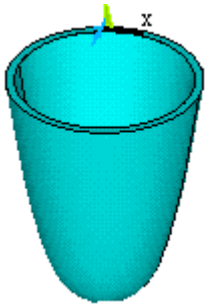

(d) Bone

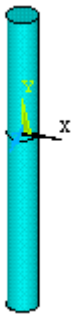

(e) Post

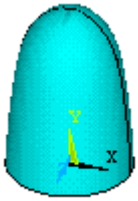

(f) Core

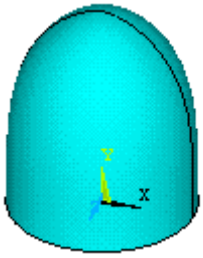

(g) Crown

Figure 2.2 Solid models of the seven components. X, Y, and Z are the coordinates.

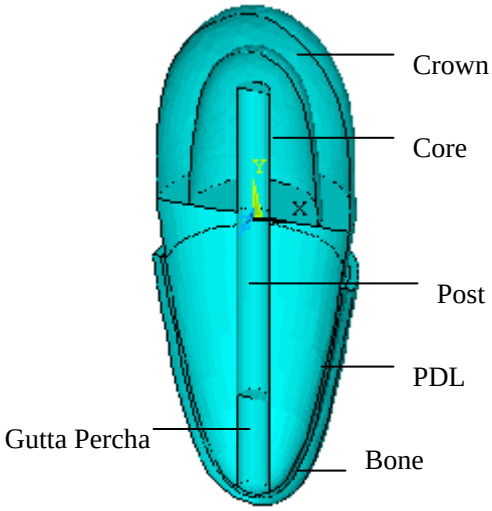

Figure 2.3 The structure of post-core restored endodontic treated tooth

virtually “glued” together to make two neighbour components share one common surface and nodes since it is assumed that all the components have perfect bonding and that any cement material, if present effectively, has no thickness.

2.4.3 Mesh

The mesh generation is an important procedure to subdivide the solid geometry into elements. Fine mesh requires considerable computing time and memory space. On the other hand, coarse mesh reduces the computing time and memory space, but will cause inaccurate results. In this work, proper meshing is determined based on the convergence test, which is discussed in the later section. Regarding the types of the elements, Prep7 is a processor in ANSYS to define model’s element types, element constants, material properties, and the model geometries, which is used in this work. ANSYS library contains

Figure 2.4 Element SOLID92 (Adapted from ANSYS Help Manual)

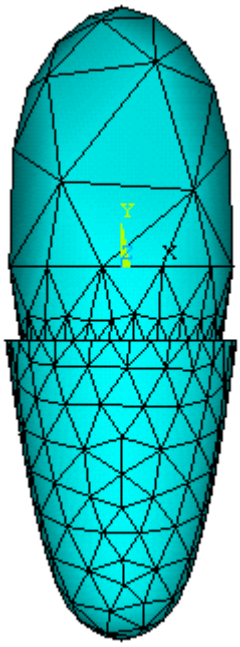

Figure 2.5 A sample of the meshed structure

over 150 element types. In this study, SOLID92 element type (shown in Figure 2.4) is used. SOLID92 element is a 3D tetrahedral structural solid of ten nodes with three degrees of freedom at each node: translations along the global coordinate axes, X, Y and Z, as shown in Figure 2.4. Such elements are well suited to model irregular meshes (such as models produced from various CAD/CAM systems). This type of element can also be used for analyzing the stresses in the structure with plasticity, creep, swelling, stress stiffing, large deflection, and large strain. Because the stress distributions in dentin and the post are the focus of the study, the mesh sizes for dentin and the post are finer than other parts such as the crown and the core. The models have about 28000 elements and 39000 nodes after meshing. The meshed structure is shown in Figure 2.5.

2.4.4 Loading and boundary condition

The concentrated force of 100 N is applied on the node of the surface vertically, horizontally, and obliquely. For the vertical loading, a load is applied on the top center of the crown. For the horizontal loading, the load is applied at a point, which is at the half height of the crown. For the oblique loading, the load is applied at a point on the crown surface, which is 7.5mm above the bottom of crown, at 45^{o} to the vertical axis (Fig 2.6). The outer surface of the bone is set to have a perfectly rigid boundary with zero displacement (Neumann boundary condition). Other surfaces are set to have a perfectly free boundary (Dirichlet Boundary Condition).

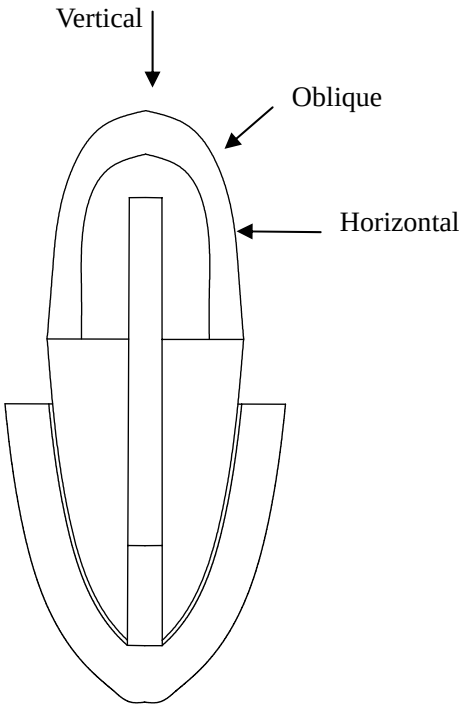

Figure 2.6 Loading location and direction

2.5 Models

A total of four models are developed in this work. Model One can be used to study the effects of different material properties of the posts and combinations of the post and the core on the stress distributions in dentin and posts under various loading. In finite element analysis program, using different posts and cores means changing the value of the elastic modulus of the posts and the cores. Model Two includes the loss of dentin along the coronal portion of the canal and can be used to study its effects on the stresses in dentin and posts. The different shapes of dentin loss, such as the L, U, and V shape, are considered. These three shapes describe the profile of the gap at the cervical region on the sectional

plane passing the vertical axis. Model Three considers the different heights of dentin ferrule and can be used to study its effects on the stress distributions in dentin and the posts. Model Four has different thickness of dentin walls and will be used to investigate the effects of the thickness of the dentin wall on the stress distributions in dentin and the posts. For each model, three loads of different directions at same magnitude of 100N are applied on the top of the crown.

2.6Convergence test

As discussed before, the number of the elements used is important for the quality of the results. Fine mesh requires considerable computing time and memory space in the computer. On the other hand, coarse mesh reduces the demand for the computing time and memory space, but will cause the inaccurate results. In the course of this research, a convergence test is conducted. The finite element model, developed above, with a stainless steel post and a vertical concentrated force of 100N applied is used. The dentin is meshed using five different mesh sizes to observe the convergence of the results. The five mesh levels are 6, 7, 8, 9, and 10. Mesh level 6 is the fine mesh, which contains 7853 elements, and mesh level 10 is the coarse mesh, which contains 529 elements. The highest stresses in dentin and the post vs. the numbers of the elements are shown in Tables 2.2 and 2.3. At mesh level below level 8, the stresses in both dentin and the post do not change greatly. Conclusion can be made that mesh level 8 satisfies the convergence requirement.

Table 2.2. Highest stresses in dentin with different mesh levels

Mesh Level	6	7	8	9	10
Number of Element	7853	5067	1344	667	529
Von Mises Stress (MPa)	4.30	4.28	4.25	4.15	4.05

Table 2.3. Highest stresses in the post with different mesh levels

Mesh Level	6	7	8	9	10
Number of Element	7050	4134	1867	1147	676
Von Mises Stress (MPa)	44.99	44.79	44.41	40.88	40.34

2.7 Verification

Joshi *et al.* (2001) built a 3D finite element model to study the effects of different post materials. The similar model was built to verify the modeling method. For horizontal and oblique loading, the highest von-Mises stress value was very close. Since the lack of the model dimension and exact loading point, the stress results for the vertical load is different from Joshi's results. We calculate the vertical force at the different section of the dentin. We find the results were very much close to the vertical force applied on the top of the crown.

Chapter 3 Simulation Results and Discussion

Using the 3D finite element model, developed in Chapter 2, five groups of simulations were conducted to investigate the effects of various factors on the stress distributions in dentin, post, core and crown of a post-core restored maxillary incisor. These factors were (*i*) post materials, (*ii*) combinations of different post and core materials, (*iii*) dentin loss at the coronal aspect of the canal, (*iv*) dentin ferrule height, and (*v*) canal diameter. Three types of loading, namely a vertical load, horizontal load, and oblique load, were applied on the top of the crown individually, and all with the magnitude of 100N. The incisor is assumed to be supported by the surrounding bone, which has a fixed outer surface. The von Mises Failure Criterion (Beer *et al.* 2002)) is often used to estimate the yield of ductile materials. It has been used to predict the failure of human teeth (Huysmans *et al.* 1993). Von Mises equivalent stress was calculated in each simulation. The stress distributions are shown in a cross section passing through the tooth longitudinal axis and loading direction since such a cross section shows the highest stresses for horizontal and oblique loading and has been used in related literature (Joshi *et al.*, 2001, Huysmans *et al.*, 1993, and Pierrisnard *et al.*, 2002).

The objective of this research is to gain an in-depth understanding of the effects of various design factors on the stress distributions of post-core restored endodontically treated teeth.

3.1 Simulation one: different post materials

The post material is believed to have significant effects on the stress distributions in post-core restored endodontically treated teeth (Joshi *et al*., 2001 and Pierrisnard *et al*., 2002). Four different types of post materials used in this study were stainless steel, titanium, ceramic, and FRC. Stainless steel has the highest elastic modulus followed by titanium, ceramic, and FRC (see Table 2.1). The dimensions, shapes and structure of the four types of posts are identical.

3.1.1 Vertical loading

3.1.1.1 Dentin

Figure 3.1 shows the Von Mises stress developed in the dentin portion of the teeth restored with the four post materials. Since the physical model is assumed axi-symmetric, the stress distribution is axi-symmetric. When the stainless steel post is used, the highest average stress in dentin is around 4.25MPa[*] and is observed in a narrow band around the apical end of the post (shown as region 1 in Figure 3.1a). At the dentin shoulder (shown as region 2 in Figure 3.1a) the mean stress is 1.75MPa. The lowest stress, which is about 0.75MPa, is observed along the upper half of the canal and at the apical third of the dentin (region 3 and 4 in Figure 3.1a). The stress at the cervical portion of the canal (region 5 in Figure 3.1a) is 0.75MPa. The stresses in the remainder of the dentin are distributed uniformly, and are around 1.25MPa. When the titanium post is used, the highest stress is reduced at the apical end of the post by 23.5% compared to that of the stainless steel post and the value is around 3.25MPa (shown as region 1 in Figure 3.1b).

[*] Note: 4.25MPa is the average stress value that would occur in this region. As can be seen from the graph at the bottom of the Figure 3.1, the maximum stress in region 1 could be as high as 4.5MPa.

The stress at the shoulder of the dentin (shown as region 2 in Figure 3.1b) has the same value 1.75MPa as that when stainless steel is used. At the apical third of the dentin and in the middle of the root, the stress is the lowest, which is about 0.75MPa (shown as regions 3 and 4 in Figure 3.1b). However, the stress increases at the upper one third of the canal (shown as 5 in Figure 3.1b) by 60% as compared with the stresses in the same area with the stainless steel post and the value is around 1.25MPa. When the ceramic post material is used, the highest stress, which occurs at the apical end of the post, is reduced by 47% as compared with that of stainless steel and the value is approximately 2.25MPa, shown as region 1 in Figure 3.1c. The stress at the shoulder area of the dentin is 1.75MPa (shown as region 2 in Figure 3.1c), which is the same as that of the model with the stainless steel post. Note that the area of region 2 increases as compared with the corresponding regions shown in Figures 3.1a and 3.1b. The lowest stress is at regions 3 and 4 with the value of 0.75MPa. However, the area of region 4 decreases significantly as compared with the corresponding regions shown in Figures 3.1a and 3.1b. The stress distribution in the rest of the regions in dentin is more even and is around 1.25MPa. When the FRC post is used, no significant stress concentration is observed at the apical end of the post, where the stress is 1.75MPa. Just below the dentin shoulder (shown as region 2 in Figure 3.1d), the stress is about 1.75MPa. Region 2 is enlarged significantly. The lowest stress is 0.75MPa and occurs at region 3. In the rest of the regions, the stress is evenly distributed with the stress value about 1.25MPa (shown as region 4 in Figure 3.1d).

The stresses in different regions of dentin with four types of post materials are summarized in Table 3.1. The results show that the stainless steel posts (with the highest elastic modulus) resulted in the highest dentin stress concentration, and that the stress concentration decreases with the decrease in the post elastic modulus. The FRC posts resulted in the lowest stress concentration and most uniform stress distributions. High stress in dentin is highly undesirable and should be avoided.

Table 3.1 Stresses in different dentin regions with four types of post materials under the vertical loading

Post Material	Region 1 (MPa)	Region 2 (MPa)	Region 3 (MPa)	Region 4 (MPa)	Region 5 (MPa)
Stainless steel	4.25	1.75	0.75	0.75	0.75
Titanium	3.25	1.75	0.75	0.75	1.25
Ceramic	2.25	1.75	0.75	0.75	1.25
FRC	1.75	1.75	0.75	1.25	1.25

3.1.1.2 Posts

Figure 3.2 shows the stress distributions in the posts under the vertical loading. The stainless steel post (high elastic modulus) has the highest stress in the middle area at about 14.4MPa (shown as region 1 in Figure 3.2a). The stress decreases in regions 2 and 3 shown in Figure 3.2a with the values of 12.2MPa. The highest stress in the titanium post is reduced by 30.6% as compared to the stainless steel post with the value of 9.99MPa, shown as region 1 in Figure 3.2b. The highest stress in the ceramic post is reduced by 61.8% as compared to the stainless steel post with the value of 5.5MPa and the changes in stress in different areas are insignificant as shown in Figure 3.2c. FRC post presents the most uniform distributed stress (Figure 3.2d) at about 1.1MPa. No stress

concentration is observed in the FRC post. Figure 3.2 shows that the stress distribution is most uniform in FRC with the lowest elastic modulus, and the least uniform is the stainless steel with the highest elastic modulus. High stresses in the stainless steel post are hazardous to the life of the post. However, it shares more load and reduces the force applied on dentin.

3.1.1.3 Cores and Crowns

Figures 3.3 and 3.4 show the stress distributions in the cores and the crowns with four different post materials under the vertical loading. Regardless of the post materials, the stress distributions in the cores and the crowns do not change significantly. Maximum stresses appear at the top of the cores and the crowns where the load is applied. For all the post materials, the maximum stress value in the cores is about 5.5MPa. The stress patterns shown in Figures 3.3 and 3.4 show that the changes in the elastic modulus of the post materials do not influence the stress distributions significantly in the cores and the crowns.

3.1.2 Horizontal load

3.1.2.1 Dentin

Figure 3.5 shows the stress distributions in the dentin with four post materials under the horizontal load. The stress distributions are similar regardless of the post materials. The dentin and the post are bent to the left in response to the horizontal load. In all cases, the highest stresses (16.4MPa) are located at the two side of the dentin, shown as 1 and 2 in Figure 3.5a-d. The stress gradually reduces from the outer surface of the dentin to the

center of the dentin. The gutta percha is easily deformable due to its low elastic modulus (0.96×10^{-3} GPa) and does not support much load. Overall, the effects of post materials on the stress distributions in dentin with a horizontal force are not significant.

3.1.2.2 Posts

Figure 3.6 shows the stress distributions in the four posts with the horizontal load. The maximum stresses in stainless steel, titanium, ceramic, and FRC post materials are 50.7MPa, 29.9MPa, 22.7MPa, and 9.0MPa, respectively. Figure 3.6a shows the highest stresses in the stainless steel post are located on the two sides of the post (shown as 1 and 2 in Figure 3.6a) in the plane containing the longitudinal axis and the force, and are reduced at the centre of the post. The high stresses are reduced significantly with lower elastic modulus material, as shown in Figures 3.6b to 3.6d, and the stress distributions are more uniform as the elastic modulus decrease. Similar observations can be made as those with the vertical loading. The advantage of using the posts with high elastic modulus is that the posts share more horizontal load.

3.1.3 Oblique load

Figures 3.7 show the stress distributions in dentin with four different post materials under an oblique load. The stress distributions are very similar among four post materials. The maximum stress in dentin is located in region 1 as shown in Figure 3.7 with the value of 12.75MPa. Also, a high stress value of 9.3MPa is observed in the dentin along the apical portion of the root (region 2 in Figure 3.7).

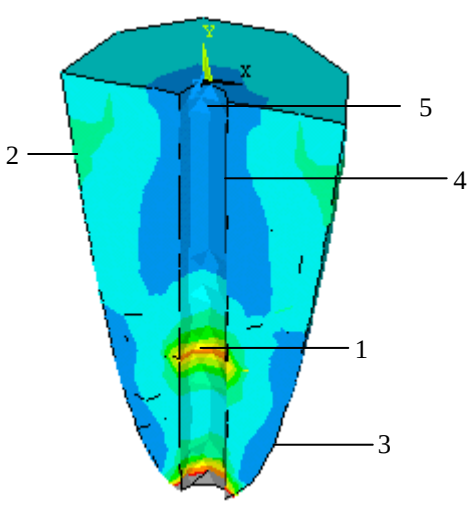

(a) With a stainless steel post

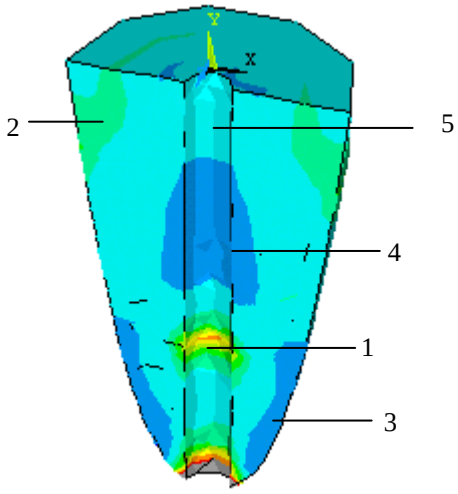

(b) With a titanium post

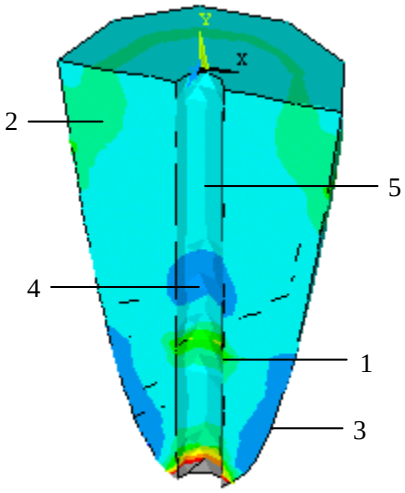

(c) With a ceramic post

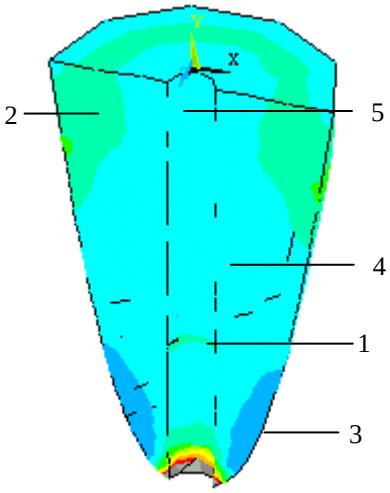

(d) With a FRC post

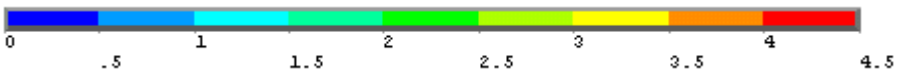

Figure 3.1 Stress distributions in dentin under a vertical load (MPa).

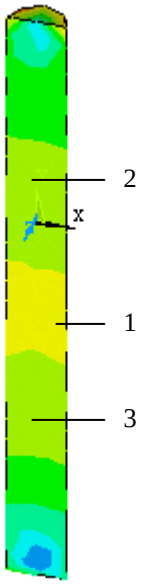

(a) With a stainless steel post

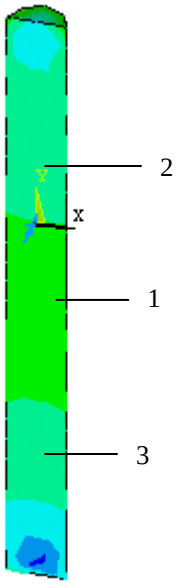

(b) With a titanium post

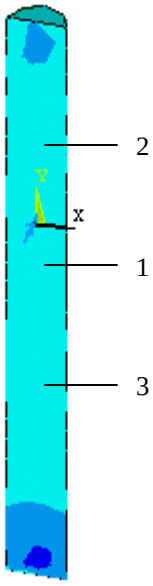

(c) With a ceramic post

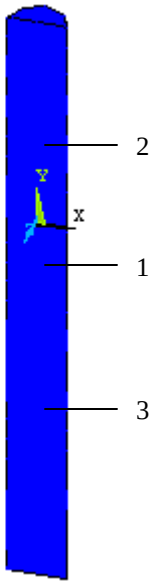

(d) With a FRC post material.

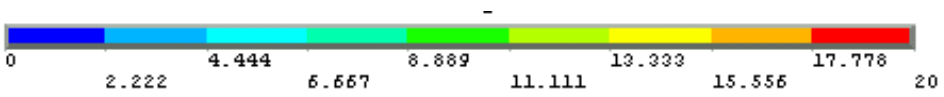

Figure 3.2 Stress distributions in posts under a vertical load (MPa).

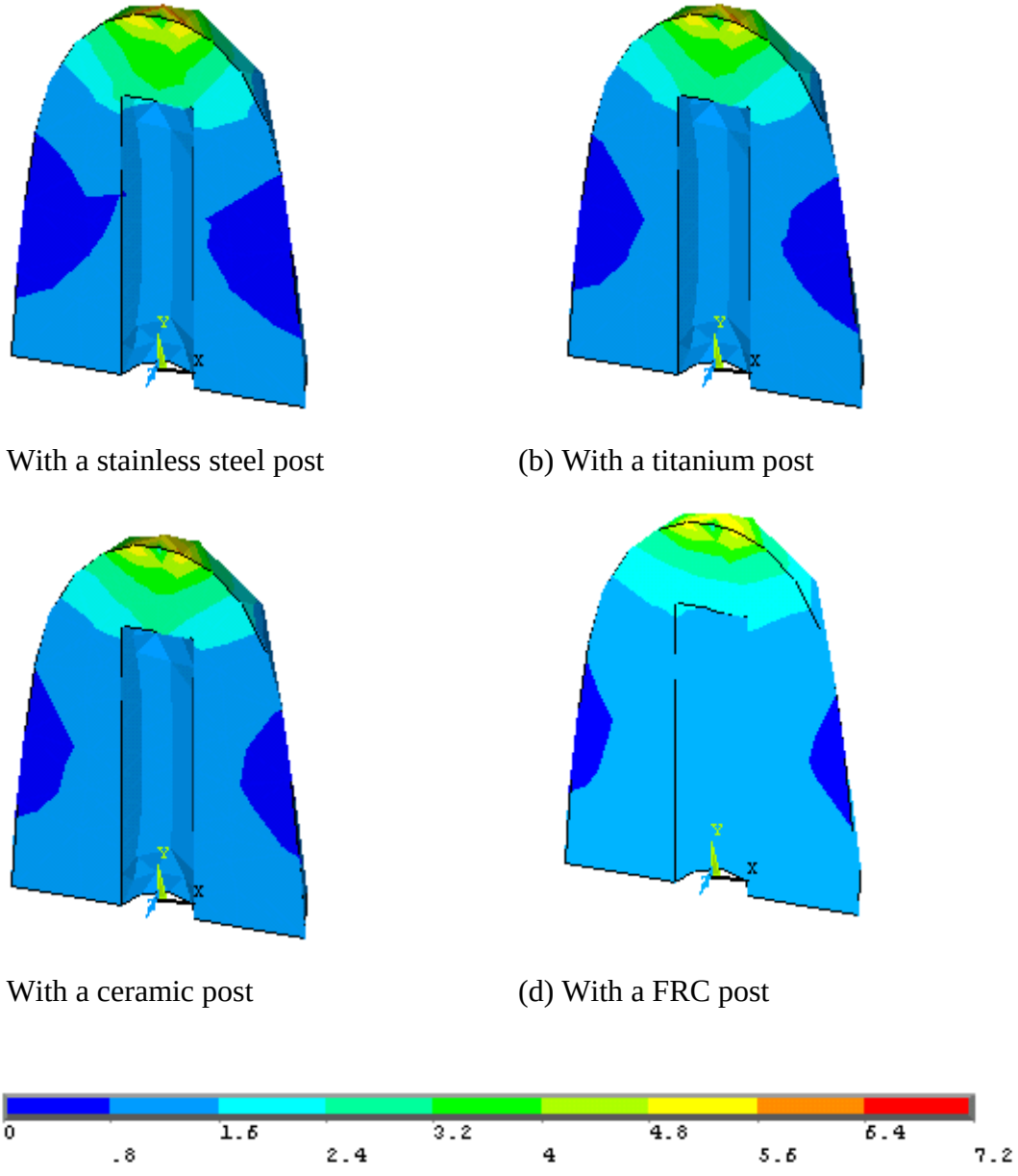

(a) With a stainless steel post

(b) With a titanium post

(c) With a ceramic post

(d) With a FRC post

Figure 3.3 Stress distributions in cores under a vertical load (MPa).

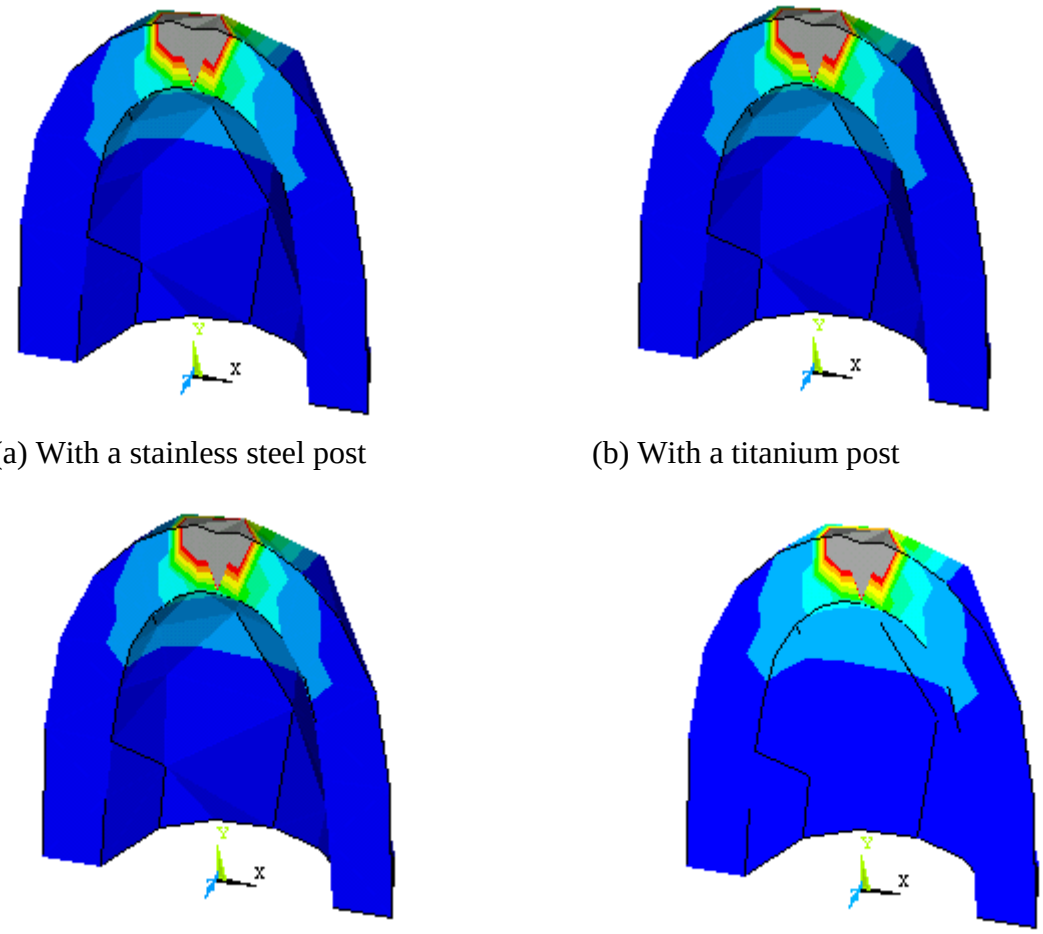

(a) With a stainless steel post (b) With a titanium post

(c) With a ceramic post (d) With a FRC post

Figure 3.4 Stress distributions in crowns under a vertical load (MPa).

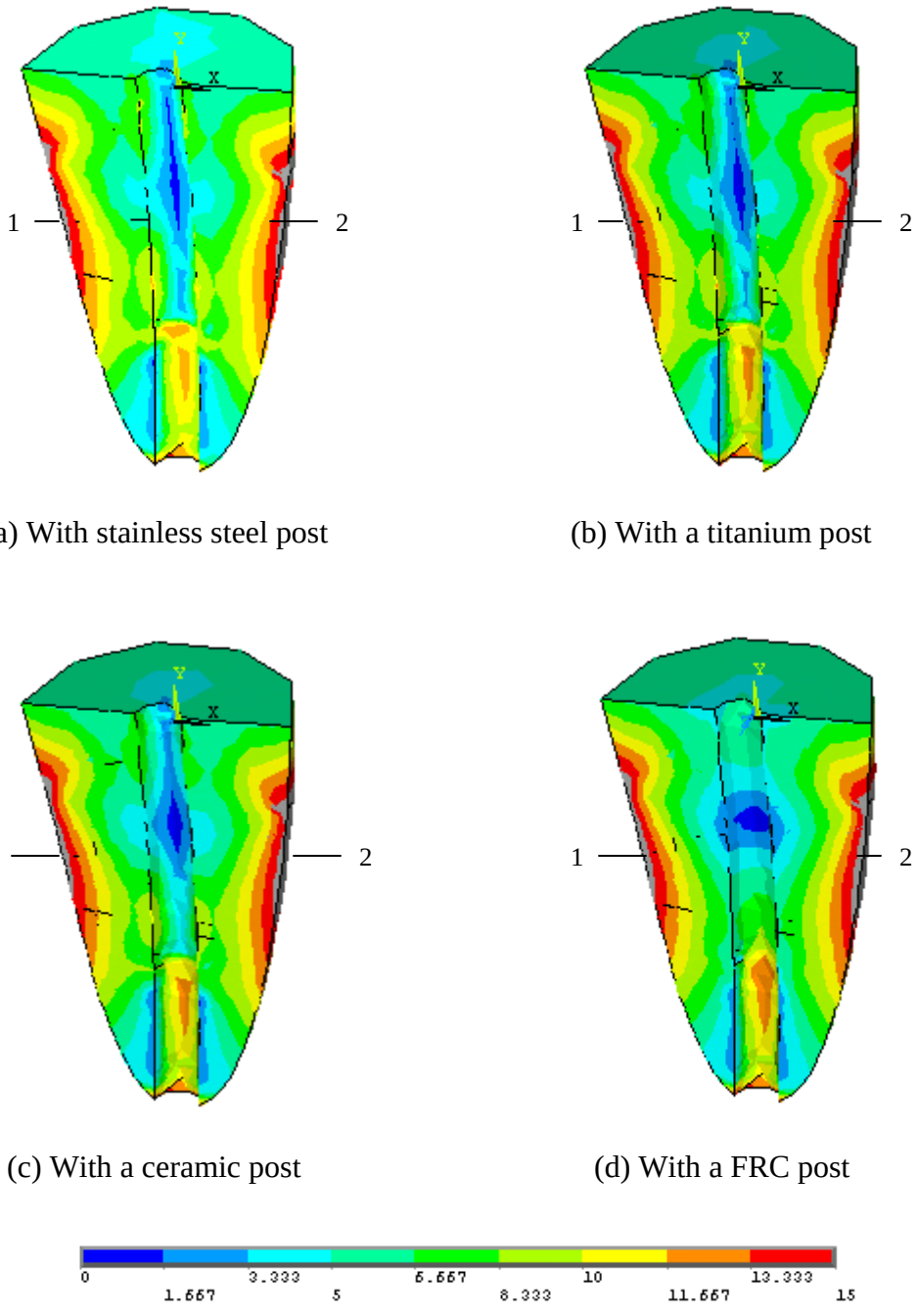

(a) With stainless steel post

(b) With a titanium post

(c) With a ceramic post

(d) With a FRC post

Figure 3.5 Stress distributions in dentin under a horizontal load (MPa).

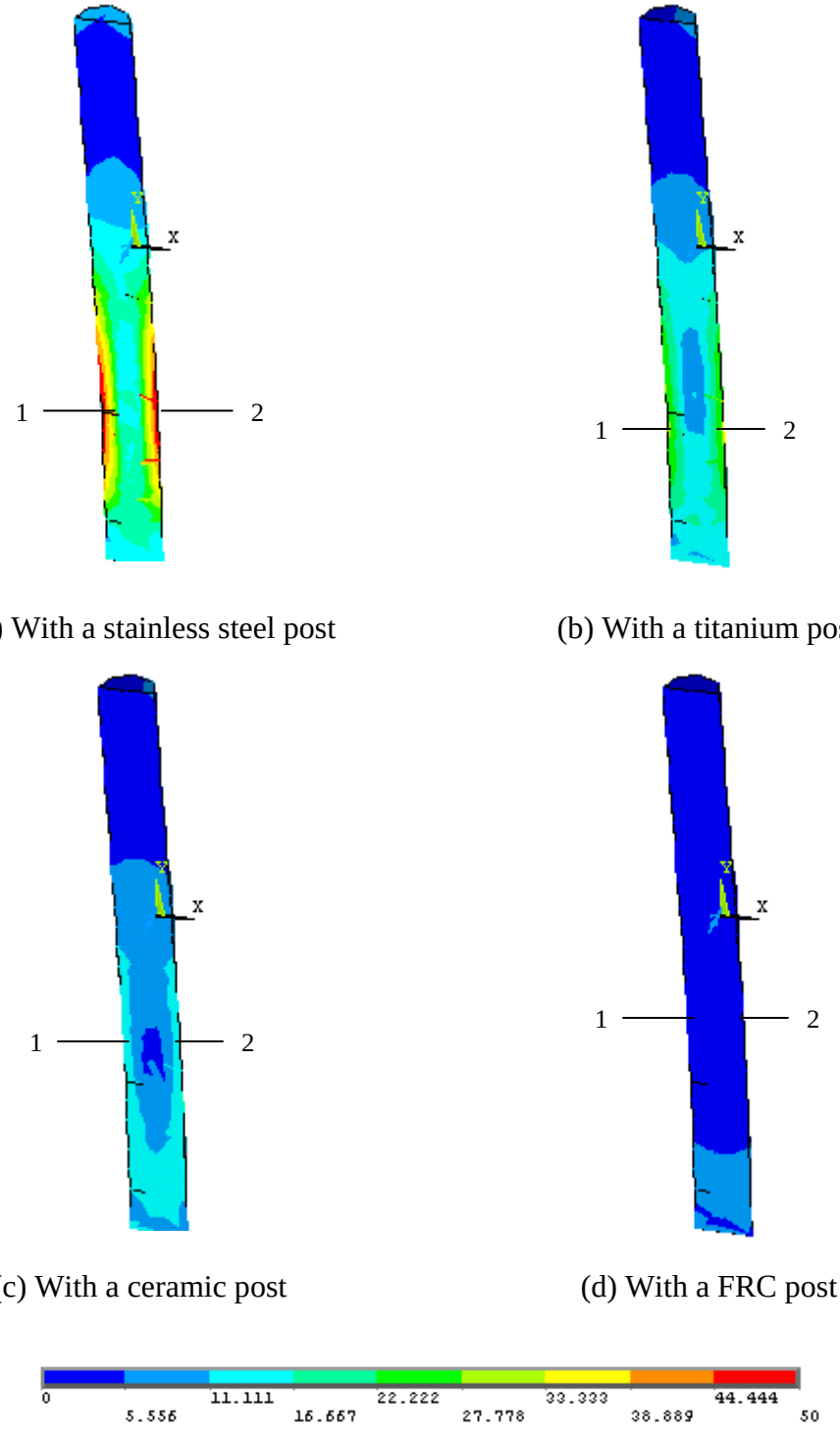

(a) With a stainless steel post

(b) With a titanium post

(c) With a ceramic post

(d) With a FRC post

Figure 3.6 Stress distributions in posts under a horizontal load (MPa).

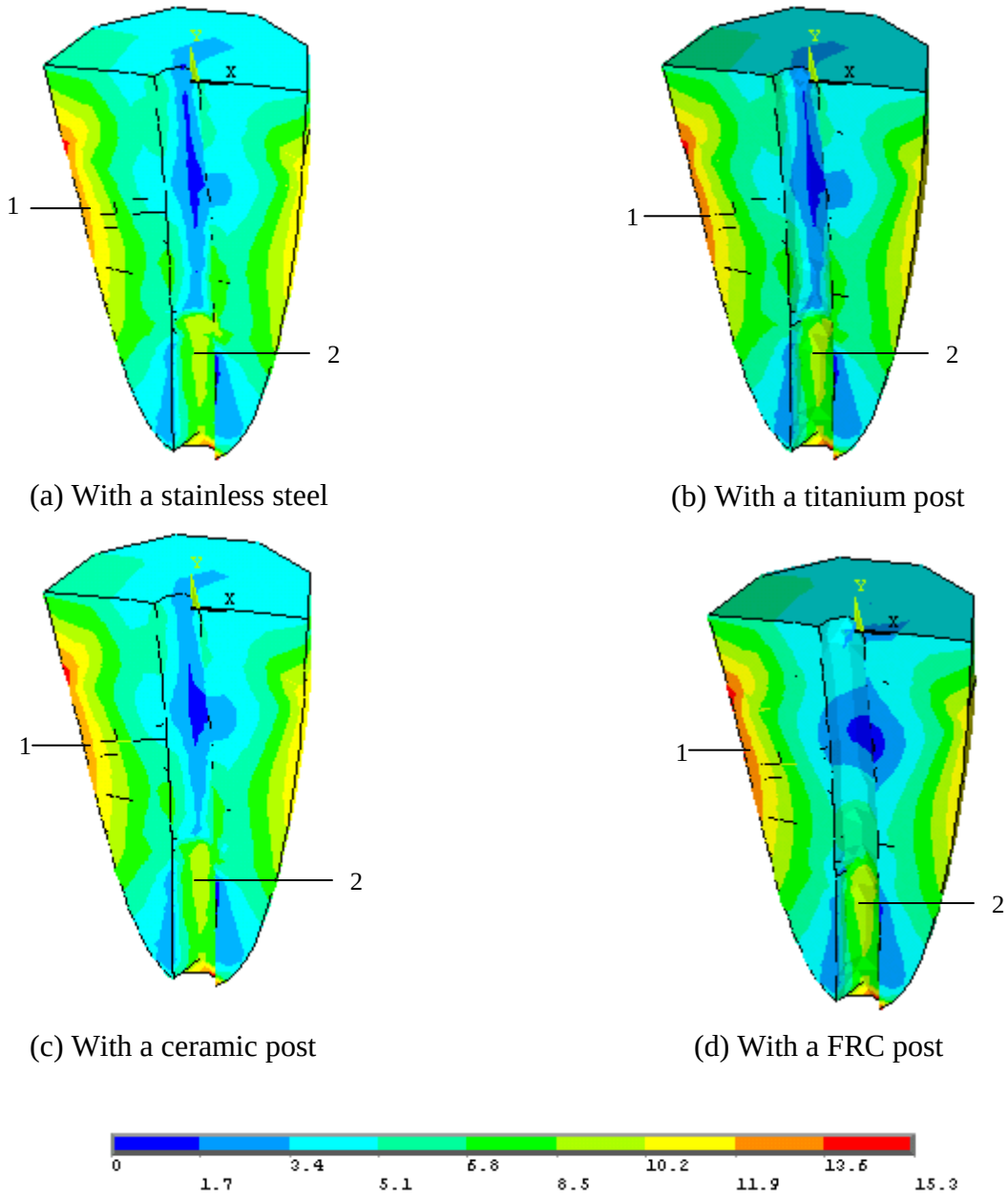

(a) With a stainless steel

(b) With a titanium post

(c) With a ceramic post

(d) With a FRC post

Figure 3.7 Stress distributions in dentin under an oblique load (MPa).

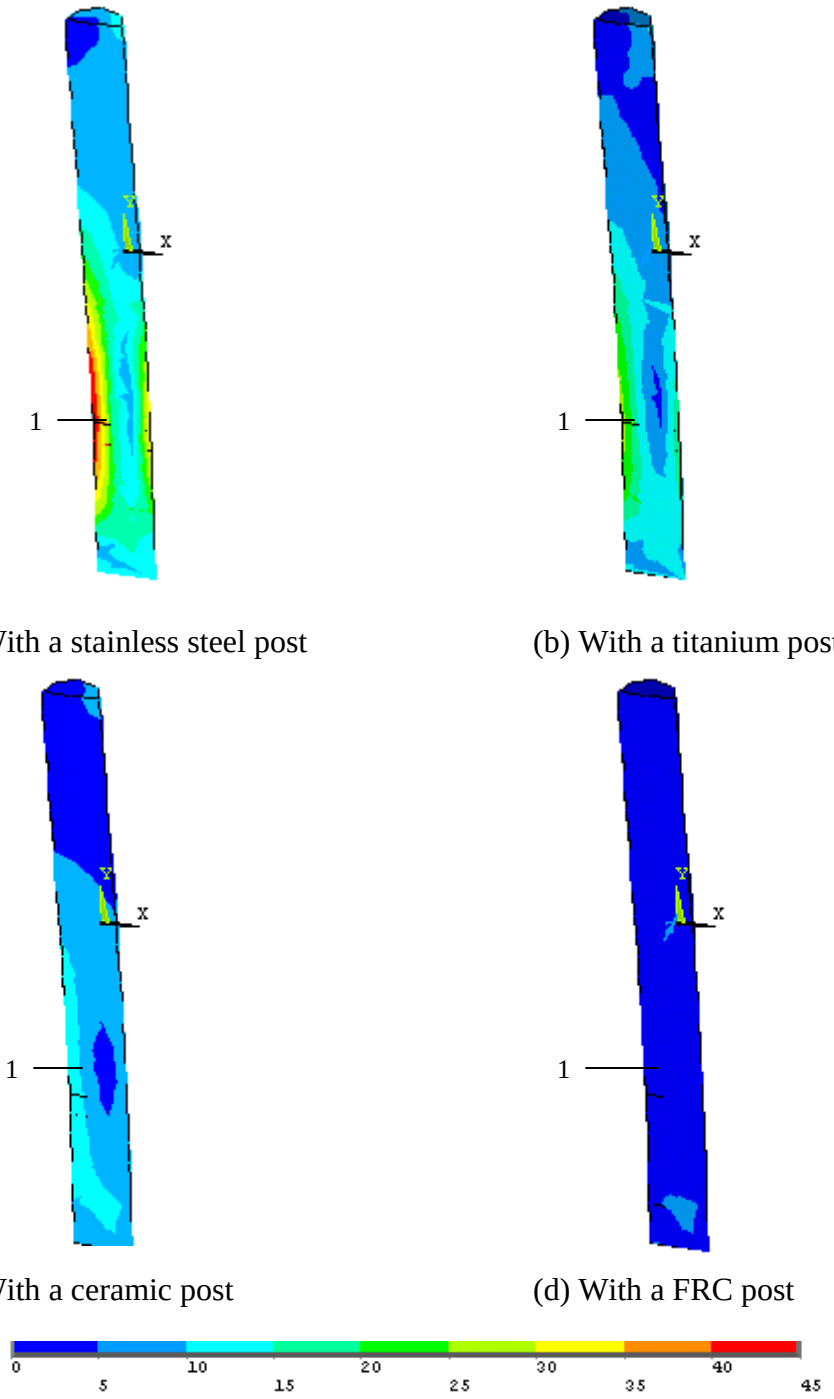

(a) With a stainless steel post

(b) With a titanium post

(c) With a ceramic post

(d) With a FRC post

Figure 3.8 Stress distributions in posts under an oblique load (MPa).

Figure 3.8 show the stress distribution in posts. The post with the highest elastic modulus shows the highest stress value, which is 45.0MPa at the side of the post (region 1 in Figure 3.8a). It is about 9 times greater than that with the FRC post (5.0 MPa shown in region 1 of Figure 3.8d). The maximum stresses in the posts decrease with the decrease in the elastic modulus of the posts.

3.1.4 Discussion

The research shows that under vertical loading the post with highest elastic modulus (i.e. stainless steel post) resulted in the highest stress concentration in the apical portion of the root. The post with highest elastic modulus supports a large amount of vertical loading. Lowest elastic modulus post material (i.e. FRC post) doesn't support much of the load. FRC post material is easily deformed. Loading is passed from the crown to the dentin, and this causes an increase in the stresses just below the dentin shoulder. Rigid post will support most of the vertical loading, and it causes high stress at the apical portion of the post. However, the stress value is much less than the stress caused by horizontal loading.

The ceramic post material produces a low stress concentration (2.25MPa) at the apical portion of the post, and no high stress is observed just below the dentin shoulder. An elastic modulus close to that of the dentin will produce less stresses at the interface between the dentin and post. Under vertical loading, post material should be chosen that will prevent the creation of high stress at the apical portion of the root and that will be able to support the load. Posts should be used only for retention of a core within remaining tooth structure when no other alternatives exist. When a post is necessary, the

stress distribution should be considered during post placement(Assif et al. 1989). The stiffness of the entire post-core system must be able to resist, with the least possible deformation, the forces of mastication (Stockton et al. 2000)

Under the horizontal and oblique loadings, highest elastic modulus post material (i.e. stainless steel post material) causes high stress along the canal, which is undesirable. High stress may eventually cause de-bonding between the post and the root. No high stress is observed along the inner wall of the canal when a low modulus post (i.e. FRC post material) is used. FRC material is more flexible and stainless steel is more rigid. FRC material allows large deformation while stainless steel material allows limited deflection. Although using a high elastic modulus post material reduces some of the stress in the root by supporting the artificial crown, the high stress created along the inner wall of the canal is not desirable and should be avoided. Even though low elastic modulus material (i.e. FRC post) doesn't cause the high stress along the inner canal wall, de-bonding of the material and long term fatigue effect still have to be considered. Under horizontal and oblique loading, post material should be chosen so that it will support the restored tooth and will prevent the creation of high stress along the inner canal wall.

The horizontal loading of a stainless steel post restored tooth causes a stress that is 3 times as high as that caused by vertical loading. Vertical loading causes high stress at the apical portion of the root. Horizontal loading causes high stress at both sides of the root. High stress concentrations are not desirable, and should be avoided. The loading direction will cause more damage to the root than the post material as long as the highest stress in

the root is considered. Horizontal loading should be avoided as much as possible. This result is in agreement with the previous work of Yang et al. (2001). They observed that greater deflections and higher stresses were generated with horizontal loading. The effect of dowel design on maximum stress and displacement was much less than the effect of the load direction.

The high stress appears at the top of the crown is not realistic, because of the point application of the load. In this research, we care about the stress in dentin. The force is transferred from the crown to the core and dentin. From the stress pattern of the core, we observed that the force is passed from the crown to the core.

3.1.5 Summary

The stresses in dentin, posts, cores and crowns have been evaluated and compared with four different post materials. Three types of loading have been applied, namely a vertical loading, a horizontal loading and an oblique loading. Since the stresses do not change significantly in the cores and the crowns, we focused on the comparisons of the stresses in dentin and the posts. The maximum Von Mises stresses in dentin and the posts are summarised in Graphs 3.1 and 3.2. The horizontal loading causes the highest stresses in dentin and posts, followed by the oblique load and finally the vertical load. The stress distributions in dentin do not change significantly when the horizontal loading is applied compared to the oblique loading regardless of the combination of the post and the core. However, they change significantly when the vertical loading is applied. We found that the post with higher elastic modulus causes higher stress concentrations and less uniform

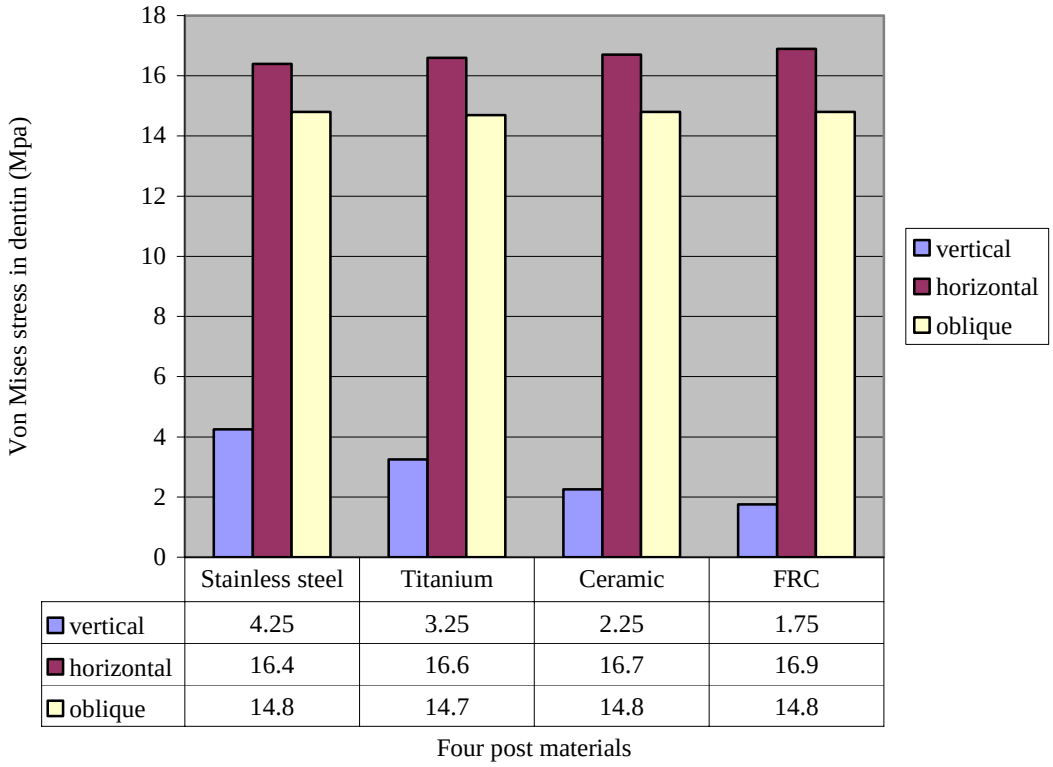

	Stainless steel	Titanium	Ceramic	FRC
vertical	4.25	3.25	2.25	1.75
horizontal	16.4	16.6	16.7	16.9
oblique	14.8	14.7	14.8	14.8

Graph 3.1 Maximum Von Mises stresses in dentin with different posts

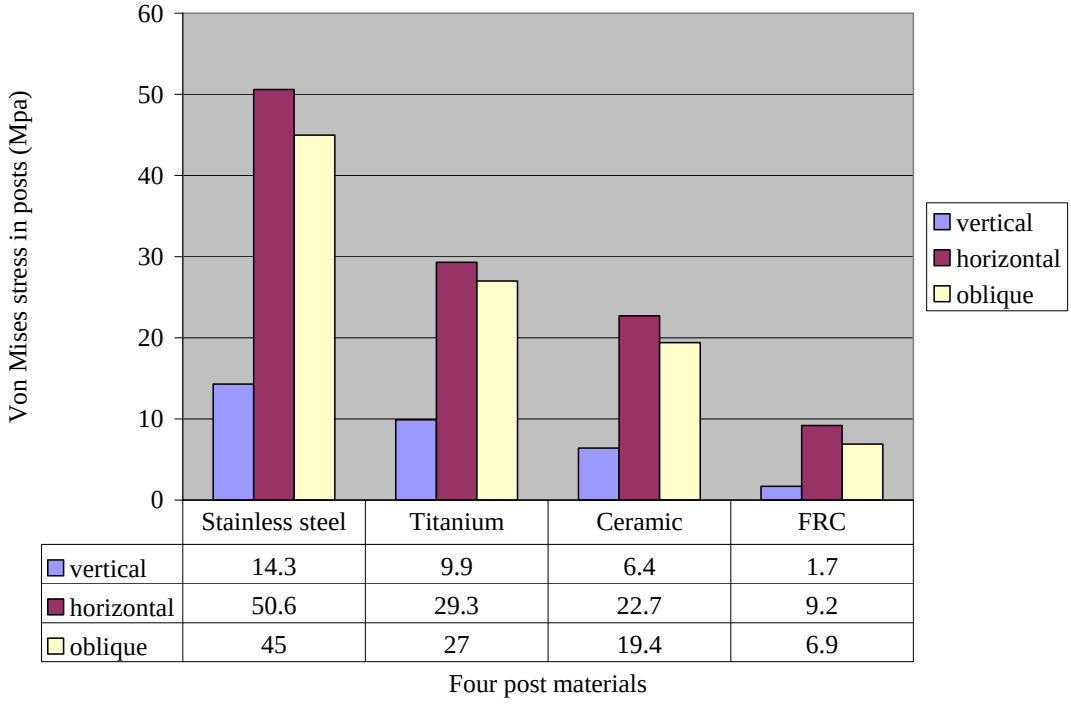

	Stainless steel	Titanium	Ceramic	FRC
vertical	14.3	9.9	6.4	1.7
horizontal	50.6	29.3	22.7	9.2
oblique	45	27	19.4	6.9

Graph 3.2 Maximum Von Mises stresses in posts

stress distributions in both dentin and the posts with the vertical loading. The posts with higher elastic modulus bear more loads. With low elastic modulus, the post flexes easily and does not support much of the load. Overall, the horizontal loading and the oblique loading are the most dangerous. The post materials do not make significant differences in the magnitudes of the stresses and their distributions in dentin.

3.2 Simulation two: combinations of different post and core

Von Mises stresses are calculated in the post-core restored endodontically treated maxillary incisor where each of the four post materials, used in Section 3.1, is combined with three different core materials. The elastic modulus of each post material is 200GPa, 120GPa, 69.0GPa, and 16.6GPa (Table 2.1). Three core materials are selected such that their elastic modulus are 5.0GPa, 16.6GPa, and 52GPa, which are below, similar to, or higher than that of dentin (18.6GPa) (Table 2.1). The Poison's ratios for the three core materials are 0.30. The elastic modulus of each post materials is much higher than that of core materials except the FRC post material. Vertical, horizontal, and oblique loading at a magnitude of 100N are applied on the top of the crown. The objective is to understand the effect of the combinations of different post and core materials on the stress distributions in dentin.

3.2.1 Vertical loading

3.2.1.1 Stainless Steel Post

Figure 3.9 shows the stress distributions in dentin with the stainless steel post and three different core materials. The elastic modulus of the post (E=200GPa) is much higher than

those of the core materials. For the core with a low elastic modulus, the highest stress appears in dentin at the apical portion of the post, shown as region 1 in Figure 3.9a, and is 4.50MPa. The stress at the shoulder of dentin, shown as region 2 in Figure 3.9a, is about 1.75MPa. The stress in the area of coronal and middle of the canal as well as the apical part of dentin (shown as regions 4 and 3 in Figure 3.9a) is about 0.75MPa, which is the lowest stress in dentin. For the core with a middle elastic modulus, which is similar to that of dentin, the highest stress appears at the apical part of post (shown as 1 in Figure 3.9b), and is 4.25MPa, which is 5.6% lower than that with low elastic modulus core. The stress at the shoulder of the dentin (shown as region 2 in Figure 3.9b) is about 1.75MPa, similar to the one with the low elastic modulus core. However, the size of region 2 is smaller than that with the low elastic modulus core. The lowest stresses appear in regions 3 and 4 at the value of 0.75MPa. When the core material with a high elastic modulus is used, the distributions and the magnitudes of the stresses are similar to those with a medium elastic modulus core except that the size of the region of shoulder stress (shown as region 2 in Figure 3.9c) is much smaller as compared with the one for the medium elastic modulus. However, it is noted that the stress at the coronal portion of the root, which is 1.25MPa (shown as 5 in Figure 3.9c), increases 67%, as comparing to those of other two core materials. When used with a stainless steel post, the core material with medium elastic modulus shows favourable stress distribution due to the low stress at the apical portion of the root, dentin shoulder and the coronal portion of the root, which is beneficial to tooth restoration.

3.2.1.2 Titanium Post

Figure 3.10 shows the stress distributions in dentin having a titanium post (E=120GPa) with the three core materials. The highest stresses in Figure 3.10 appear at the apical portion of the post with the magnitude of 3.25MPa, shown as region 1 in Figures 3.10. The stresses at the shoulder of dentin is the next highest at 1.75MPa, for all three cores shown as region 2 in Figure 3.10, but the size of region 2 reduces significantly as the elastic modulus increases. The stress along the canal (region 3, Figure 3.10) as well as at the apical portion of the dentin (shown as 3 and 4 in Figure 3.10a) is the lowest among all the core materials, which is 0.75MPa. The rest of dentin shows stress around 1.25MPa. When the cores with medium and high elastic modulus are used with a titanium post, the stress at the coronal canal (shown as 5 in Figure 3.10b and c) increases about 29% comparing to that of the low elastic modulus core material, which is 1.25MPa. When used with a titanium post, Core materials with high and medium elastic modulus show low stress at the apical portion of the root and dentin shoulder, which is beneficial to tooth restoration.

3.2.1.3 Ceramic Post

Figure 3.11 shows the stress distributions in dentin with three core materials and a ceramic post (E=69GPa). The highest stresses for three cases are located at the apical portion of the post, shown as region 1 in Figure 3.11, and is about 2.25MPa. When the low elastic modulus core material is used, the stress along the canal has the lowest value comparing to the other two core materials, shown as region 4 in Figure 3.11. It is 0.75MPa and is 40% lower than that of the other two core materials. Under the dentin

shoulder (region 2 in the Figure 3.11a), the stress is 1.75MPa. The area of region 2 is larger than that using other two core materials. The stress patterns in dentin with middle and high elastic modulus core materials are similar. At the apical portion of the post (shown as region 1 in Figure3.11b and c), the highest stress (2.25MPa) is observed. The stress at the shoulder of the dentin is high (shown as 2 in Figure 3.11b and c), which is 1.75MPa. The area is smaller than that of the core material with the lowest stiffness. The majority of the dentin shows stress value at 1.25MPa. The bottom portions of the dentin (region 3 in Figure 3.11) are similar for the three core material and the values are 0.75MPa. When used with ceramic posts, the core materials with high and medium elastic modulus show low stress at the apical portion of the root and dentin shoulder, which is beneficial to tooth restoration with ceramic post material.

3.2.1.4 FRC Post

Figure 3.12 shows the stress distributions in dentin with three core materials and a FRC post under vertical loading. Stresses in region 1 are all 1.75MPa. When the low elastic modulus core material is used, the highest stress appears at the shoulder of the dentin (shown as 2 in Figure 3.12a) and the stress value is about 1.75MPa. The lowest stress appears at the bottom portion of the dentin (shown as region 3 in Figure 3.12a) at value of 0.75MPa. In the rest of the dentin (shown as region 4 in Figure 3.12a), the stress is uniformly distributed at the stress value of 1.25MPa. In the coronal portion of the canal (region 5 in Figure 3.12), the stress is between 0.75MPa and 1.25MPa. When the core material of the middle elastic modulus is used, the greatest stress appears at the dentin shoulder (shown as 2 in Figure 3.12b) at the value of 1.75MPa. The lowest stress is

located at the bottom portion of the dentin (shown as region 3 in Figure 3.12b) with the value of 0.75MPa. The value is the same as that of the lowest elastic modulus. In the rest of the dentin (region 4 in Figure 3.12b), the stress is evenly distributed at value of 1.25MPa. When the high elastic modulus core material is used, the highest stress is observed at the coronal portion of the root (shown as region 5 in Figure 3.12c) with stress value of 1.75MPa. The stress has increased 40% when compared to that of the low elastic modulus core. The lowest stress is located at the bottom portion of dentin (shown as region 3) at the value of 0.75MPa. For the rest of the dentin, the stress is 1.25MPa and the stress pattern is similar to that of other two core materials. Middle elastic modulus core material shows low stress at dentin shoulder, which is beneficial to tooth restoration with FRC post material.

The stresses in different regions of dentin for each post combined with three core materials are shown in Table 3.2. The results show that the stress distribution is the most uniform when the material properties of the post, the core and dentin are similar as is the case of the FRC post and the core, both with the elastic modulus of 16.6Gpa, which is close to the one of dentin (18.6GPa). The results also show that the stress concentration is high when the elastic modulus of the post, the core and dentin are different. When the stainless steel (the highest elastic modulus of 200GPa) and the core of lowest elastic modulus of 5Gpa are used, the highest stress concentration results. High stress

Table 3.2 Stresses in different regions with different combinations of posts and cores under vertical loading

Post materials	Cores materials E (GPa)	Region 1 (MPa)	Region 2 (MPa)	Region 3 (MPa)	Region 4 (MPa)	Region 5 (MPa)
Stainless steel	5.0	4.25	1.75	0.75	0.75	0.75
	16.6	4.25	1.75	0.75	0.75	0.75
	52	4.25	1.75	0.75	0.75	1.25
Titanium	5.0	3.25	1.75	0.75	0.75	1.25
	16.6	3.25	1.75	0.75	0.75	1.25
	52	3.25	1.75	0.75	0.75	1.25
Ceramic	5.0	2.25	1.75	0.75	0.75	1.25
	16.6	2.25	1.75	0.75	0.75	1.25
	52	2.25	1.75	0.75	0.75	1.25
FRC	5.0	1.75	2.25	0.75	1.25	1.25
	16.6	1.75	1.75	0.75	1.25	1.25
	52	1.75	1.75	0.75	1.25	1.75

concentrations in dentin are highly undesirable and should be avoided. As can be seen in Table 3.2, when the elastic modulus of the post and core are similar to that of dentin (16.6MPa), the stress in all 5 regions falls to comparatively low values.

3.2.2 Horizontal loading

3.2.2.1 Stainless Steel Post

3.2.2.1.1 Dentin

Figure 3.13 shows the stress distributions in dentin with a stainless steel post and three different elastic modulus core materials. The stress patterns are very similar for the three types of the core materials. The greatest stresses are observed at both sides of the dentin

(shown as 1 and 2 in Figure 3.13), and is 16.0MPa. High stress concentration is observed at region 3 in Figure 3.13 with a value of 12.445MPa. Lowest stresses are located at the centreline of the canal (shown as 4 in Figure 3.13), and is about 1.6MPa. For most of the area the stresses value are around 6.6MPa. Changing the core material has no significant influence on the stress distribution in the dentin.

3.2.2.1.2 Stresses in Posts

Figure 3.14 shows the stress distribution in the stainless steel post. Stress patterns for all three core materials are similar, and the highest stress for all four post materials appears at both sides of the apical portion of the post, and is 47.2MPa (shown as 1 and 2 in the Figure 3.14). With the high elastic modulus core material, the stress at the coronal area of the post (region 3 in Figure 3.14c) increases to 8.30MPa. This is two times higher than that of lowest elastic modulus core material.

3.2.2.2 Titanium Post

Figure 3.15 show the stress distributions in dentin with a titanium post and three different elastic modulus core materials. Regardless of the core material used, the stress distributions in dentin are similar. The highest stress is located at both sides of the dentin (shown as 1 and 2 in Figure 3.15), and is 16.5MPa. At the centreline of the apical portion of the root, a stress concentration is observed and the value is about 12.4MPa (region 3 in Figure 3.15). Along the centreline of the canal (shown as 4 in Figure 3.15), the lowest stress is noticed, which is 0.75MPa. For the rest of the dentin, the stress is about 7.5MPa. Changing core materials has no significant influence on stress distribution. With three

different core materials, the stress distributions in posts are not different, and are similar to the stress pattern shown in Figure 3.5b.

3.2.2.3 Ceramic Post

Figure 3.16 shows the stress distributions in dentin with ceramic post material and three different elastic modulus core materials. The stress distributions for the three core materials are very similar. The largest stress is located at both sides of the dentin (shown as 1 and 2 in Figure 3.16), which is 16.5MPa. At the centreline of the apical area of the canal (shown as 3 in Figure 3.16), the high stress concentration is observed and the stress value is 12.4MPa. The lowest stresses are observed along the centreline of the canal (shown as 4 in Figure 3.16), which is 0.75MPa. The change of core material has no significant influence on the stress distribution of the dentin. With three different core materials, the stresses distributions in posts show no difference, and are similar to the stress pattern shown in Figure 3.6(b).

3.2.2.4 FRC Post

3.2.2.4.1 Stresses in Dentin

Figure 3.17 shows the stress distributions in dentin with a FRC post. The stress patterns are similar with three core materials. The greatest stresses are located at the both sides of the dentin (shown as 1 and 2 in Figure 3.17), and the stress value is about 16.0MPa. Along the centerline of the apical portion of the root (shown as 3 in Figure 3.17), the stress is 12.5MPa. In the middle portion of the root, a low stress value is observed (shown

as 4 in Figure 3.17). The stress value is about 0.8MPa. Changing the core materials has no significant effect on the stress distribution in dentin.

3.2.2.4.2 Stresses in Post

Figure 3.18 shows the stress distribution of the post under horizontal load with FRC post material and three different core materials. The stress distribution of the post is similar for the three types of the core materials. For most of the post (shown as 1 in Figure 3.18), the stress value is about 4.5MPa. At the apical area of the post (shown as 2 in Figure 3.18), the stress is higher than the other area, which is 7.8MPa average. Compared to other post material, the stress in FRC post material is low.

3.2.3 Oblique loading

Figure 3.19 shows the stress distributions in dentin with a stainless steel post and three different core materials. Changing core materials has no significant influence on the stress distribution of the dentin. The high stress appears at the one side of the dentin (shown as 1 in Figure 3.19), and is about 14.8MPa. The stress value in the centreline of the apical canal is as high as 9.3MPa (shown as 2 in Figure 3.19).

Figure 3.20 shows the stress distribution of the post when used with three types of core materials. The stress distributions are very similar. The highest stress (14.8MPa) is located at one side of the post (shown as 1 in Figure 3.20), and is opposite to the loading direction. For lowest elastic modulus core materials, the stress at the coronal post (region 2 in Figure 3.20a) is about 2.5MPa. For highest elastic modulus core materials, the stress

at the coronal post (region 2 in Figure 3.20c) is about 7.5MPa. The highest elastic modulus core material causes the stress to be almost 3 times higher than that caused by lowest elastic modulus core material.

Figure 3.21 shows the stress distributions in dentin with ceramic post and core materials. No matter what core material is used, the stress distributions are similar. The stress concentration is along the one side of the dentin (shown as region 1 in Figure 3.21) and the maximum stress value is 14.7MPa. The lowest stress is at the centreline of the canal (shown as region 2 in Figure 3.21), and is 0.85MPa. For most part of area, the stress is uniformly distributed and is about 9.4MPa.

Figure 3.22 show the stress distributions of the posts under oblique loading with ceramic post and three core materials. The stress patterns are very similar. The coronal area of the post (shown as 1 in Figure 3.22) shows the lowest stress value, which is about 2.5MPa. One side of the post (shown as 2 in Figure 3.22), which is opposite to the loading force, show the highest value of 12.5MPa.

3.2.4 Discussion

Three types of core materials have dramatically different elastic modulus (5.0GPa, 16.6GPa, and 52GPa). One core material is close to that of the dentin (18.6GPa). Through this simulation, we try to find the effects of different post-core combination on stress distribution in dentin under different load directions. The force is applied to the surface of the crown which transfers the load to the core and dentin (Peter, 1982).

For the stainless steel post material under vertical loading, we find that flexible core material yields high stress at the dentin shoulder. Load is transferred from the crown to the dentin. Flexible core material takes less vertical loading. Higher elastic core material yield high stress at the cervical opening of the canal. From the Figure 3.9, the stainless steel post material with middle elastic modulus core material (which elastic modulus is also close to that of the dentin) shows the best results. Under horizontal and oblique loading, the stress patterns with all core material are very similar.

For the titanium post under vertical load, the stress patterns are very similar with the middle and highest elastic modulus core materials. At the apical portion of the post, the stress in dentin is reduced. The combination with middle elastic modulus core (the elastic modulus of which is close to that of dentin) yields best results. Under horizontal and oblique load, stress patterns are very similar. The combination of the post and core materials has no effect on the stress distribution in dentin under the horizontal and oblique loading.

For the ceramic post material under vertical loading, we found the middle elastic modulus core material yields best results. The combination of ceramic post material and middle elastic modulus core material cause less stress at the dentin shoulder or smaller size of the high stress area. Under horizontal and oblique loading, the stress patterns in dentin are very similar. The stress distribution is influenced most by the direction of the loading.

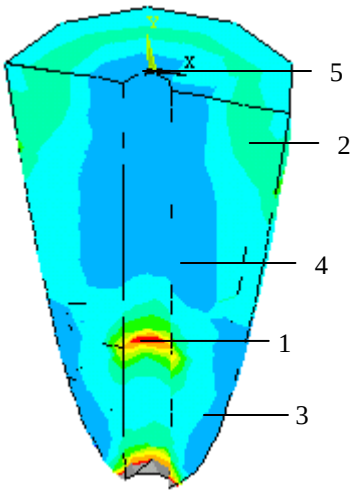

(a) With lowest elastic modulus core

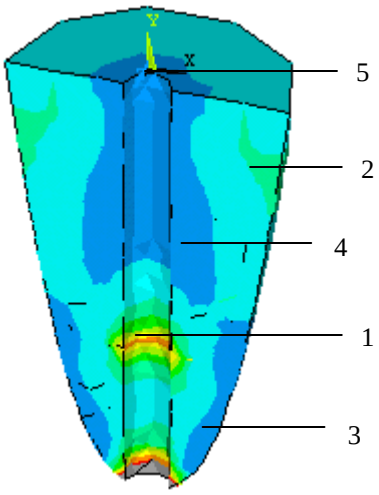

(b) With middle elastic modulus core

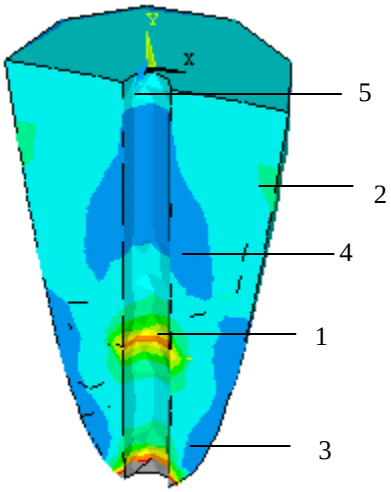

(c) With highest elastic modulus core

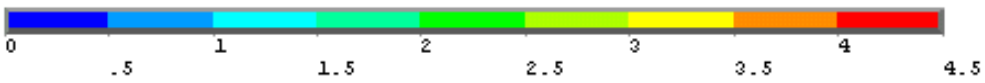

Figure 3.9. Stress distributions in dentin of a restored tooth with a stainless steel post and three different core materials under a vertical load (MPa).

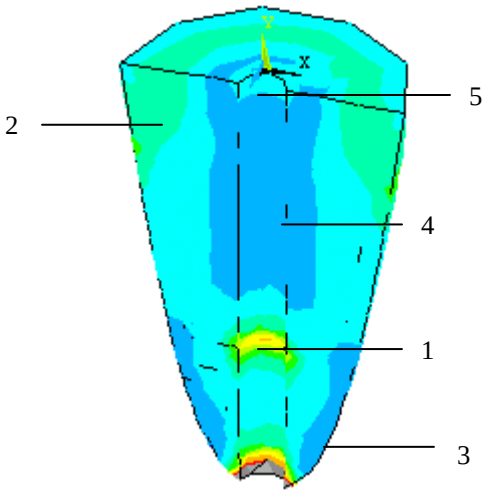

(a) With lowest elastic modulus core

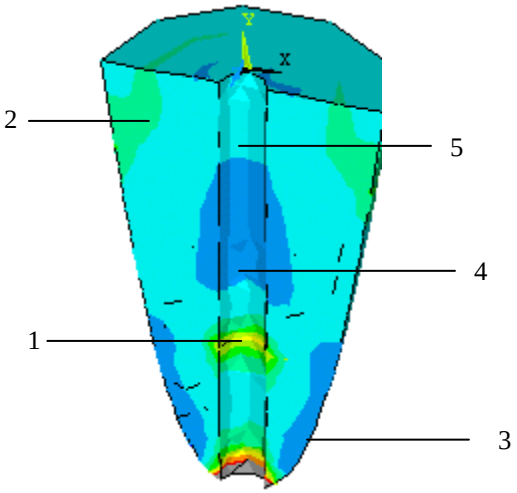

(b) With middle elastic modulus core

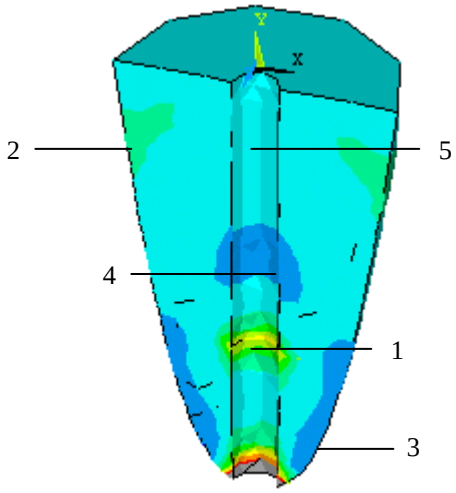

(c) With highest elastic modulus core

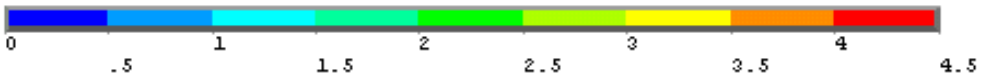

Figure 3.10 Stress distributions in dentin of a restored tooth with a titanium post and three core materials under a vertical load (MPa).

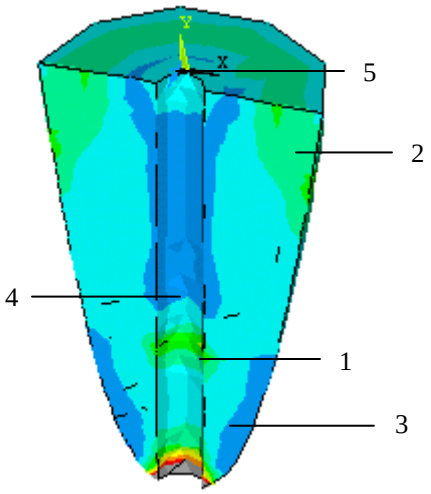

(a) With low elastic modulus core material

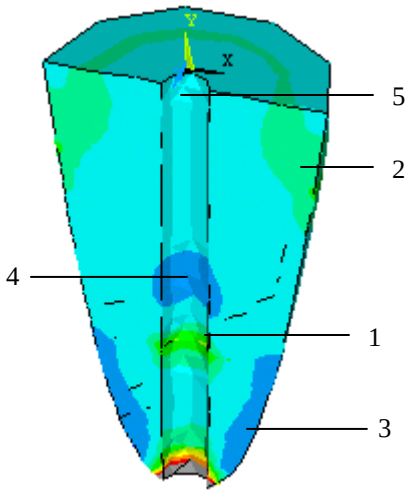

(b) With middle elastic modulus core material

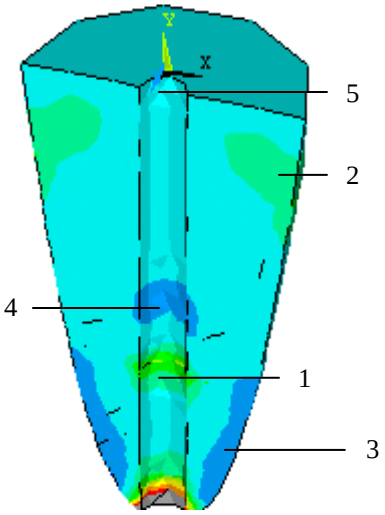

(c) With high elastic modulus core material

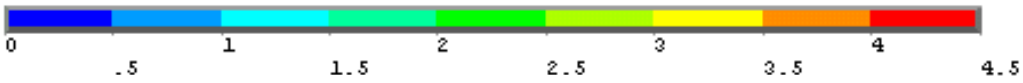

Figure 3.11. Stress distributions in dentin of a restored tooth with a ceramic post and three core materials and under a vertical load (MPa).

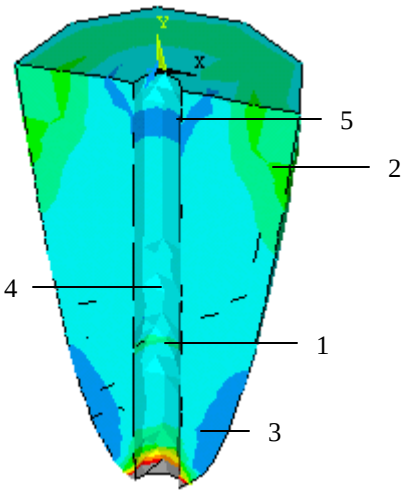

(a) With low elastic modulus core material

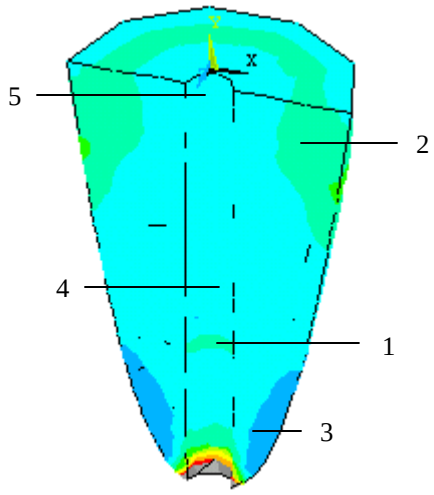

(b) With middle elastic modulus core material

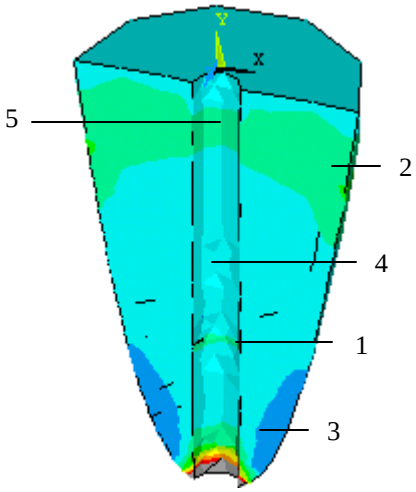

(c) With high elastic modulus core material

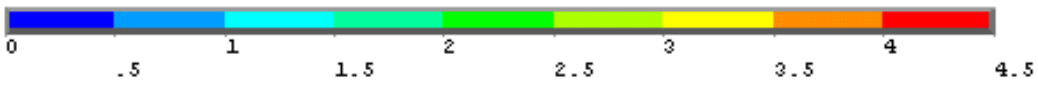

Figure 3.12. Stress distributions in dentin of a restored tooth with a FRC post and three core materials and under a vertical load (MPa).

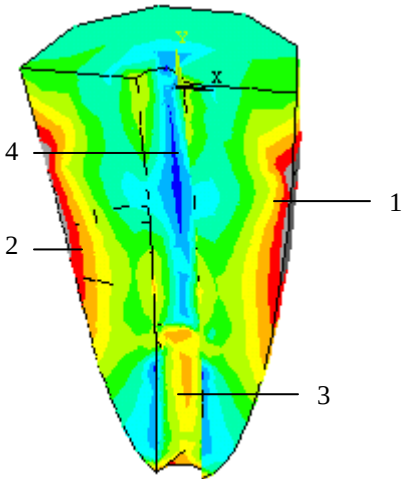

(a) With lowest elastic modulus core

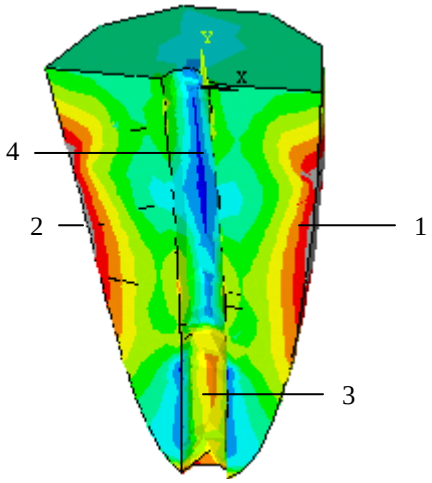

(b) With middle elastic modulus core

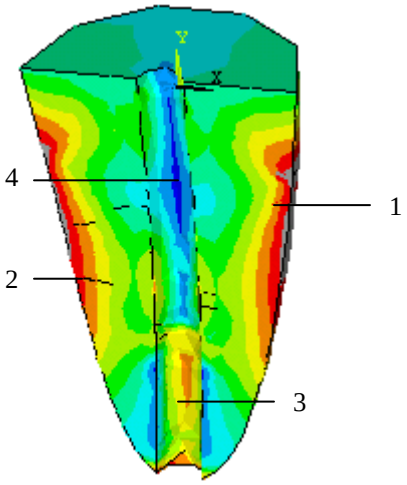

(c) With highest elastic modulus core

Figure 3.13 Stress distributions in dentin of a restored tooth with a stainless steel post and three core materials and under a horizontal load (MPa).

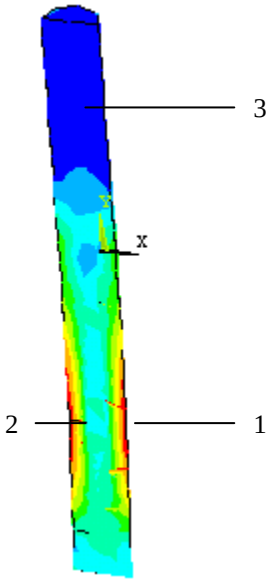

(a) With lowest elastic modulus core

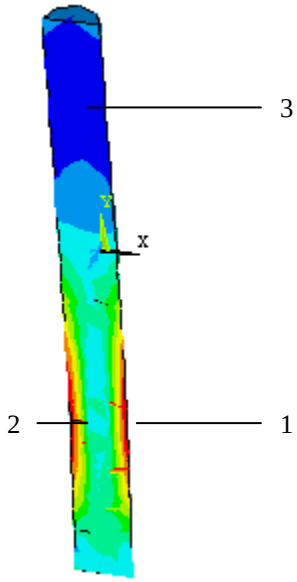

(b) With middle elastic modulus core

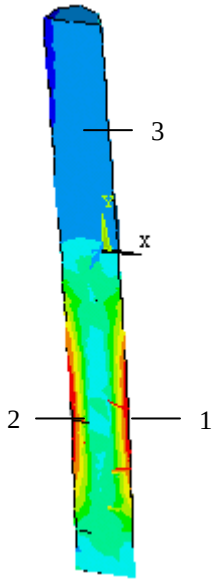

(c) With highest elastic modulus core

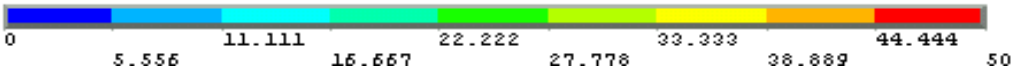

Figure 3.14 Stress distributions in the post of a restored tooth with a stainless steel post and three core materials and under a horizontal load (MPa).

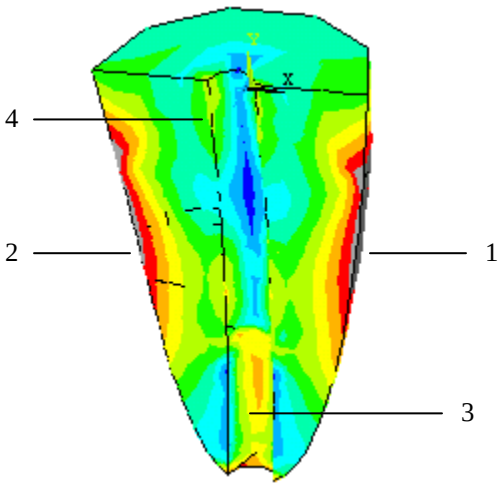

(a) With lowest elastic modulus core

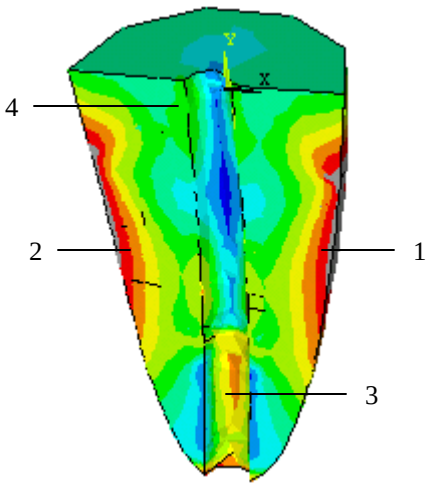

(b) With middle elastic modulus core

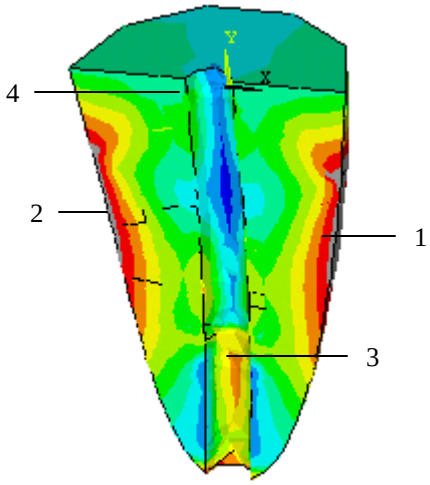

(c) With highest elastic modulus core

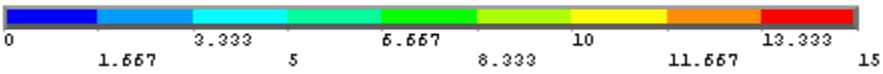

Figure 3.15. Stress distributions in dentin of a restored tooth with a titanium post and three core materials and under a horizontal load (MPa).

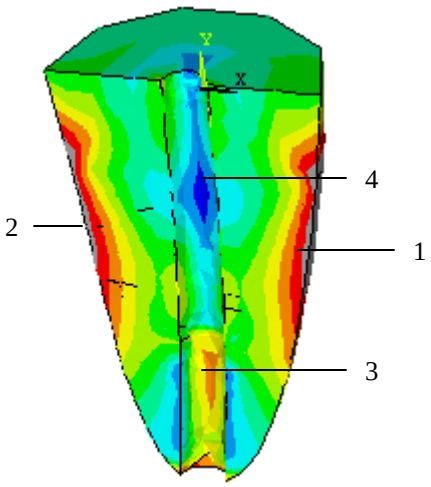

(a) With lowest elastic modulus core

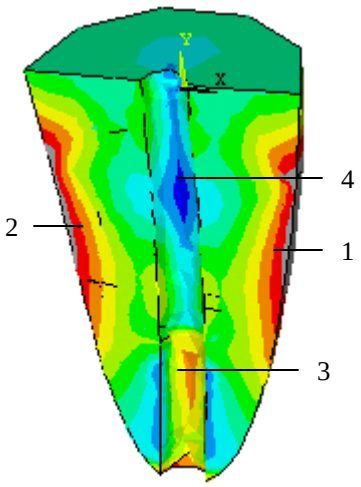

(b) With middle elastic modulus core

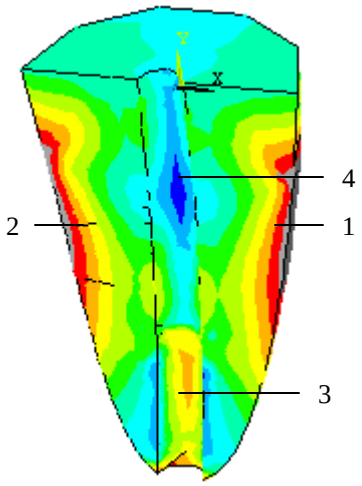

(c) With highest elastic modulus core

Figure 3.16 Stress distributions in dentin of a restored tooth with a ceramic post and three core materials and under a horizontal load (MPa).

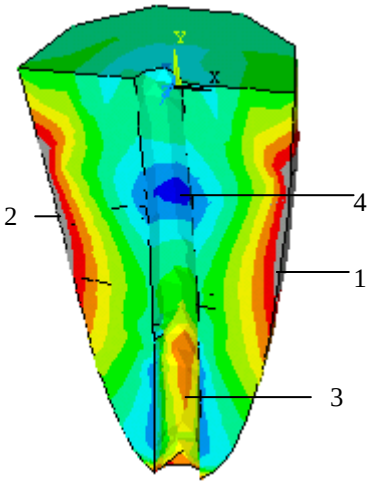

(a) With lowest elastic modulus core

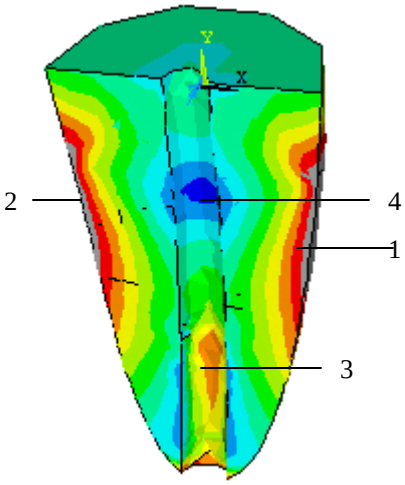

(b) With middle elastic modulus core

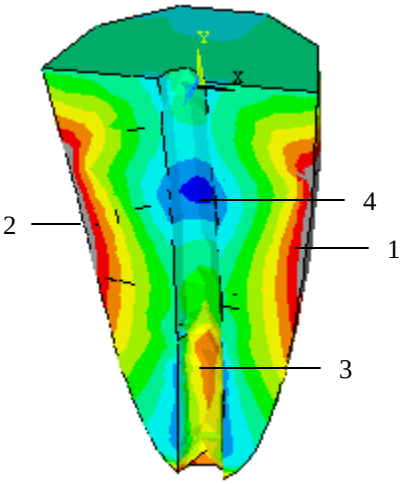

(c) With highest elastic modulus core

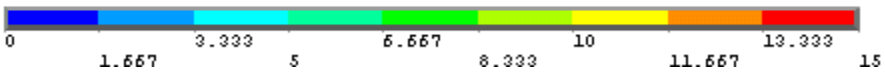

Figure 3.17 Stress distributions in dentin of a restored tooth with a FRC post and three different core materials and under a horizontal load (MPa).

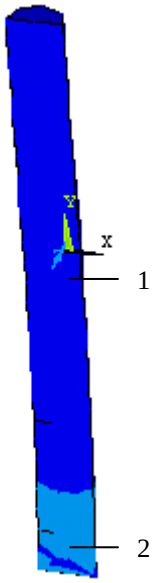

(a) With lowest elastic modulus core

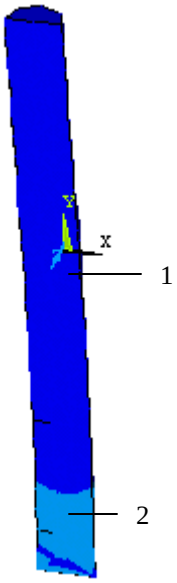

(b) With middle elastic modulus core

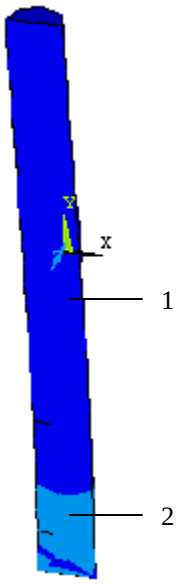

(c) With highest elastic modulus core

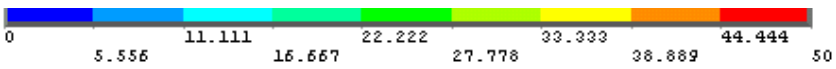

Figure 3.18 Stress distributions in FRC post with three different core materials under a horizontal load (MPa).

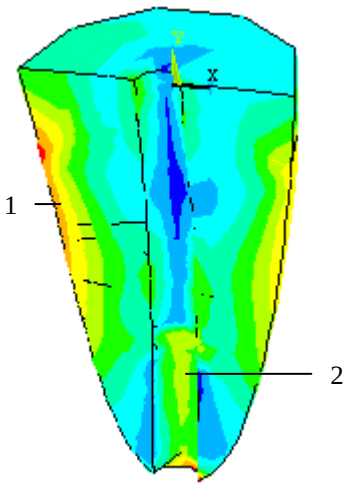

(a) With lowest elastic modulus core

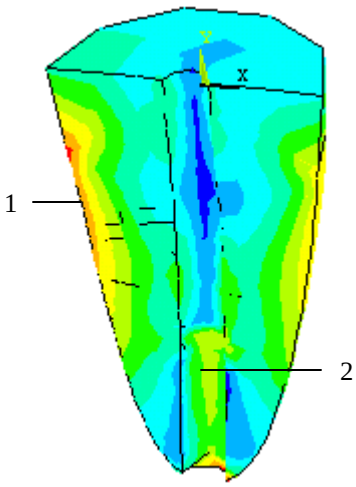

(b) With middle elastic modulus core

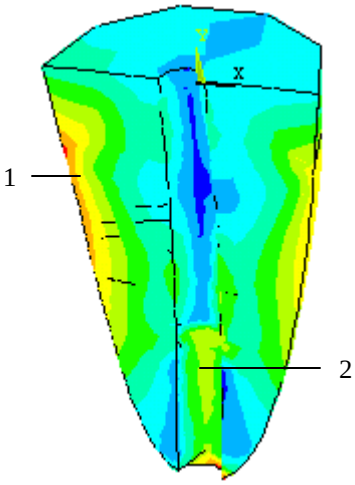

(c) With highest elastic modulus core

Figure 3.19 Stress distributions in dentin of a restored tooth with a stainless steel post and three core materials and under an oblique load (MPa).

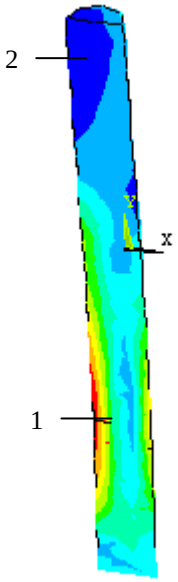

(a) With lowest elastic modulus core

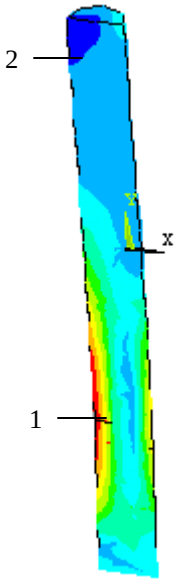

(b) With middle elastic modulus core

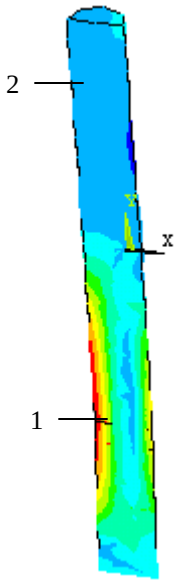

(c) With highest elastic modulus core

Figure 3.20 Stress distributions in post of a tooth restored with a stainless steel post and three core materials under an oblique load (MPa).

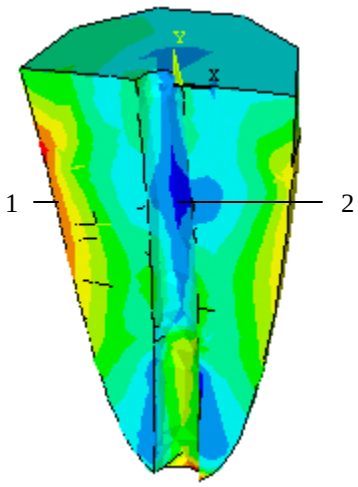

(a) With lowest elastic modulus core

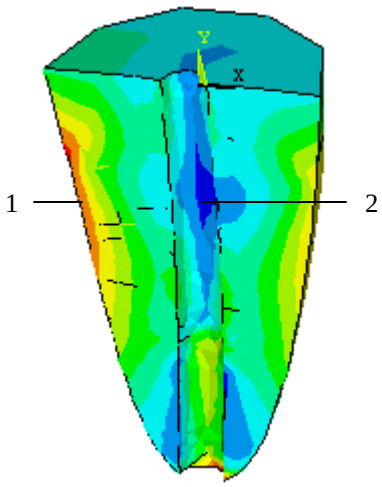

(b) With middle elastic modulus core

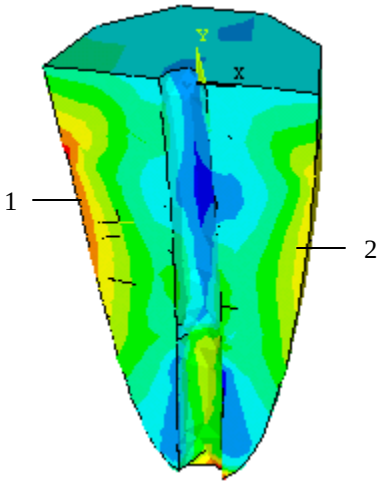

(c) With a highest elastic modulus core

Figure 3.21 Stress distributions in dentin of a restored tooth with ceramic post and three core materials and under an oblique load (MPa).

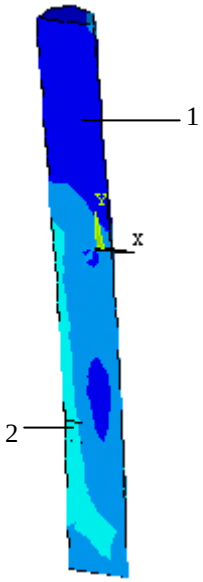

(a) With a lowest elastic modulus core

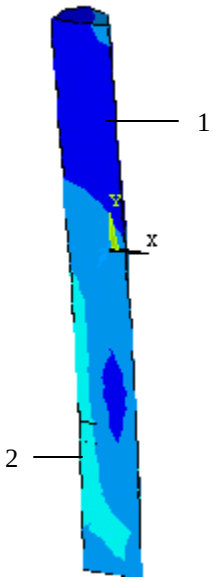

(b) With a middle elastic modulus core

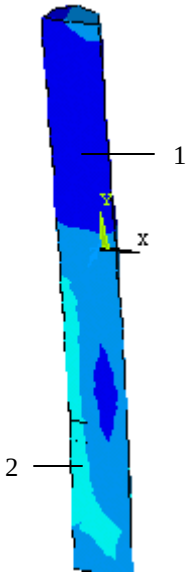

(c) With a highest elastic modulus core

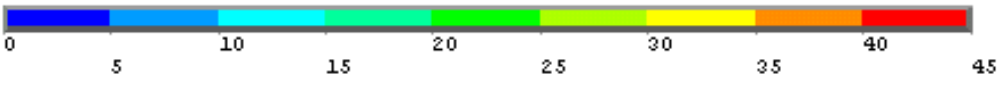

Figure 3.22 Stress distributions in the post of a restored tooth with ceramic post and three core materials and under an oblique load (MPa).

Even though stress distribution is mostly influenced by the loading direction, different combinations result in different stress distribution in dentin under vertical loading. Before a combination of post and core is used, stress distribution created by it should be studied.

3.2.5 Summary

The stresses in dentin and posts have been evaluated and compared when each of four different post materials is combined with three different cores. Three types of loading have been applied, namely a vertical, a horizontal and an oblique loading. The maximum Von Mises stresses in dentin are summarized in Graph 3.3. Under the vertical load, when the elastic modulus of the core is similar to that of the post and dentin, the stress distribution is the most uniform. When the elastic modulus of the post, the core and

(a) Highest stress in dentin with a stainless steel post

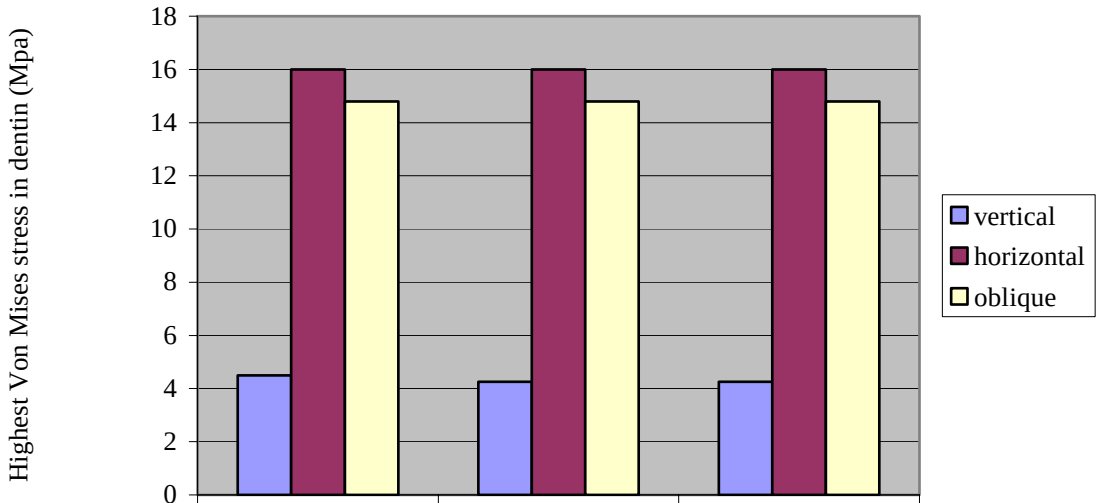

	core1 (E=5.0GPa)	core2 (E=16.6GPa)	core3 (E=52GPa)
vertical	4.5	4.25	4.25
horizontal	16	16	16
oblique	14.8	14.8	14.8

Different core materials

(b) Highest stress in dentin with a titanium post

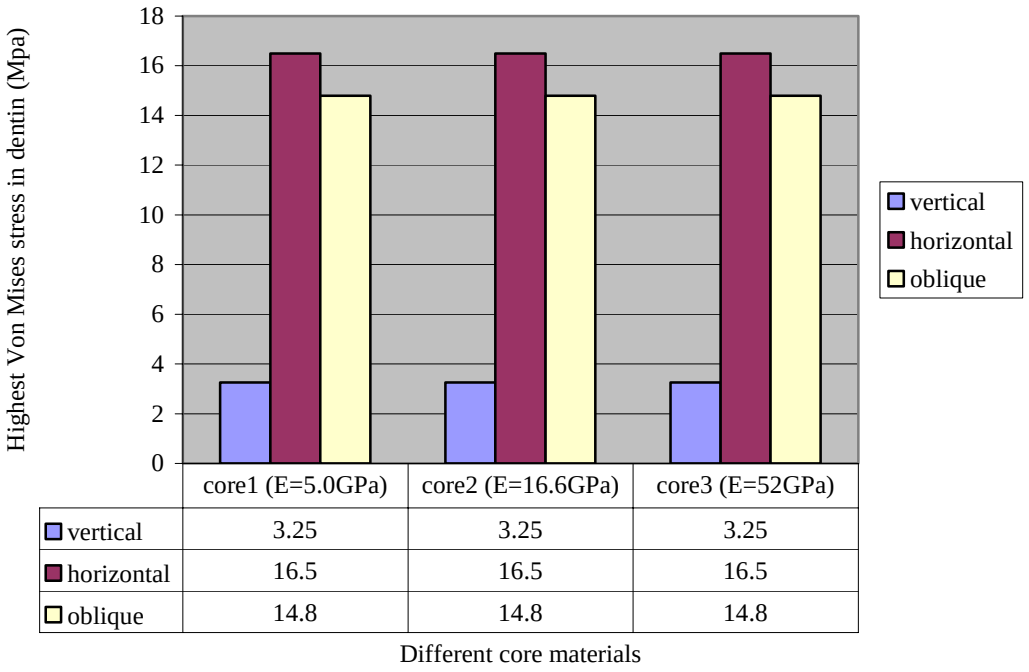

	core1 (E=5.0GPa)	core2 (E=16.6GPa)	core3 (E=52GPa)
vertical	3.25	3.25	3.25
horizontal	16.5	16.5	16.5
oblique	14.8	14.8	14.8

(c)Highest stress in dentin with a ceramic post

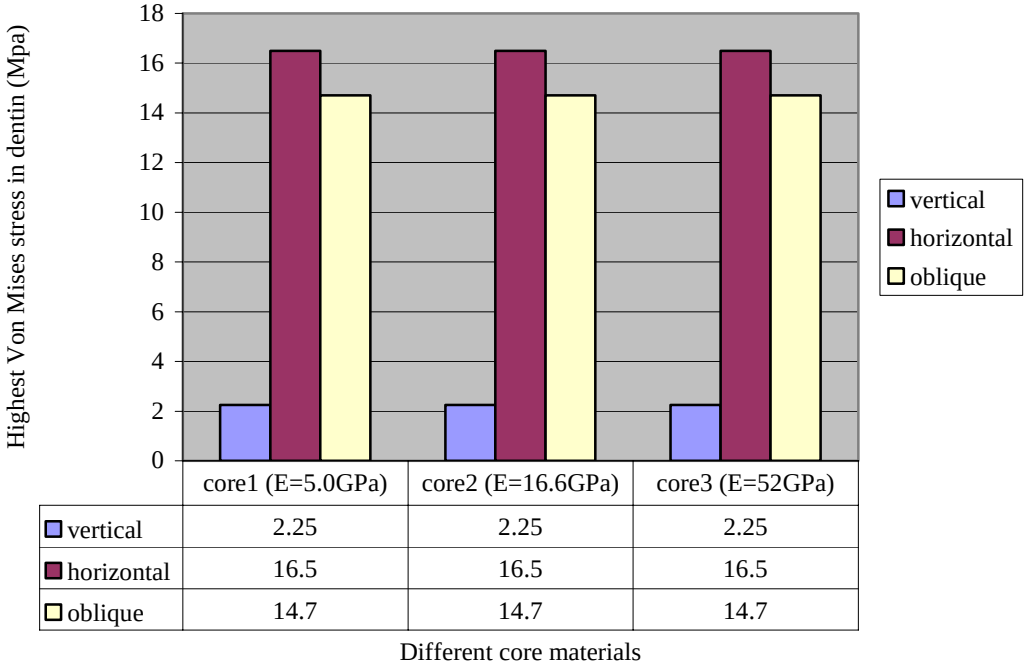

	core1 (E=5.0GPa)	core2 (E=16.6GPa)	core3 (E=52GPa)
vertical	2.25	2.25	2.25
horizontal	16.5	16.5	16.5
oblique	14.7	14.7	14.7

(d) Highest stress in dentin with a FRC post

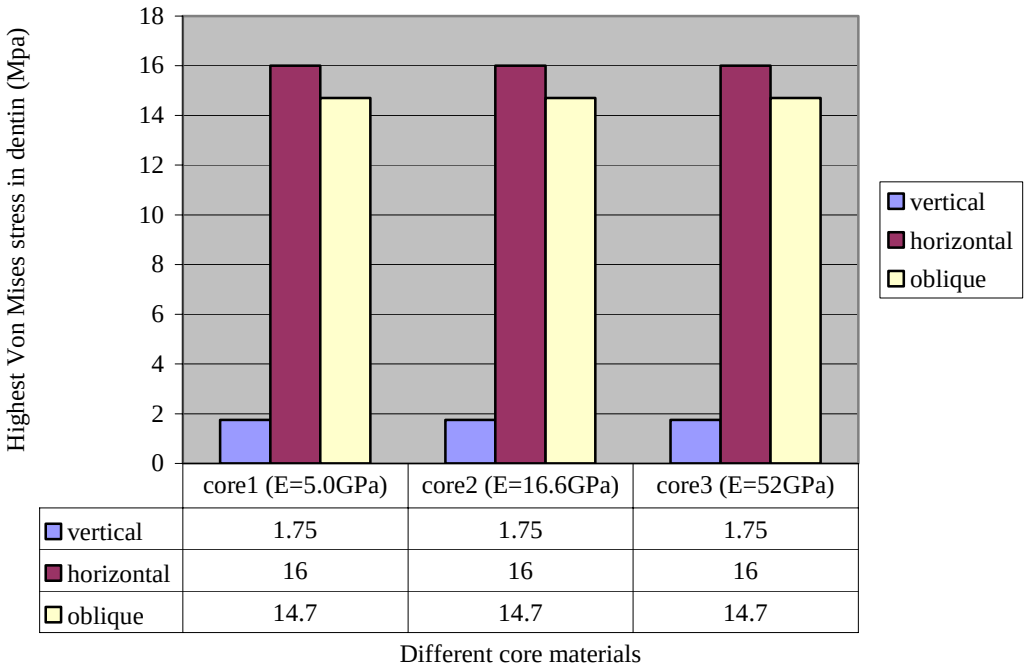

	core1 (E=5.0GPa)	core2 (E=16.6GPa)	core3 (E=52GPa)
vertical	1.75	1.75	1.75
horizontal	16	16	16
oblique	14.7	14.7	14.7

Graph 3.3 Maximum stresses in dentin with different combinations of the post and the core.

dentin are very different, the stresses at the apical portion of the root and at the dentin shoulder are high. Low stresses at the apical portion of the root and dentin shoulder will reduce the probability of fracture. Under horizontal and oblique loading, the stress distributions in dentin are similar. Thus, changing the core materials has very little effect on stress distributions under horizontal and oblique loading.

3.3 Simulation Three: Effect of Cervical Dental Loss

The effects of the dentin loss at cervical region on the stress distributions in dentin are evaluated in this study. Stainless steel post is used. The elastic modulus of the post, core material is 200GPa and 16.6GPa respectively. To simplify the model, the dentin loss is

assumed to be continuous along the circle of the cervical opening of the root canal. Three types of dentin loss, which are viewed in the sectional plane passing through the vertical axis, are: L-shape (Figure 3.23), U-shape (Figure 3.24), and V-shape (Figure 3.25). Except for the model without dentin loss, the width at the top of the canal is always 2.5mm. The depth of the dentin loss is 0.5mm, 1.0mm, and 2.0mm.

3.3.1 Vertical loading

The stresses in different regions of dentin due to the cervical dentin loss under vertical loading are shown in Table 3.3. Figure 3.26 shows the stress distribution in dentin with the L-shape dentin loss under vertical load. Without the dentin loss, the highest stress is located at the apical portion of the post (shown as region 1 in Figure 3.26a) with the value of 4.5MPa. Stress observed under the dentin shoulder, shown as region 2 in Figure 3.24a, is 1.75MPa. The stress located along the canal and at the apical portion of the root (shown as regions 4 and 3 in Figure 3.26a) is 0.75MPa. The remainder shows uniformly distributed stress at a value of 1.25MPa. With the L-shape dentin loss at the 0.5mm depth, the highest stress is located at the apical portion of the post (shown as 1 in Figure 3.26b), which is about 4.5MPa. At the shoulder of dentin, shown as region 2 in Figure 3.26b, the stress is observed at value of 1.75MPa. The lowest stress are observed at region 3 and 4 in Figure 3.26b, which are along the canal and the apical portion of the root, and the values are 0.75MPa. The stress at the cervical region (region 5 in Figure 3.26b) is about 1.75MPa. The remainder of the dentin shows uniformly distributed stress at value of 1.25MPa. The stress distribution in dentin with a 0.5mm depth is almost identical to the

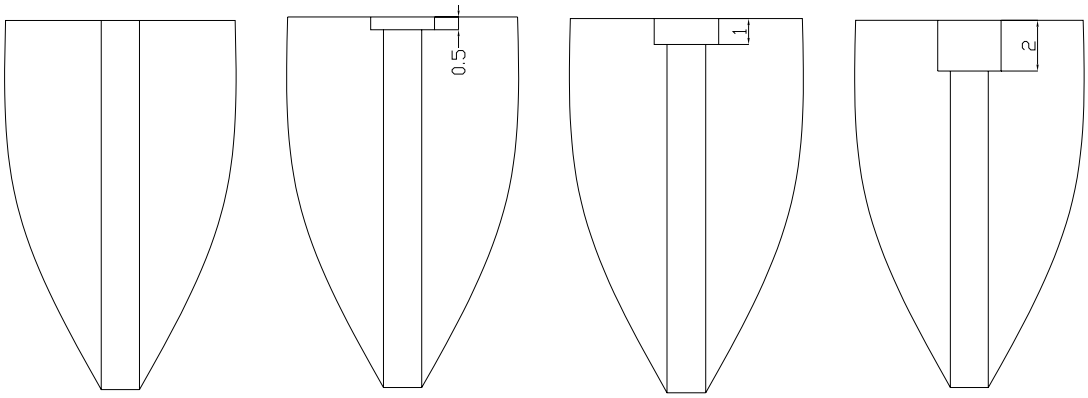

(a) No dentin loss (b) 0.5mm depth (c) 1.0mm depth (d) 2.0mm depth

Figure 3.23. Diagram of dentin with the L-shape dentin loss at different depth.

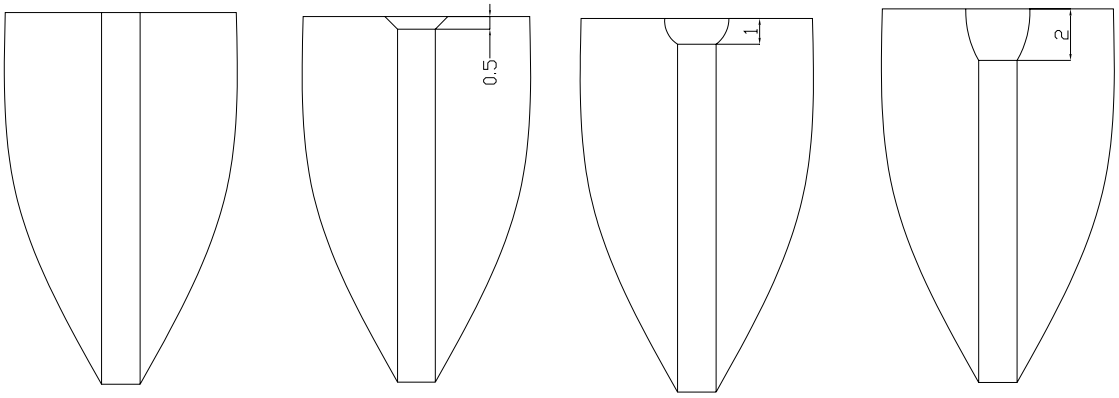

(a) No dentin loss (b) 0.5mm depth (c) 1.0mm depth (d) 2.0mm depth

Figure 3.24. Diagram of dentin with the U-shape dentin loss at different depth.

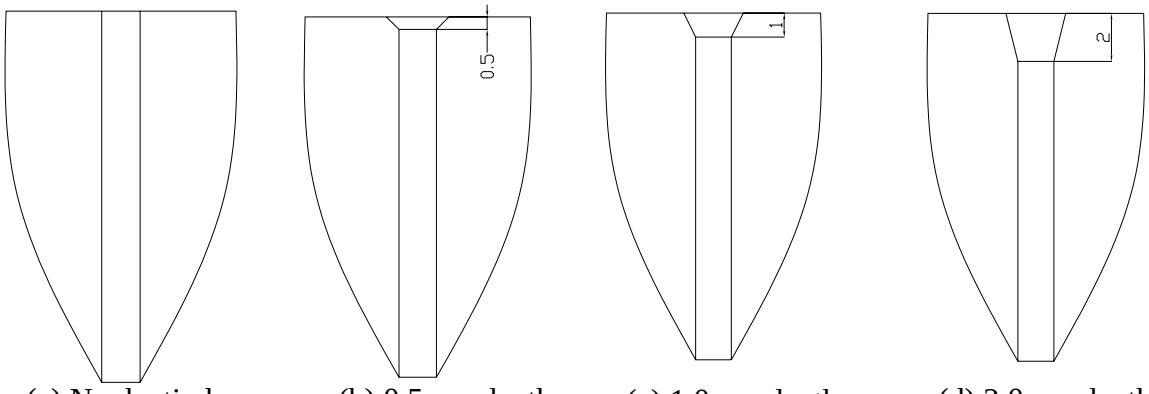

(a) No dentin loss (b) 0.5mm depth (c) 1.0mm depth (d) 2.0mm depth

Figure 3.25. Diagram of dentin with the V-shape dentin loss at different depth.

one without dentin loss except for the cervical region. With 1.0mm depth, the highest stress at the apical portion of the post (shown as region 1 in Figure 3.26c) is 4.25MPa, which is 15% lower than that without dentin loss. Under the dentin shoulder (region 2 in Figure 3.26c), the stress is 1.75MPa. The stresses in regions 3 and 4 are 0.75MPa. Along the cervical area (shown as region 5 in Figure 3.26c), the stress value is 1.25MPa, which is 29% lower than that without dentin loss. With a dentin loss of 2mm depth, the maximum stress at the apical portion of the post (shown as 1 in Figure 3.26d) reduces 25% (3.75MPa) compared to that without dentin loss. At the bottom of dentin loss (shown as region 5 in Figure 3.26d), the stress is about 1.75MPa, which is the same as that of 0.5mm depth. Stress in the other areas has a similar pattern to that without dentin loss. The stress under the dentin shoulder (region 2 in Figure 3.26d) is 1.75MPa. The stresses at region 3 and 4 in Figure 3.26d are 0.75MPa.

Figure 3.27 shows the stress distributions in dentin with U-shape dentin loss of various depths under vertical loading. The stress distribution without dentin loss is shown in Figure 3.26a. With the gap depth of 0.5mm, the highest stress is observed at the apical portion of the root (shown as region 1 in Figure 3.27a) with a value of 4.25MPa, which is 15% lower than the one without dentin loss. At the dentin shoulder (shown at region 2 in Figure 3.27a), a high stress is observed at the value of 1.75MPa. At the top ring of the cervical opening (shown as region 5 in Figure 3.27a), a high stress is observed at value of 1.75MPa. The lowest stresses appear along the root canal and at the bottom portion of the dentin (shown as region 3 and 4 in Figure 3.27a) with value of 0.75MPa. In the rest of the dentin, the stress is uniformly distributed at value of 1.25MPa. With the gap depth of

1.00mm, stress pattern is very similar to that of the gap length of 0.5mm. However, the stress at the coronal dentin, shown as region 5 in Figure 3.27b, decrease to 1.25Mpa, which is 28% lower than that of 0.5mm dentin loss. The stresses in region 1, 2, 3, and 4 are 4.25MPa, 1.75MPa, 0.75MPa, and 0.75MPa respectively. With the depth of 2.0mm, the highest stress appears at the apical portion of the root (shown as 1 in Figure 3.27c) with the value of 4.25MPa. At the cervical region (shown as region 5 in Figure 3.27c), the stress value is 1.25MPa, which is 29% lower than that caused by L-shape. The stresses in regions 2, 3, 4 are 1.75MPa, 0.75MPa, and 0.75MPa respectively.

Figure 3.28 shows the stress distribution in dentin with V-shape dentin loss under the vertical load. Highest stresses for the three cases are located at the apical portion of the post (region 1 in Figure3.28), and the values are 4.25MPa, 4.25MPa, and 3.75MPa respectively. The stresses in region 2, 3, and 4 are 1.75MPa, 0.75MPa, and 0.75MPa respectively. With the increase of the depth, the area of high stress at the cervical region increases (shown as region 5 in Figure 3.28). The stress at the cervical area is similar to that of the U-shape.

The results show that regardless of the type of dentin loss as shown in Figures 3.23 to 3.25, the depth of 2.0mm of the gap slightly reduces the stresses at the apical portion of the root. However, the dentin loss causes an increase in stresses at the cervical region (shown as region 5 in Figures 3.26-3.28). The magnitude of the stresses in other regions is not affected.

Table 3.3 Stresses in different regions due to the cervical dentin loss under vertical loading

Dentin loss shape	Depth (mm)	Region 1 (MPa)	Region 2 (MPa)	Region 3 (MPa)	Region 4 (MPa)	Region 5 (MPa)
No loss	0.0	4.25	1.75	0.75	0.75	0.75
L-shape	0.5	4.5	1.75	0.75	0.75	1.75
	1.0	4.25	1.75	0.75	0.75	1.25
	2.0	3.75	1.75	0.75	0.75	1.75
U-shape	0.5	4.25	1.75	0.75	0.75	1.75
	1.0	4.25	1.75	0.75	0.75	1.25
	2.0	4.25	1.75	0.75	0.75	1.25
V-shape	0.5	4.25	1.75	0.75	0.75	1.25
	1.0	4.25	1.75	0.75	0.75	1.25
	2.0	3.75	1.75	0.75	0.75	1.25

3.3.2 Horizontal load

Figure 3.29 shows the stress distributions of the dentin with L-shape dentin loss of different depths. The stresses at the bottom of dentin loss (shown as 1 in Figure 3.29) are high with the values of 11MPa, 13MPa, and 15MPa, corresponding to the depth of 0.5mm, 1mm, and 2mm. The stress distributions have a similar pattern in all three cases. The high stresses also appear at both sides of the dentin (shown as 2 and 3 in Figure 3.29), which is 13.0MPa. Stresses appear high along the centerline of dentin apex, which is about 11.0MPa (shown as 4 in Figure3.29). The lowest stress is located along the centreline of the canal (shown as 5 in Figure 3.29), which is about 1.0MPa. The deeper dentin loss causes higher stress at the interface between the post and dentin at the cervical region.

Figure 3.30 shows the stress distribution in dentin with U-shape dentin loss. Stress distributions for all three cases are similar. High stress is located at the two sides of the dentin (shown as region 1 and 2 in Figure 3.30), and is about 13.6MPa. High stress is also observed at the centreline of dentin apex (region 4 in Figure 3.30), which is about 10.4MPa. The stress concentrates at the interface between the dentin and post at the cervical region (region 3 in Figure 3.30), which is about 12.0MPa. The lowest stress is located along the centreline of the canal (shown as 5 in Figure 3.30), which is about 1.0MPa.

Figure 3.31 shows the stress distribution in dentin, which has V-shape dentin loss. For the three different depths, the greatest stress is at both sides of the dentin (shown as region 1 and 2 in Figure 3.31), and is 13.6MPa. The lowest stress appears along the centreline of the upper half of the canal (region 5 in Figure3.31), which is 0.8MPa. High stress is also observed at the interface between the post and dentin at the cervical region (shown as region 3 in Figure 3.31). The values are 10.4MPa, 12.0MPa, and 12.0MPa respectively. With the increase of the depth, the stress increases at the interface. High stress is also observed at the centreline of dentin apex (region 4 in Figure 3.31), which is about 10.4MPa. V-shape dentin loss causes the least stress concentration at the interface comparing to other shapes, and yields the best results under the horizontal loading.

3.3.3 Oblique loading

Figure 3.32 shows the stress distribution of the dentin with different amounts of U-shape dentin loss. Under oblique loading, the stress distribution is similar for all three amounts

of dentin loss. The highest stress is located at the one side of the dentin (shown as region 1 in the Figure 3.32), and is 12.8MPa. Other side of the dentin (region 2 in Figure 3.32) has lower stress, and is 11.1MPa. High stress appears at the interface between the post and dentin at the cervical region (shown as region 3 in Figure3.32), which is about 11.1MPa. High stress is also observed at the centreline of dentin apex (region 4 in Figure 3.32), which is about 9.4MPa. Lowest stress is observed along the upper half of the canal (region 5 in Figure 3.32), and the value is 0.9MPa. The results show that no significant stress concentration appears at the interface.

3.3.4 Discussion

The U-shape and V-shape show the best results. No obvious high stress at the bottom of the gap. U-shape and V-shape have smoother surface along the dentin canal comparing to that of the L-shape. L-shape shows high stress at the bottom of the gap.

For the L-shape under vertical loading, the size of high stress area is parallel with the depth of the gap. With the increase of the gap depth, the area of high stress at the bottom of the gap increase.

Under horizontal loading, the gap with L-shape is also the worst case. The stress at the bottom of the gap is much higher than the stress value with U-shape and V-shape. Notches and gapes should be avoided because high stress concentrations were observed in this research in that area.

3.3.5 Summary

The maximum von Mises stress in dentin are summarized in Graph 3.4. The effects of dentin loss between post and dentin at the cervical region on the stress distributions in dentin are evaluated in this study. Three types of dentin loss, L-shape, U-shape and V-shape, with the depth of 2.0mm, 1.5mm, and 0.5mm are considered. In the sectional view, the width at the top of all gaps is 0.5mm. The same three types of loading are applied. It was found that horizontal loading causes the higher stress concentrations than other types of loading. The L-shape gap always results in the highest stress concentration at the apical portion of the root and at the bottom of the dentin loss. The U-shape and V-shape dentin loss both show low stress concentrations regardless of the loading. The stresses are not sensitive to the shape of dentin loss when a horizontal or oblique load is applied. For vertical loading, the high stresses at the apical portion of the post and the bottom of the dentin loss decrease as the increase of the depth. Overall, the sharp angle and notch, which can cause stress concentration, should be avoided in tooth restoration.

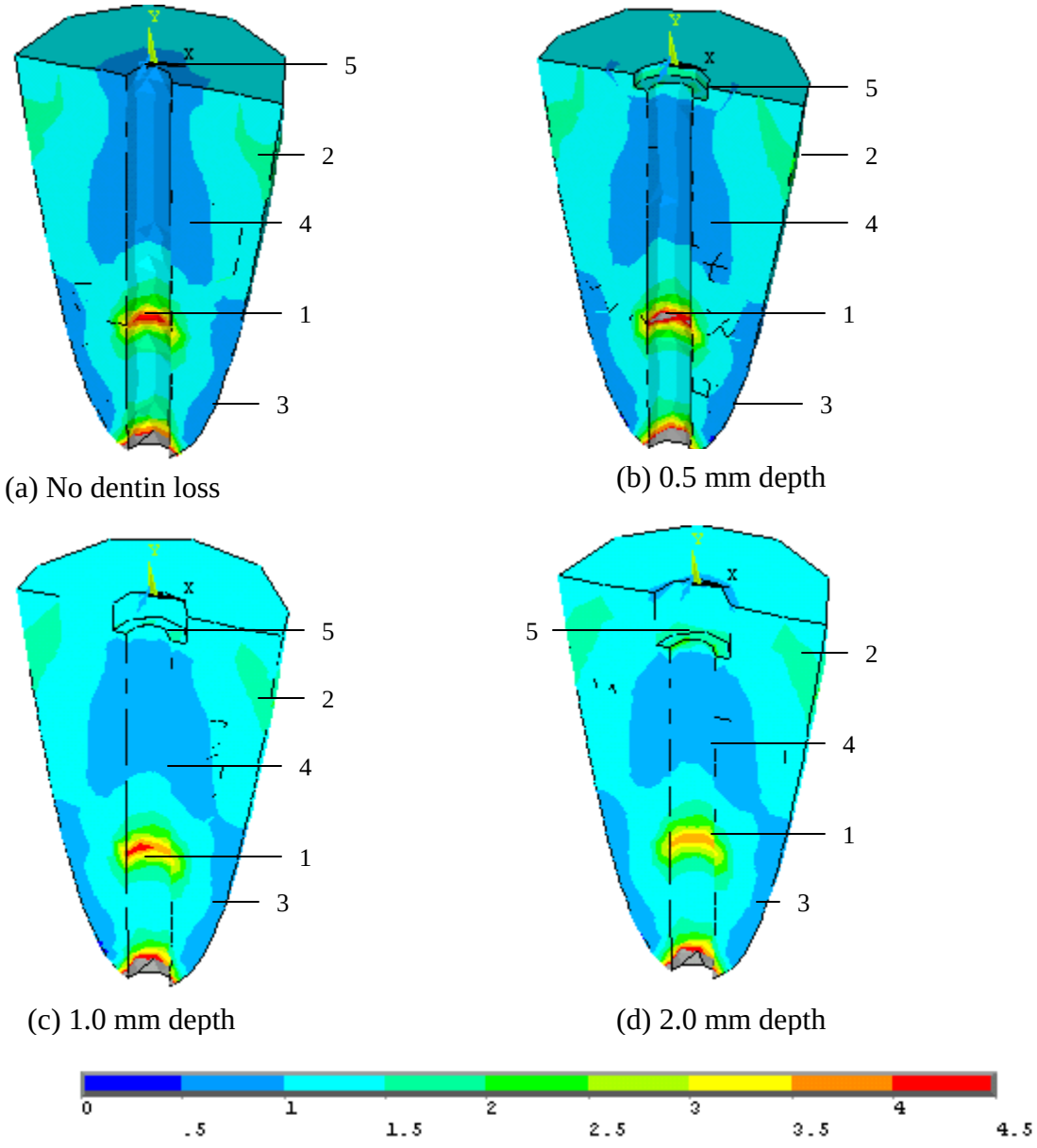

Figure 3.26 Stress distributions in dentin of a restored tooth with the L-shape dentin loss and under a vertical load (MPa).

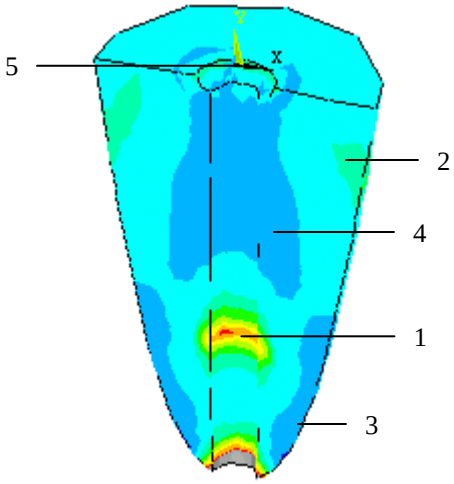

(a) With 0.5 mm depth

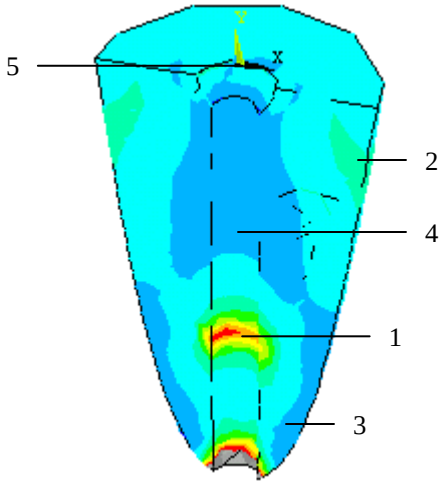

(b) With 1.0 mm depth

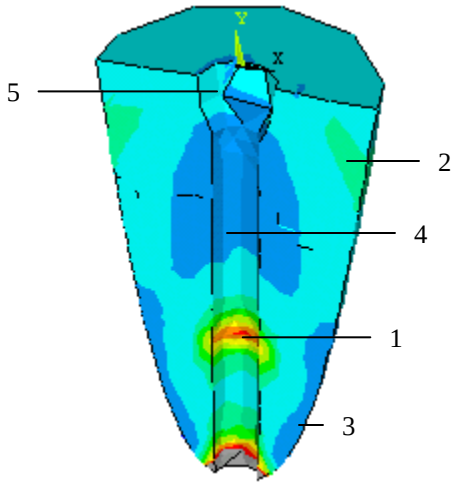

(c) With 2.0 mm depth

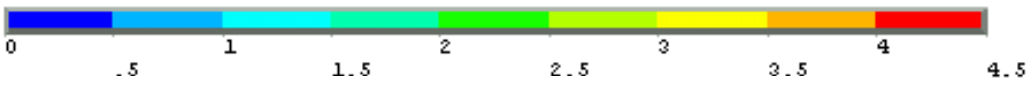

Figure 3.27 Stress distributions in dentin of a restored tooth with the U-shape dentin loss and under a vertical load (MPa).

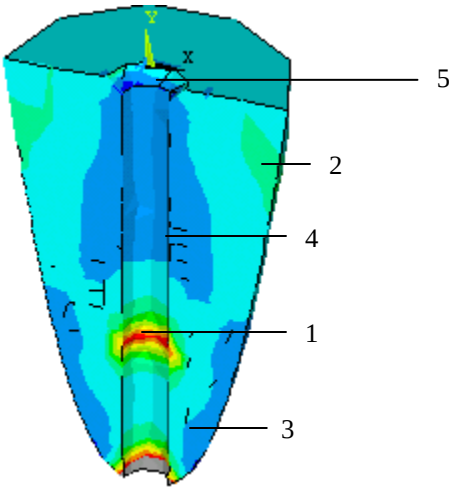

(a) With 0.5 mm depth

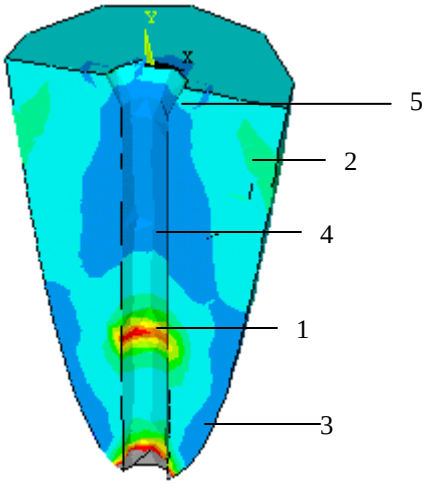

(b) With 1.0 mm depth

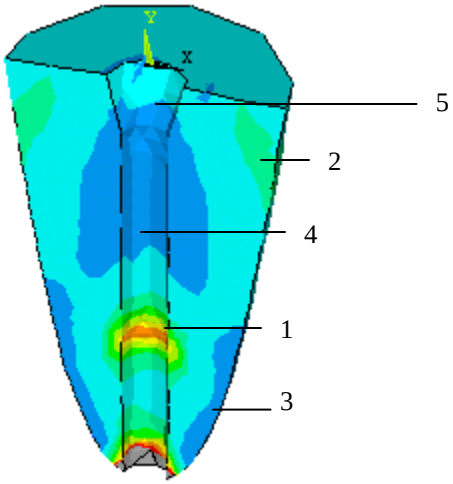

(c) With 2.0 mm depth

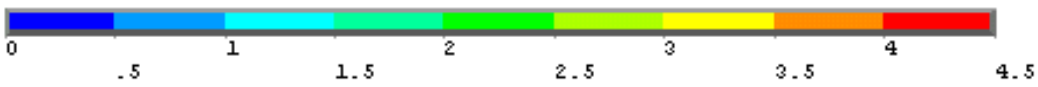

Figure 3.28 Stress distributions in dentin of a restored tooth with the V-shape dentin loss and under a vertical load (MPa).

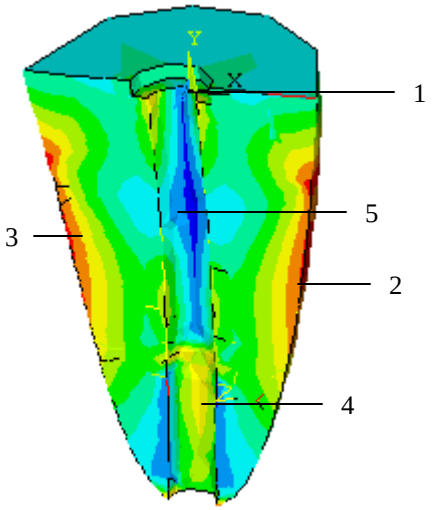

(a) With 0.5 mm depth

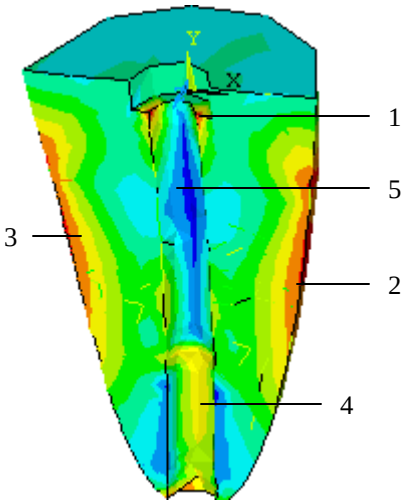

(b) With 1.0 mm depth

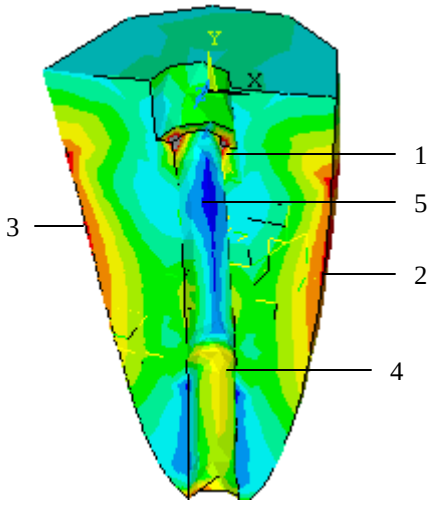

(c) With 2.0 mm depth

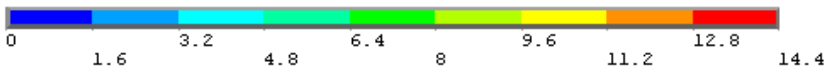

Figure 3.29 Stress distributions in dentin of a restored tooth with the L-shape dentin loss and under a horizontal load (MPa).

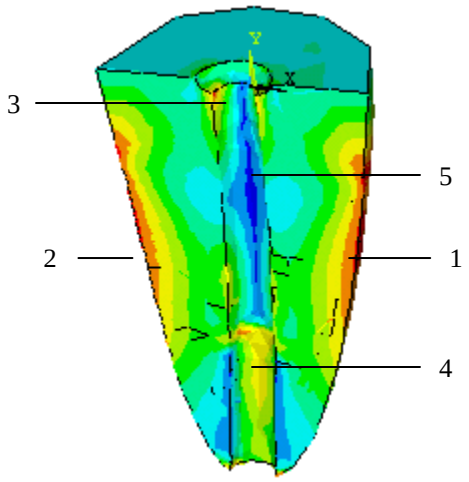

(a) With 0.5 mm depth

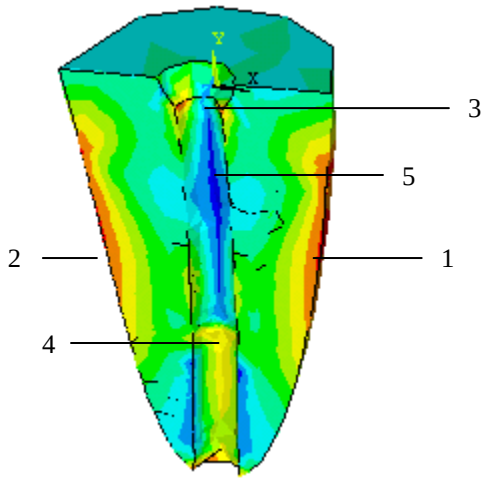

(b) With 1.0 mm depth

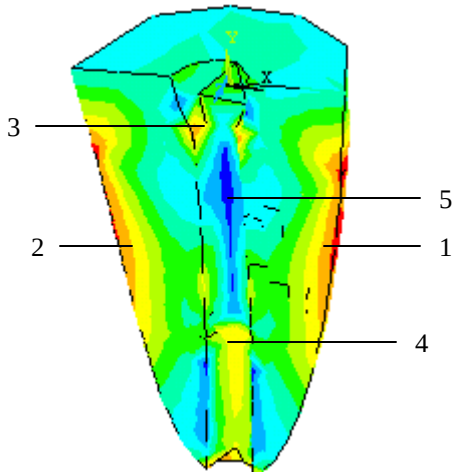

(c) With 2.0 mm depth

Figure 3.30 Stress distributions in dentin of a restored tooth with the U-shape dentin loss and under a horizontal load (MPa).

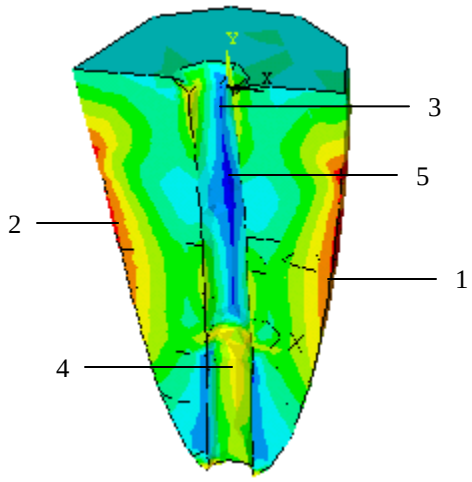

(a) With 0.5 mm depth

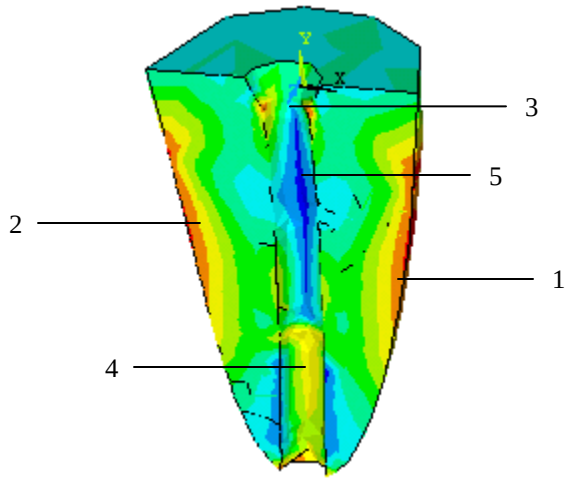

(b) With 1.0 mm depth

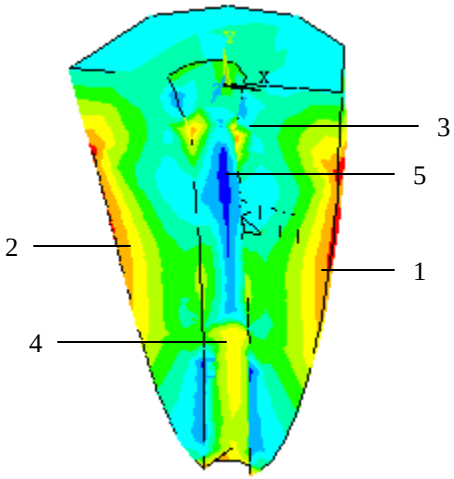

(c) With 2.0 depth

Figure 3.31 Stress distributions in dentin of a restored tooth with the V-shape dentin loss and under a horizontal load (MPa).

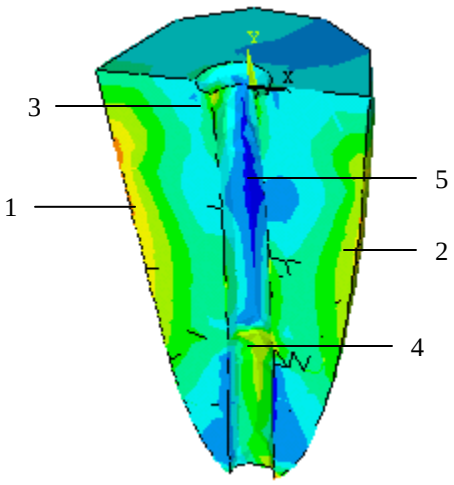

(a) With 0.5 mm depth

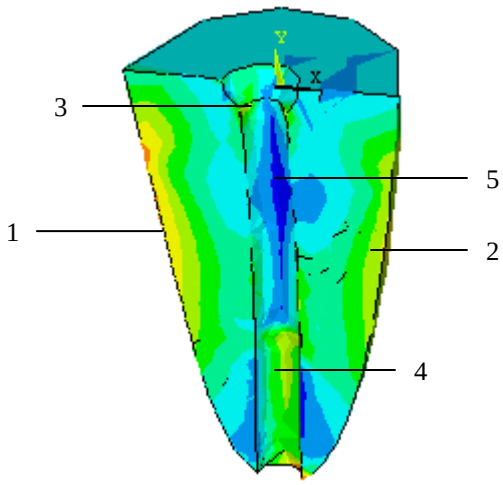

(b) With 1.0 mm depth

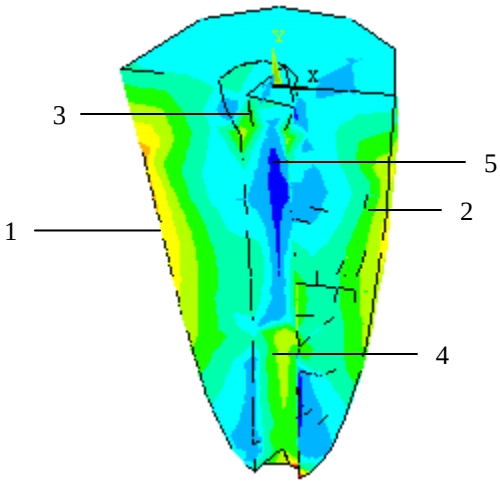

(c) With 2.0 mm depth

Figure 3.32 Stress distributions in dentin of a restored tooth with the U-shape dentin loss and under an oblique load (MPa).

(a) Highest stress in dentin with different dentin loss under vertical loading

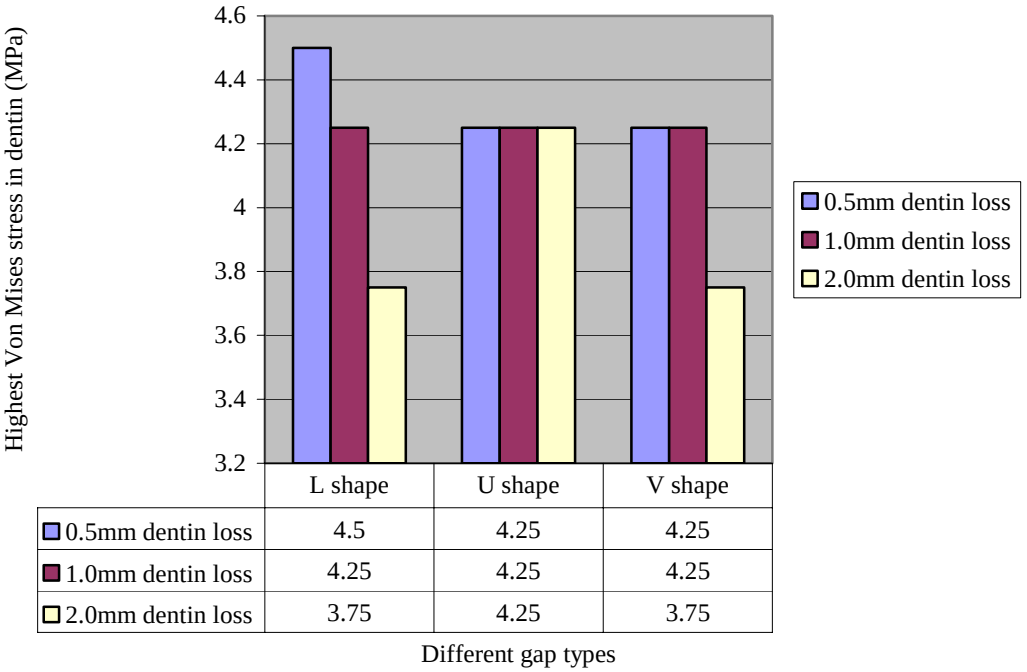

	L shape	U shape	V shape
0.5mm dentin loss	4.5	4.25	4.25
1.0mm dentin loss	4.25	4.25	4.25
2.0mm dentin loss	3.75	4.25	3.75

(b) Highest stress in dentin with different dentin loss under horizontal loading

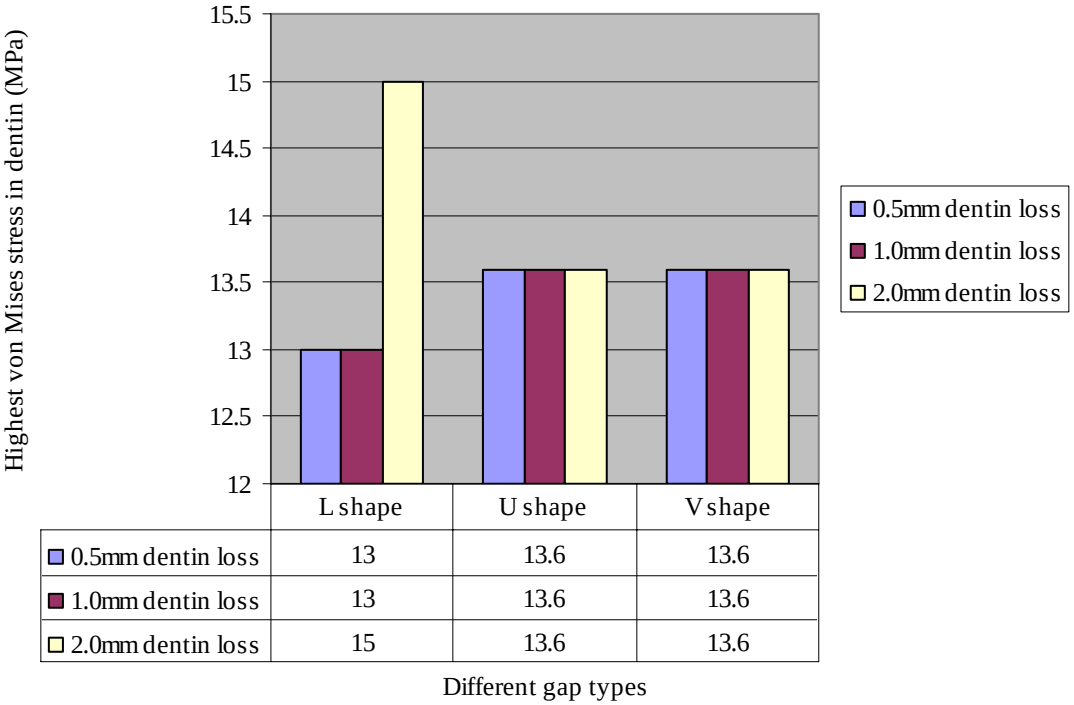

	L shape	U shape	V shape
0.5mm dentin loss	13	13.6	13.6
1.0mm dentin loss	13	13.6	13.6
2.0mm dentin loss	15	13.6	13.6

(c) Highest stress in dentin with U shape dentin loss under oblique loading

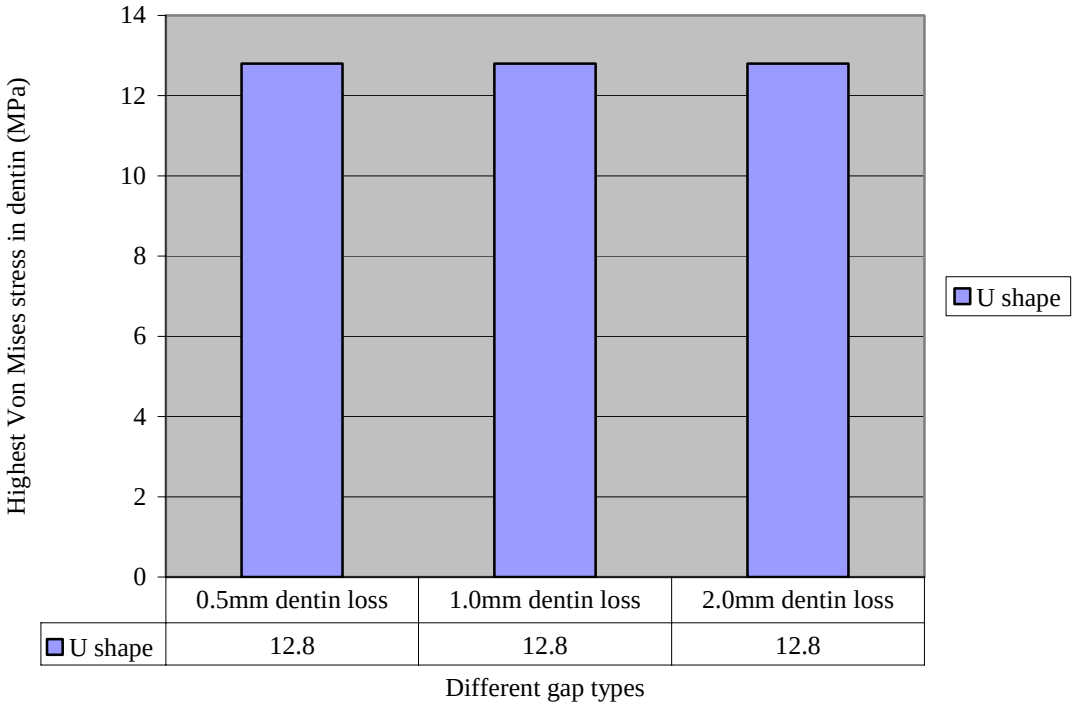

Graph 3.4 Maximum stresses in dentin with different cervical dentin loss

3.4 Simulation Four: different level of dentin ferrule

In order to enhance the retention of the restoration, a ferrule often is created on the crown. To accommodate the ferrule, the coronal portion of the dentin is reduced as show in Figure 33.3a-d. In this simulation, the effects of different heights of dentin ferrule on the stress distributions in dentin and the post are evaluated. The heights of the ferrules and therefore the vertical dentin reduction are 0.0mm, 1.75mm, 3.50mm, and 5.25mm, respectively as shown in Figure 3.33. The dentin is reduced laterally to create a cone-like configuration as shown in Figure 3.33. the elastic modulus of the post and core material are 200GPa and 16.6GPa respectively.

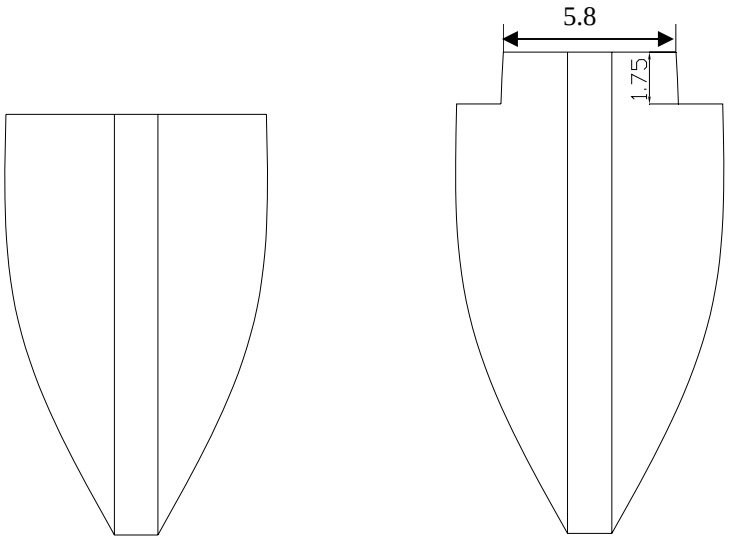

(a) Ferrule Height 0.00mm (b) Ferrule Height 1.75mm

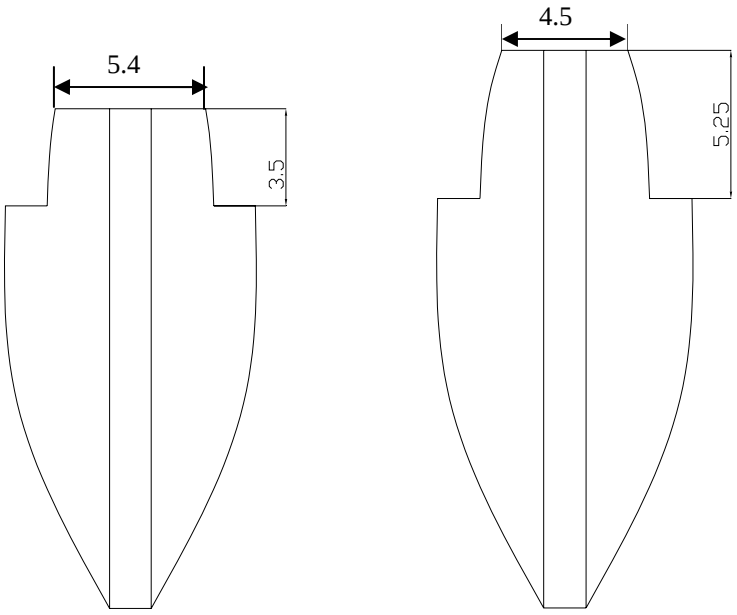

(c) Ferrule Height 3.5mm (d) Ferrule Height 5.25mm

Figure 3.33 Diagrams of dentin with different ferrule heights.

3.4.1 Vertical loading

Stresses in different regions of dentin due to different ferrule height are listed in Table 3.4. Figure 3.34 shows the stress distribution in dentin with different ferrule heights under vertical loading. When the ferrule height is zero, the highest stress occurs at the apical end of the post, and the value is 4.25MPa (shown as region 1 in Figure 3.34a). Just below the dentin shoulder (shown as region 2 in Figure 3.34a), the stress is 1.75MPa. The lowest stress appears at the apical portion of the dentin (0.75MPa), which is shown as region 3, 4, and 5 in Figure 3.34a. For most area of the dentin, the stresses are distributed uniformly (1.25MPa). When the ferrule height is 1.75mm, the stress distribution is very similar to the one when the ferrule height is zero, except that the lowest stress (0.75MPa) also appears at the coronal ferrule (shown as region 5 in Figure 3.34b) in addition to the apical portion of the root (shown as region 3 in Figure 3.34b). For the rest of the dentin, the stresses are distributed uniformly (1.25MPa). When the height is 3.5mm, the maximum stress is located at the apical portion of the post (shown as region 1 in Figure 3.34c) at the value of 4.25MPa. High stress shows just below the dentin shoulder (shown as region 2 in Figure 3.34c) at the value of 1.75MPa. The lowest stress appears at the bottom sides of the dentin, the top of the ferrule and cervical opening of the canal (shown as regions 3, 4 and 5 in Figure 3.34c) at value of 0.75MPa, which is similar to that of zero ferrule height. The rest of the dentin show uniformly distributed stress at the value of 1.25MPa. When the ferrule height is 5.25mm, the highest stress is observed at the apical portion of the post (shown as 1 in Figure 3.34d) at the value of 4.25MPa, which is the same as that when the ferrule height is zero. The lowest stresses appear at the sides of the coronal ferrule and the apical portion of the dentin (shown as regions 3 and 5 in Figure

3.34d), and is 0.75MPa. The stresses in region 2 and 4 are 1.75MPa and 0.75MPa respectively.

Figure 3.35 shows the stress distribution in post with different ferrule heights under vertical loading. Regardless of the ferrule heights, the stress distributions of the post are similar. The highest stress appears at the middle of the post (shown as 1 in Figure 3.35), which is about 11.0MPa. In the both end of the post, the stress value gradually reduces. The lowest value is at the end of the post (shown as 2 in Figure 3.35), and is about 3.0MPa. Thus, under vertical loading, the stress distributions in the post are not sensitive to the heights of dentin ferrule.

Table 3.4 Stresses in different regions of dentin due to different ferrule height under vertical loading

Ferrule Height (mm)	Region 1 (MPa)	Region 2 (MPa)	Region 3 (MPa)	Region 4 (MPa)	Region 5 (MPa)
0.0	4.25	1.75	0.75	0.75	0.75
1.75	4.25	1.75	0.75	0.75	0.75
3.5	4.25	1.75	0.75	0.75	0.75
5.25	4.25	1.75	0.75	0.75	0.75

3.4.2 Horizontal loading

Figure 3.36 shows the stress distributions of the dentin with different ferrule heights. The greatest stress appears at both sides of the dentin (shown as region 1 and 2 in Figure 3.36), which is about 13.6MPa. High stress is also located along the centreline of the apical canal (shown as region 3 in Figure 3.36), which is about 11.2MPa. The low stress appears

along the canal. The stresses at the coronal area of the ferrule are 2.4MPa, 0.8MPa, and 0.8MPa respectively. Along the center line of upper half of the canal (region 4 in Figure 3.36), stress is about 0.8MPa. Changes in ferrule height do not affect the stress distributions in dentin except that with the higher ferrule, less stress appears at the top of the ferrule.

Figure 3.37 shows the stress distributions of the post with different ferrule heights. Regardless of the ferrule heights, the stress distributions of the post are similar. Both sides of the post (shown as region 1 and 2 in Figure 3.37) show the stress concentrations of 40.8MPa. The lowest stress appears at the top of the post (shown as region 3 in Figure 3.37), which is about 2.5MPa. Changes in ferrule heights have little effect on the stress distributions of post.

3.4.3 Oblique loading

Figure 3.38 show the stress distributions in dentin with different ferrule heights. The highest stress happens at one side of the dentin (shown as 1 in Figure 3.38), and is about 9.6MPa. The stresses at the top of the dentin (shown as region 2 in Figure 3.38) are 1.8MPa, 0.8MPa, and 0.8MPa corresponding to dentin ferrule heights of 1.75mm, 3.50mm, and 5.25mm, respectively. The lowest stress value appears along the centreline of the canal (shown as region 3 in Figure 3.38), which is about 0.6MPa. The results show that the high ferrule has the advantage of low stress distribution at the top of the ferrule, but it does not affect the stress distributions in dentin.

Figure 3.39 show the stress distributions in posts. Regardless of the ferrule heights, the stress distributions of the post are very similar. The highest stress appears at one side of the post that is opposite to the direction of the loading. The value is about 32.0MPa (region 1). The lowest stress is located at the top of the post, which is about 2.0MPa (region 2). Changes in the ferrule height have insignificant effect on stress distributions of post.

3.4.4 Discussion

Except for the area of the dentin ferrule, the stress distribution seems very similar. Even though the dimensions of the structure are changed, the structure is assumed to be bonded very well. Force is transferred from elements to elements. No bonding failure happens at the bonding area.

The higher the ferrule is, the lower the stress appears to be at the top of the ferrule. When fatigue strength is considered, the low stress at the top of the helpful for the life of the dentin. Undamaged tooth should be kept as much as possible so that high stress doesn’t happen at the interface between the ferrule and the core.

3.4.5 Summary

Highest stresses in dentin with different ferrule height are summarized Graph 3.5. The effects of ferrule heights on the stress distributions in dentin and the posts have been studied. The research has found that the ferrule heights do not affect the stress

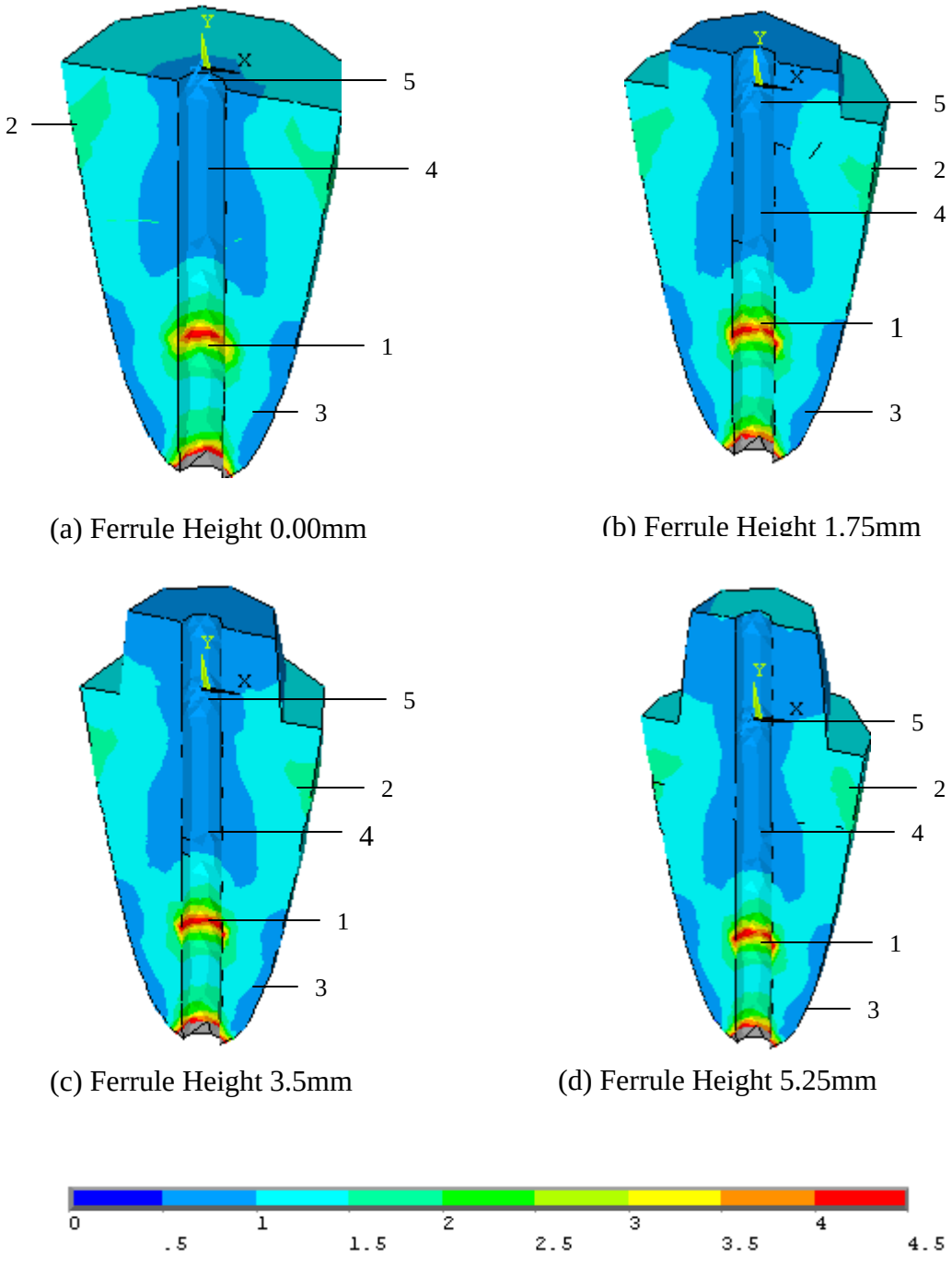

(a) Ferrule Height 0.00mm

(b) Ferrule Height 1.75mm

(c) Ferrule Height 3.5mm

(d) Ferrule Height 5.25mm

Figure 3.34 Stress distributions in dentin with different ferrule heights under a vertical load (MPa).

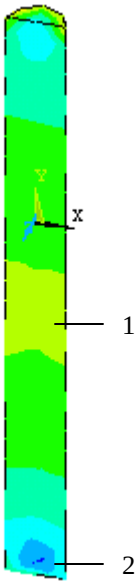

(a) Ferrule Height 0.00mm

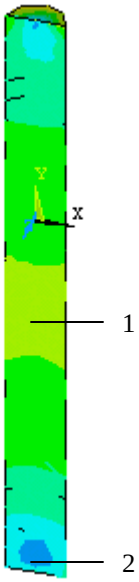

(b) Ferrule Height 1.75mm

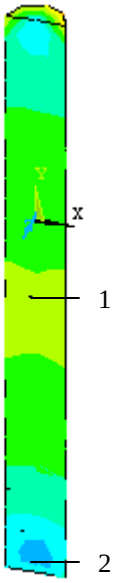

(c) Ferrule Height 3.5mm

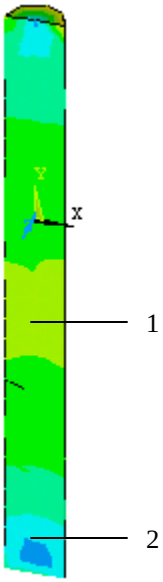

(d) Ferrule Height 5.25mm

Figure 3.35 Stress distributions in the posts with different ferrule heights under a vertical load (MPa).

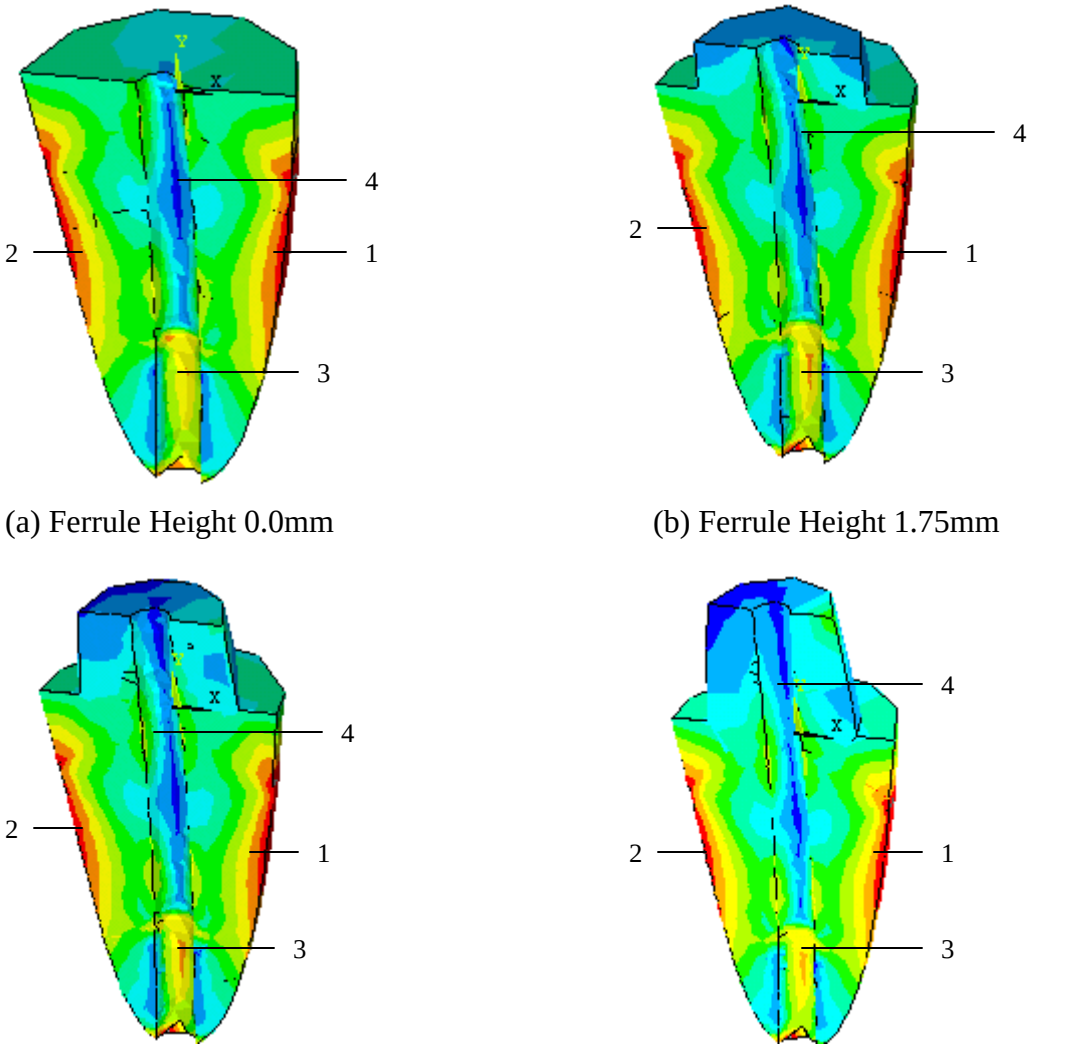

Figure 3.36 Stress distributions in dentin with different ferrule heights under a horizontal load (MPa).

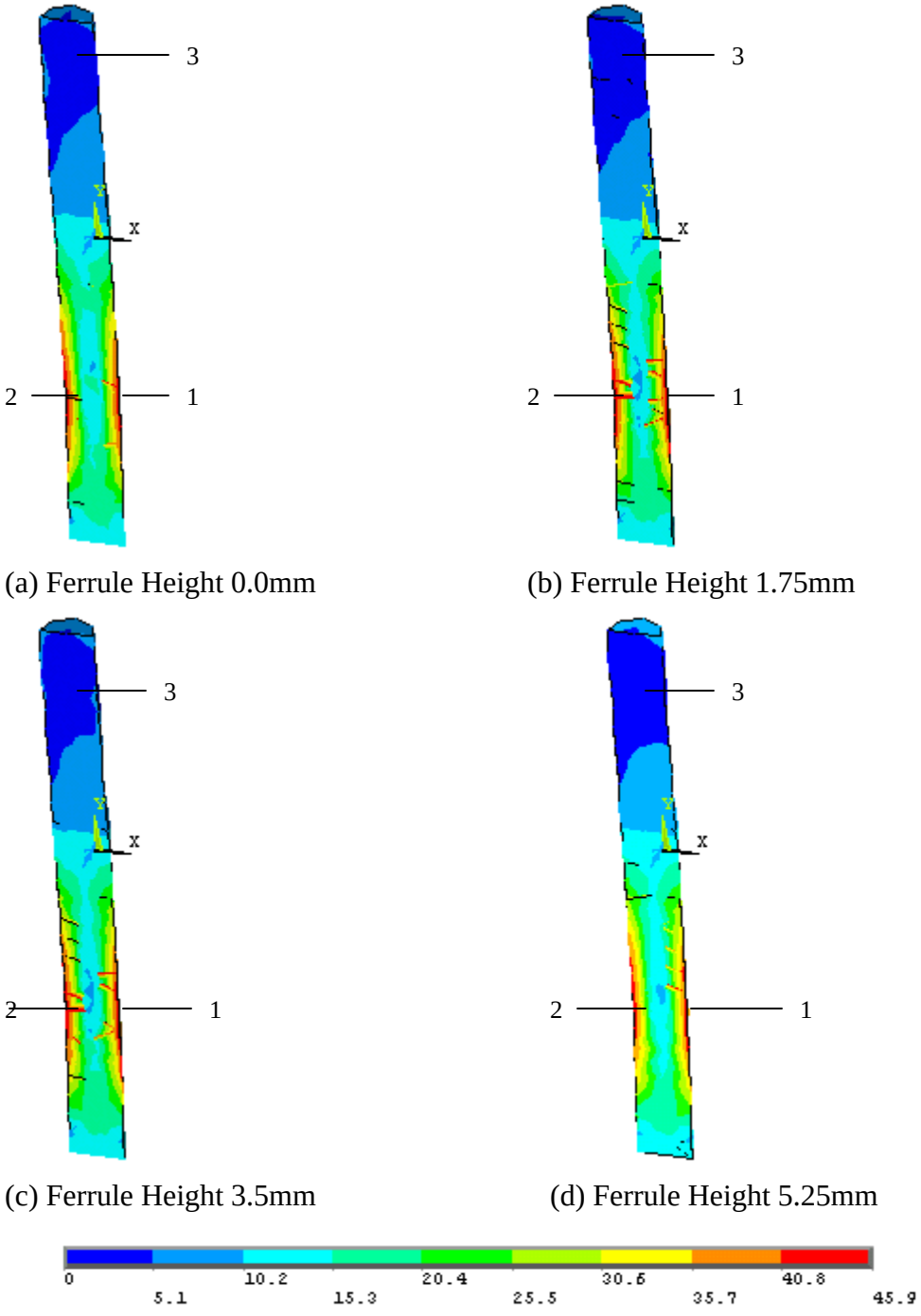

(a) Ferrule Height 0.0mm

(b) Ferrule Height 1.75mm

(c) Ferrule Height 3.5mm

(d) Ferrule Height 5.25mm

Figure 3.37 The stress distribution in the posts with different ferrule heights under horizontal loading (MPa).

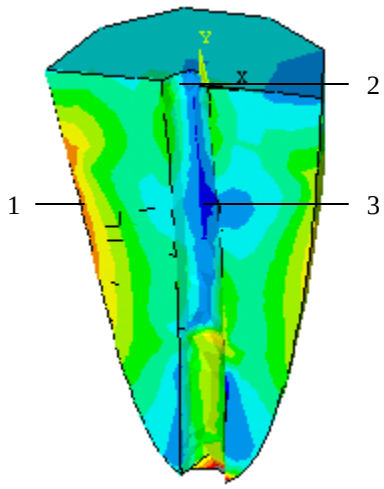

(a) Ferrule Height 0.0mm

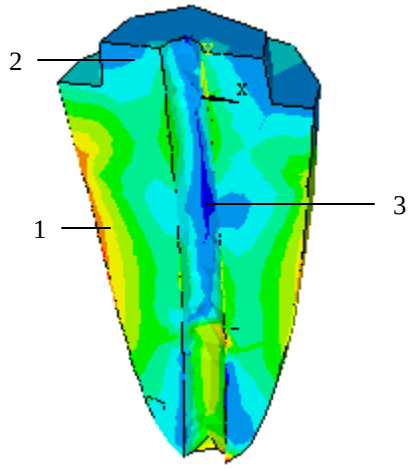

(b) Ferrule Height 1.75mm

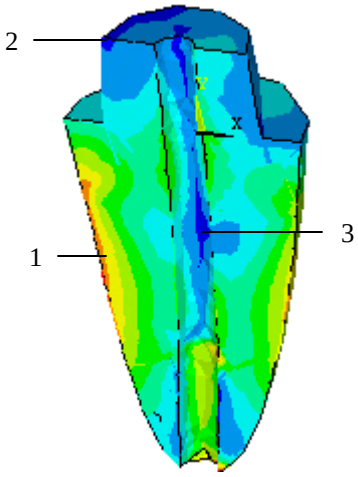

(c) Ferrule Height 3.5mm

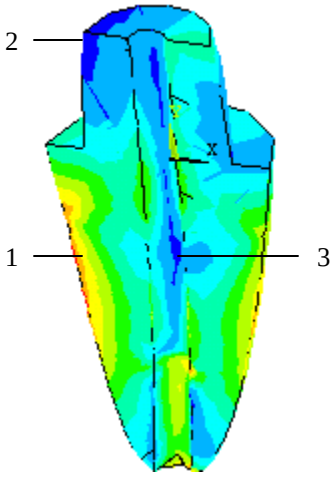

(c) Ferrule Height 5.25mm

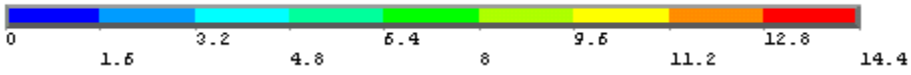

Figure 3.38 Stress distributions in dentin with different ferrule heights under an oblique load (MPa).

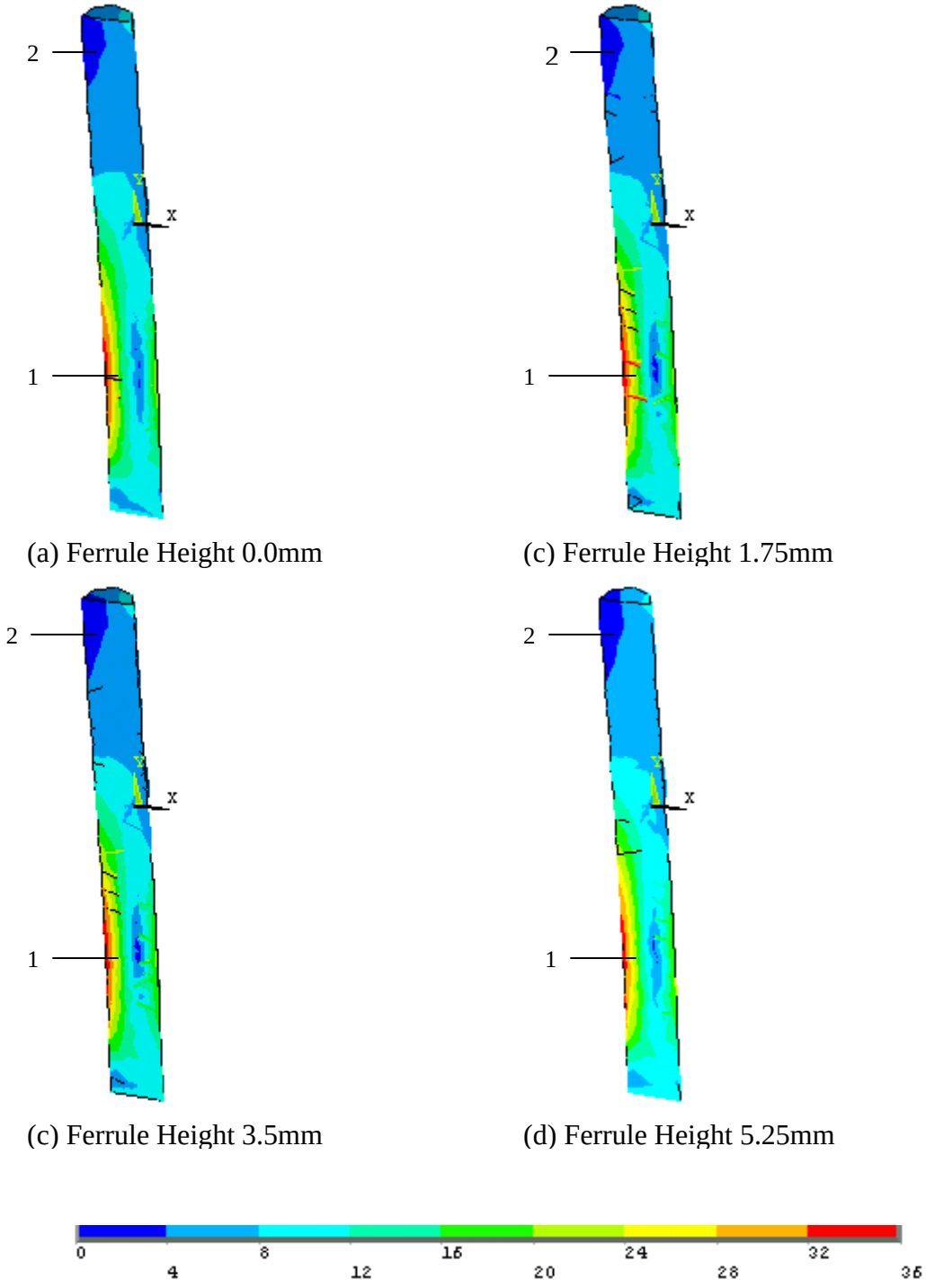

(a) Ferrule Height 0.0mm

(c) Ferrule Height 1.75mm

(c) Ferrule Height 3.5mm

(d) Ferrule Height 5.25mm

Figure 3.39 Stress distributions of the posts with different ferrule heights under an oblique load (MPa).

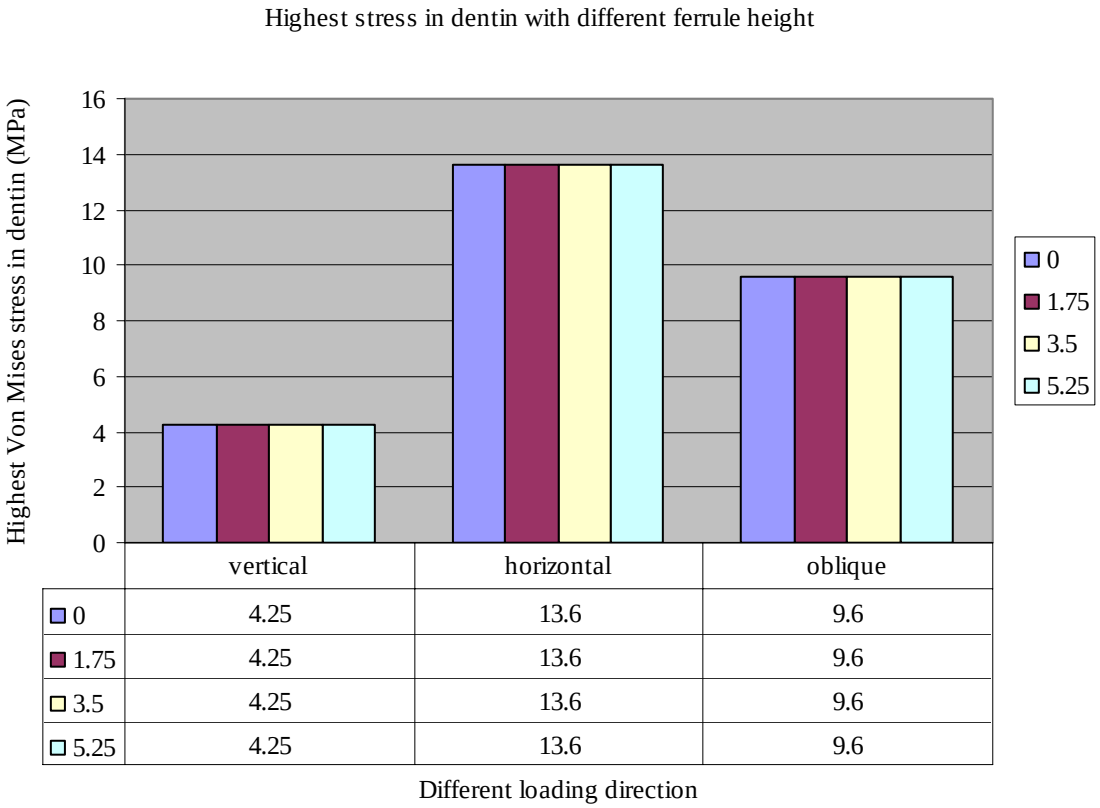

Graph 3.5 Maximum stresses in dentin with different ferrule height

distributions in the post and dentin significantly. However, higher ferrule shows lower stress at the top of the ferrule. The remaining structure of a damaged tooth should be retained as much as possible.

3.5 Simulation Five: Different Canal Diameters

In this simulation, the effects of different canal diameters on the stress distributions in dentin and posts are studied. Different canal diameters are prepared for post placement. Canal diameters, considered in this simulation, are 1.5mm, 2.0mm, and 2.5mm, respectively. To perfectly bond a post in the canal, post diameter is assumed to be the

same as the canal diameter. The thickness of dentin is reduced because of the enlarged canal diameter. Except for the change in the diameter of the post, the inner core, and the canal, all the other sizes of the restoration structure are the same as in the other simulations. The diameter of the apical canal is fixed as 1.5mm. The canal is smoothed at the apical portion of the root to avoid sharp corners. The elastic modulus of the post, core material is 200GPa and 16.6GPa respectively.

3.5.1 Vertical loading

Figure 3.40 shows the stress distributions of dentin with different canal diameters under the vertical loading. For three different canal diameters, the stress distributions are similar. The high stresses appear at the apical portion of the post (shown as region 1 in Figure 3.40), and is 4.25MPa. The medium stress appears at the shoulder of the dentin (shown as 2 in Figure 3.40) with the value of 1.25MPa. The area of medium stress at the dentin shoulder reduces with the increase of the canal diameter, whereas the area with high stress at the apical portion of the root increases significantly with the increase in the canal diameters. The stress in the rest area is 1.25MPa). Changes of canal diameter do not affect the stress distributions in dentin under vertical loading significantly.

Figure 3.41 shows the stress distributions in post with three different canal diameters. When the canal diameter is 1.5mm, the stress in the middle of the post (shown as region 1 in Figure 3.41a) is 9.7MPa. When the canal diameter increases to 2.00mm, the greatest stress (shown as region 1 in Figure 3.41b) reduces 15% to 8.2MPa comparing to that of 1.5mm canal diameter. When the canal diameter increases to 2.50mm, the greatest stress

(shown as 1 in Figure 3.41c) is 5.7MPa, which is 41% lower than that of 1.5mm post diameter. The increase in post diameter leads to the reduction of stress and more uniform stress distributions in the post. The lowest stress appears at the apical portion of the post (region 2 in Figure 3.41) and it is 2.25MPa.

Table 3.5 Stresses in different regions of dentin due to different canal diameters under vertical loading

Canal diameter (mm)	Region 1 (MPa)	Region 2 (MPa)	Region 3 (MPa)	Region 4 (MPa)	Region 5 (MPa)
1.5	4.25	1.25	0.75	0.75	0.75
2.0	4.25	1.25	0.75	0.75	0.75
2.5	4.25	1.25	0.75	0.75	0.75

3.5.2 Horizontal loading

Figure 3.42 shows the stress distribution in dentin with different canal diameters under horizontal loading. The maximum stresses are 10.4MPa, 10.4MPa, and 13.6MPa respectively at the apical portion of the root (shown as region 1 in Figure 3.42) corresponding to the canal diameter of 1.5mm, 2.0mm and 2.5mm. The stress at the apical portion of the root increases significantly using the large size of the post diameter. Compared to the stresses with a 1.5mm canal diameter, the stress increases about 31% with the usage of 2.5mm canal diameter. The stresses at the two sides of the dentin (shown as regions 2 and 3 in Figure 3.42) are 13.6MPa, 12.0MPa, and 12.0MPa corresponding to the post diameters of 1.5mm, 2.0mm and 2.5mm, respectively. The stress decreases 12% compared to that of 1.5mm canal diameter. An increase in canal

diameter causes the stress reduction at two sides of the dentin. However, a large canal diameter increases the stress at the apical portion of the root. Large canal diameters should be avoided for obtaining the lowest stress at the apical portion of the root.

Figure 3.43 shows the stress distributions in post with different canal diameter under horizontal loading. The greatest stress is located at the two sides of the post (shown as 1 and 2 in Figure 3.43). The stress values are 45MPa, 53MPa, and 58MPa corresponding to the canal diameters of 1.5mm, 2.0mm and 2.5mm, respectively. For 2.5mm canal diameter, stress increases 29% comparing to that of 1.5mm diameter. The 2.5mm diameter post is stressed less than the 1.5mm diameter post.

3.5.3 Oblique loading

Figure 3.44 shows the stress distributions in dentin with different canal diameters under oblique loading. The stress patterns are similar. When the canal diameter is 1.5mm, the greatest stress is located at one side of dentin (shown as 1 in Figure 3.44a) at the value of 9.0MPa. Stress concentration is observed in the apical portion of the root (shown as region 2 in Figure 3.44a), and this is about 6.8MPa. The lowest stress is along the centreline of the canal (shown as 3 in Figure 3.44a), and is about 0.6MPa. When the canal diameter is 2.0mm, the maximum stress is located at one side of the dentin (shown as region 1 in Figure 3.44b) at value of 7.8MPa. The highest stress reduces about 13%. At the apical portion of the root (shown as region 2 in Figure 3.44b), the stress value is about 6.8MPa, which is the same as 1.5mm canal diameter. The lowest stress appears at the centerline of the canal (shown as region 3 in Figure 3.44b), and is about 1.8MPa, which is

3 times that observed with a 1.5mm canal. When the canal diameter is 2.5mm, the stress at the outer surface of the dentin (shown as region 1 in Figure 3.44c) reduces 13%, which is about 7.8MPa. The stress at the apical portion of the post (shown as region 2 in Figure 3.44c) increases to 7.8MPa. The stress along the centreline of the canal (shown as region 3 in Figure 3.44c) is about 1.2MPa. The increase in the canal diameter increases the stress in the apical portion of the root.

Figure 3.45 shows the stress distribution in the post of the restored teeth with different canal diameters under oblique loading. The stress patterns are similar. The greatest stress is located at one side of the posts (shown as region 1 in Figure 3.45). The stress value increases with the increase of the diameter at 34.2MPa, 37.8MPa, and 39.6MPa, respectively. The highest stress in the 2.5mm-diameter post is 16% higher than that of the 1.5mm post diameter. The post with the 2.5mm diameter supports more load than that of the post with the 1.5mm diameter.

3.5.4 Discussion

The thickness of the dentin wall is directly proportional to the ability of the tooth to withstand the horizontal loading (Assif et al., 1989). Thin dentin wall with post of large diameter yielded lower stresses at outer surface of the dentin. The large size post is found withstand most of the horizontal load. a post with too small diameter could bend and the bending would likely occur at its coronal end under horizontal stress (Nergiz 2002).

The danger of thin dentin walls is not obvious under the vertical loading. However, the decrease of the dentin wall thickness and the corresponding increase of the post diameter cause a high stress concentration at the apical portion of the post, which is not desirable.

3.5.5 Summary

The effects of different canal diameters on the stress distributions in dentin and posts are studied. The results show that the increase of canal diameter reduces the stress at the two

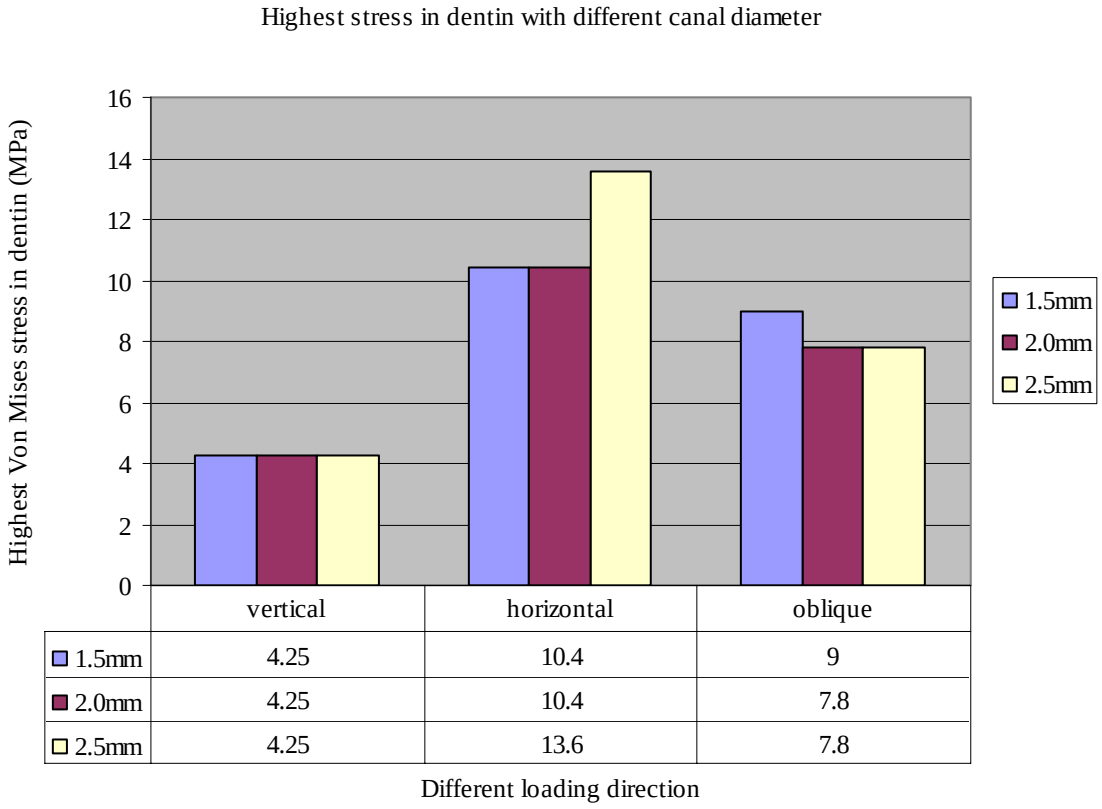

	vertical	horizontal	oblique
1.5mm	4.25	10.4	9
2.0mm	4.25	10.4	7.8
2.5mm	4.25	13.6	7.8

Graph 3.6 Maximum stresses in dentin with different canal diameters under different loading direction.

sides of dentin under the horizontal loading and the oblique loading. Posts with large diameters support more loads. However, since a tooth restored with a larger diameter post has a thinner dentin wall, high stress concentrations at the apical portion of the post result, and this is not desirable. The maximum stresses in dentin with different canal diameter are summarized in Graph 3.6.

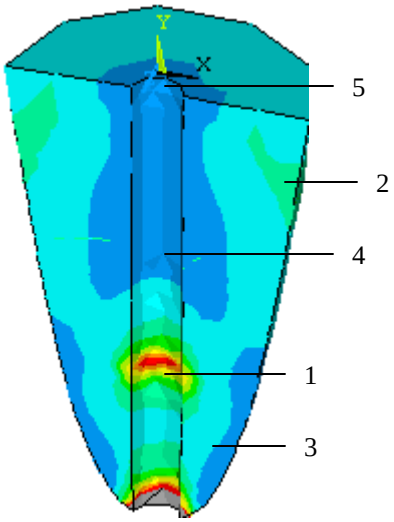

(a) 1.50mm canal diameter

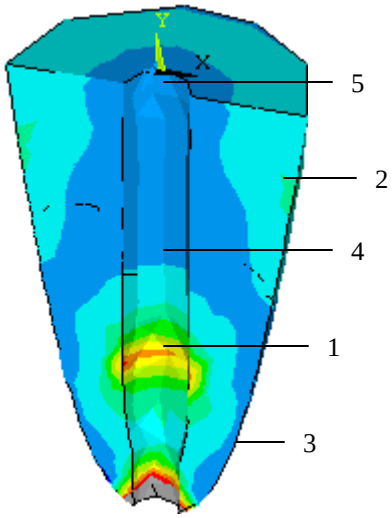

(b) 2.00mm canal diameter

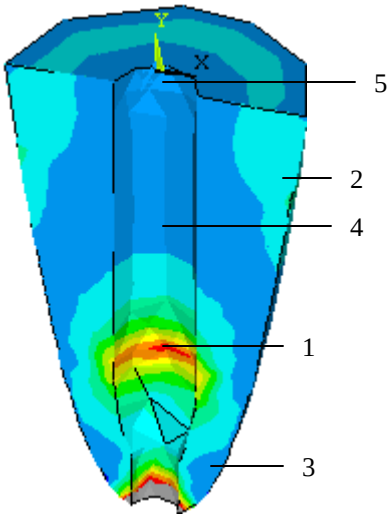

(c) 2.50mm canal diameter

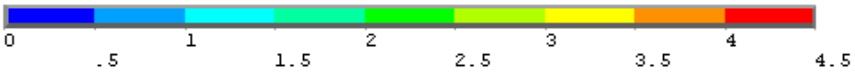

Figure 3.40 Stress distributions in dentin with three different canal diameters and under a vertical load (MPa).

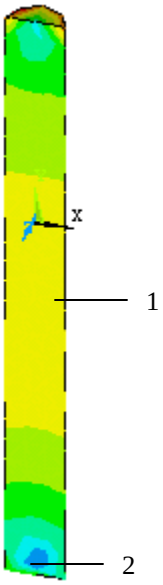

(a) 1.50 mm canal diameter

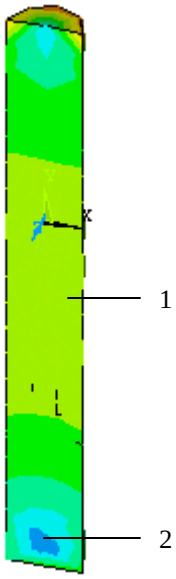

(b) 2.00 mm canal diameter

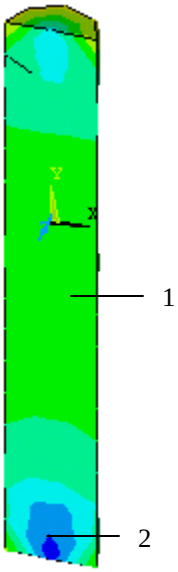

(c) 2.50 mm canal diameter

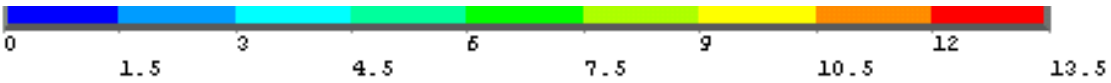

Figure 3.41 Stress distributions in the posts with three different canal diameters and under a vertical load (MPa).

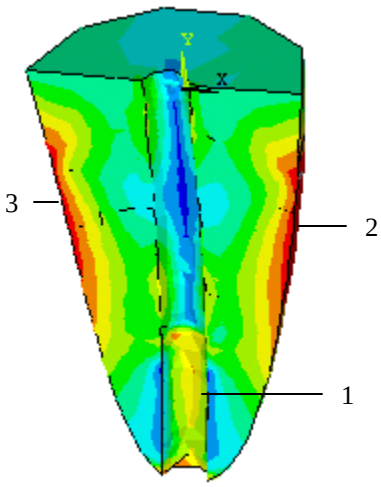

(a) 1.50 mm canal diameter

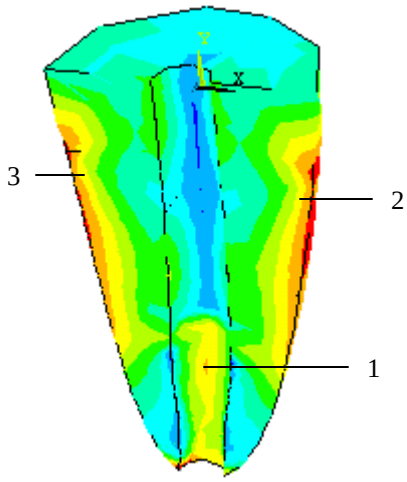

(b) 2.00 mm canal diameter

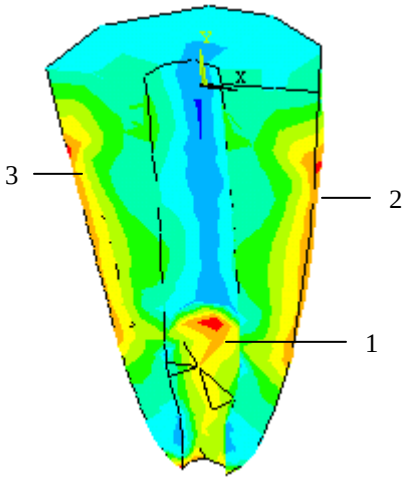

(c) 2.50 mm canal diameter

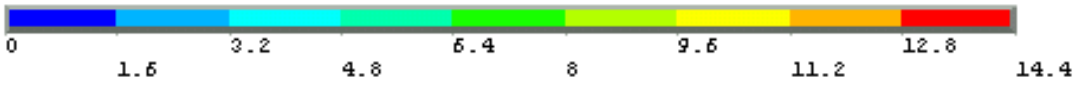

Figure 3.42. Stress distributions in dentin with different canal diameters under a horizontal load (MPa).

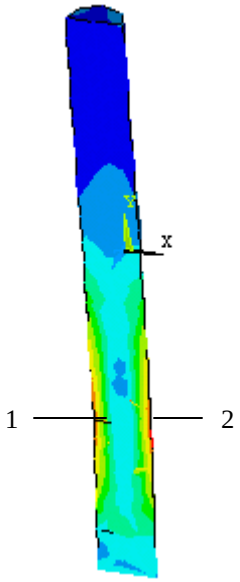

(a) 1.50 mm canal diameter

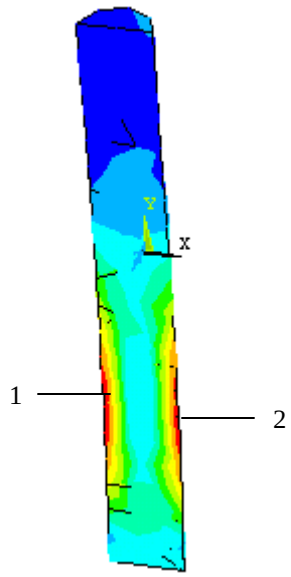

(b) 2.00 mm canal diameter

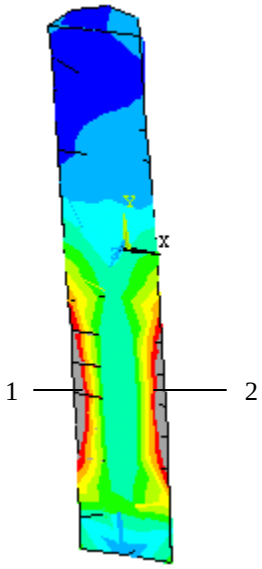

(c) 2.50 mm canal diameter

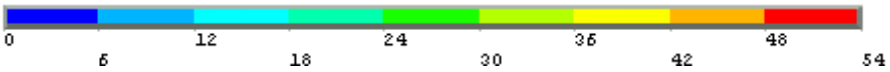

Figure 3.43. Stress distributions in posts with different canal diameters under a horizontal load (MPa).

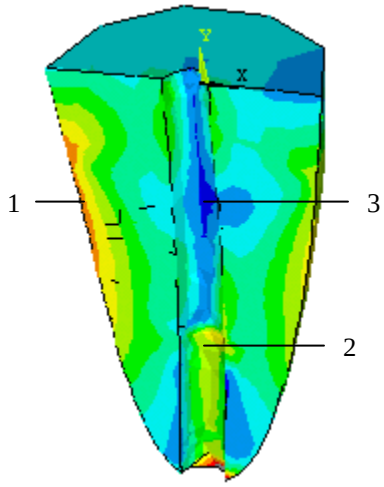

(a) 1.50 mm canal diameter

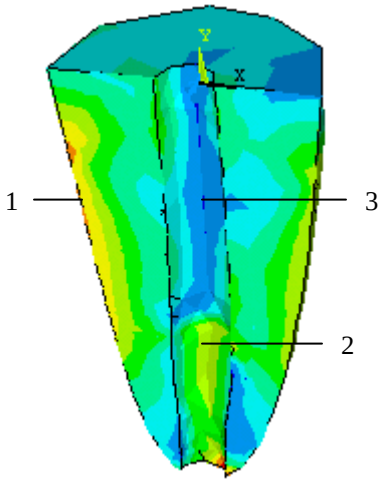

(b) 2.00 mm canal diameter

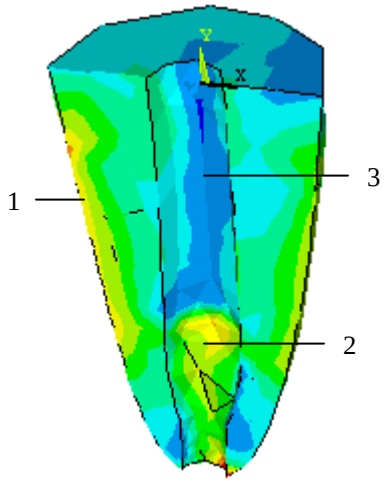

(c) 2.50 mm canal diameter

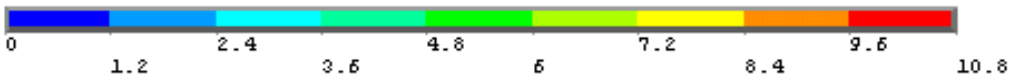

Figure 3.44. Stress distribution in dentin with different canal diameters under an oblique load (MPa).

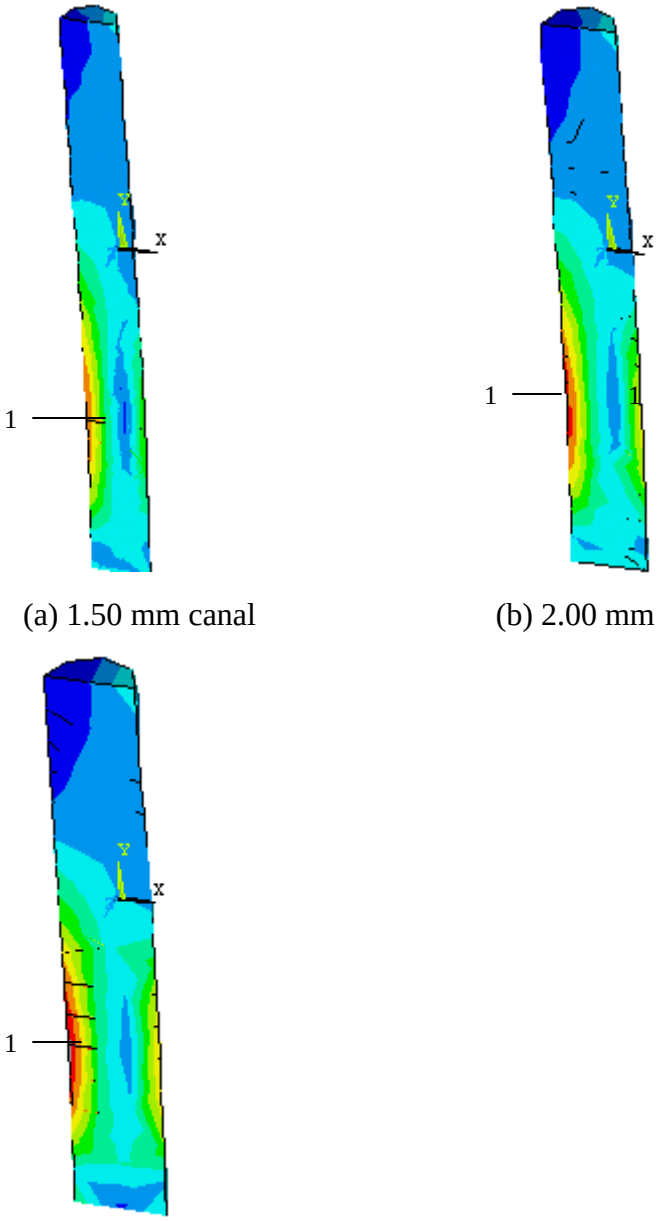

(a) 1.50 mm canal (b) 2.00 mm canal

(c) 2.50 mm canal diameter

Figure 3.45 Stress distributions in the posts of restored teeth with different canal diameters under an oblique loading (MPa).

Chapter 4 Conclusions

In this thesis, a 3D finite element model of a post-core restored endodontically treated maxillary incisor has been developed to study the stress distributions under a variety of loading conditions. The model has then been used to conduct simulations to investigate the effects of various parameters on stress distributions. The goal is to gain an in-depth understanding of the mechanical performance of the post-core restored endodontically treated teeth so that improvements can be made to post and core design and to tooth preparation. The contributions, made in this work, are detailed below.

(1) Development of the finite element model:

Post-core restored endodontically treated teeth are complex systems due to the small dimensions, structural complexities, multiple components with significantly different material properties, and variations in loading directions and the magnitudes. A 3D finite element model has been developed, which includes dentin, PDL, bone, gutta percha, post, core and crown. Because of their elastic modulus being similar to dentin, the cementum and any luting agents are included in the dentin portion of the tooth. All components have been assumed to be perfectly bonded, and all materials have been assumed to be homogenous, isotropic, linear and elastic. Various loadings have been considered. The geometrical model has been built using Pro/Engineer, and the commercial finite element analysis package ANSYS has been used for the generation of the finite element model, stress calculations and post processing. A convergence test has been conducted to determine the proper number of the elements. Von Mises equivalent stresses in dentin,

posts, cores and crowns have been calculated, and the results have been shown in graphic forms. Due to the lack of experimental results, model validation has not been conducted. However, the results of one simulation have been compared with the similar work from the literature, and they match reasonably well.

(2) Simulations of the effects of various design parameters on the stress distributions

The effects of various factors on the stress distributions have been investigated using the finite element model, developed here. The factors include post materials, combinations of the posts and the cores, ferrule heights, post and dentin contacts at the dentin coronal surface, and thicknesses of root.

The effects of different post materials on the stress distributions in dentin, posts, cores and crowns have been first evaluated. Four popular post materials have been included in the finite element model. It has been found that, for the vertical load, the stress distributions are sensitive to the post materials. A post with high elastic modulus (stainless steel posts) causes high stress concentrations in dentin and the posts. The stress distributions in both dentin and the post are the most uniform without stress concentrations when the elastic modulus of the post is similar to that of dentin (FRC). High stresses in dentin are highly undesirable because they may cause the fracture of dentin and failure of the restored tooth. High stresses in posts are desirable since more of the load is shared by the post. The stress distributions in the cores and crowns are similar regardless of the post materials. The horizontal loading causes the highest stresses in dentin and posts, followed by the oblique load. The vertical load gives the lowest stress.

The stress distributions do not change significantly with the changes in the post materials under the horizontal and the oblique loading. Overall, the horizontal loading is the most dangerous and differences in post materials do not make significant differences in the magnitudes of the stresses and their distributions. The above findings agree reasonably well with those from previous work (Joshi *et al.*, 2001).

In the second simulation, the effects of the combinations of different posts and cores on the stress distributions in dentin and posts have been studied. Each of the four post materials, used in the first simulation, is combined with three different core materials, of which the elastic modulus are below, similar to, and higher than that of dentin. The Poison's ratios for the three core materials are the same. Under the vertical load, when the elastic modulus of the core is similar to that of the post and dentin, the stress distribution is the most uniform. As the elastic modulus of the post, the core and dentin differ significantly, the stresses at the apical portion of the root and dentin shoulder are high. Low stresses at the apical portion of the root and dentin shoulder would be expected to reduce the incidence of the tooth restoration failure. Under horizontal and oblique loading, the stress distributions in dentin are similar, and the stresses are significantly higher than those under a vertical load. Thus, changes in the elastic modulus of the core material have insignificant impact on stress distributions under horizontal and oblique loading.

The effects of dentin loss at the cervical region on the stress distributions in dentin are important, but have not been investigated before. In this simulation, such effects are studied. Three types of dentin loss at the coronal entrance of the canal, L-shape, U-shape

and V-shape, viewed in the sectional plane passing the vertical axis, have been considered. The width at the top of the dentin loss is fixed, but the depths of the gap are varied. This research found that horizontal loading causes higher stress concentrations than the other types of loading. The L-shape gap always results in the highest stress concentration at the apical portion of the root and at the bottom of the dentin gap, and the U-shape and V-shape dentin gap have shown low stress concentrations regardless of the type of loading. The stresses are not sensitive to the depth and the shape of dentin gap when horizontal and oblique loads are applied. For vertical loading, the high stresses at the apical portion of the root and the bottom of the dentin gap decrease with the increase of the depth of the gap. Overall, sharp angles and notches, which can cause stress concentration, should be avoided in tooth restorations.

Due to the fact that damage to the tooth crown varies in extent, a dentin ferrule is created on the remaining undamaged tooth. The effects of different ferrule height on the stress distributions in dentin have not been investigated before, and therefore are studied in this simulation. This research found that regardless of the ferrule heights, the changes of the stress distributions in dentin and the post are insignificant except that increased ferrule height creates lower stresses at the top of the ferrule.

The effects of different canal diameters on the stress distributions in dentin and posts have been studied in this simulation. Different canal diameters were prepared for the post placement, which reduces the thickness of dentin. The results show that the posts with large diameters support more of the load, and the increase of canal diameter reduces the

stress in the boundary areas of dentin under the horizontal loading and the oblique loading. However, the posts with large diameters cause high stress concentrations at the apical portion of the root, which is not desirable.

The 3D finite element model is a powerful tool for the stress analysis of post-restored endodontically treated teeth and in the design of post-core systems. With the finite element method, various parameters, such as geometry of the structure, post-core design, material properties, the magnitude and the direction of the load can be changed, and simulations can be conducted easily as demonstrated in this work. Most of the simulation results, such as the effects of the combinations of the post and the core, the dentin loss at cervical region, ferrule heights and the thickness of dentin have not been reported before. Such results enable us to gain physical insights into the mechanical performance of post-core restored endodontically treated teeth. The finite element model can also facilitate the optimal design of the post and core systems.

The results obtained in this thesis are only a first step in the development of the 3D finite element model for stress analysis of post-core restored endodontically treated teeth. In the future, work can be extended. For example, the support of the tooth (i.e. PDL) should be modeled more realistically as a flexible support rather than a rigid support. The post and the core, the post and dentin, and the core and dentin may not be perfectly bonded. Proper bonding conditions should be considered. More importantly, experimental validation of the finite element model is imperative since the post-core restored endodontically treated

teeth consists of a number of parts, of which the material properties are significantly different, the dimensions are small and the structure of each part is complex.

References

1. Abu-Hassan, M.I., Abu-Hammad, O.A., and Harrison, A., Stress distribution associated with loaded ceramic onlay restorations with different designs of marginal preparation, an FEA study. *Journal of Oral Rehabilitation*, **27**, 294-298, 2000
2. Akpinar, I., Anil, N. and Parnas, L., A natural tooth's stress distribution in occlusion with a dental implant, *Journal of Oral Rehabilitation*, **27**, 538-545, 2000
3. Arola, D., Galles, L.A., and Sarubin, M.F., A comparison of the mechanical behaviour of posterior teeth with amalgam and composite MOD restorations, *Journal of Dentistry*, **29**, 63-73, 2001
4. Assif, D., Oren, E., Marshak, B.L. and Aviv, I., Photoelastic analysis of stress transfer by endodontically treated teeth to the supporting structure using different restorative techniques, *Journal of Prosthetic Dentistry*, **61**, 535-43, 1989
5. Atmaram, GH and Mohammed, H, Estimation of physiologic stresses with a natural tooth considering fibrous PDL structure, *Journal of Dental Research*, **60** 873-877, 1981
6. Barbier, L., Sloten, S., J., Krzesiski, G., Schepers, E. and Van Der Perre, G., Finite element analysis of non-axial versus axial loading of oral implants in the mandible of the dog, *Journal of Oral Rehabilitation*, **25**, 847-858, 1998
7. Barink, M., Van der Mark, P.C.P., A 3D finite element model of the polymerization process in dental restorations, *Biomaterials*, **24**, 1427-1435, 2003
8. Beer, Johnson and DeWolf, Mechanics of Materials, 3rd Edition, McGraw-Hill, 2002

9. Bouillaguet, S., Troesch, S., Wataha, J., Krejci, I., Meyer, J., and Pashley, D.H., Microtensile bond strength between adhesive cements and root canal dentin, *Dental Materials*, **19**, 199-205, 2003
10. Burns, D.A., Krause, W.R., Douglas, H.B., and Burns, D.R., Stress distribution surrounding endodontic posts, *Journal of Prosthetic Dentistry*, **64**, 412-418, 1990
11. Canadian Academy of Endodontics (CAE), Standards of Practice, 1998
12. Cailleteau, J., Rieger, M.R. and Akin, J.E., A comparison of intracanal stresses in a post-restored tooth utilizing the finite element method, *Journal of Endodontics*, **18**, 540-544, 1992
13. Caputo AA, and Standlee JP. Biomechanics in clinical dentistry. Quintessence Publisher co, 1987
14. Cohen, B.I., Musikant, B. L., and Deutsch, A.S., Comparison of the Photoelastic Stress for a Split-Shank Threaded Post Versus a Threaded Post, *Journal of Prosthodontics*, **3**, 53-55, 1994
15. Cohen, B.I., Condos, S., Musikant, B.L., and Deutsch, A.S., Pilot study comparing the photoelastic stress distribution for four endodontic post systems, *Journal of Oral Rehabilitation*, **23**, 679-685, 1996
16. Chang, C.H., Lin, C.L., Wang, C.H. and Lee, H.E. Stress analysis at cervical region of human teeth, *Advances in Bioengineering, ASME*, **43**, 251-252, 1999
17. Chimko, J., Stress analysis in human teeth due to the insertion of metal posts, *B.Sc. Thesis*, Department of Mechanical Engineering, University of Manitoba, 2001

18. Darendeliler, S., Darendeliler, H. and Kinoglu, T., Analysis of a central maxillary incisor using a three-dimensional finite element method, *Journal of Oral Rehabilitation*, **19**, 371-383, 1992
19. Davy, D.T., Dilley, G.L. and Krejci, R.F., Determination of stress patterns in root-filled teeth incorporating various dowel designs, *Journal of Dent Research*, **60**, 1301-1310, 1981
20. De Santis, R., Prisco, D., Apicella, A., Ambrosio, L., Rengo, S. and Nicolais, L., Carbon fiber post adhesion to resin luting cement in the restoration of endodontically treated teeth, *Journal of Materials Science: Materials in Medicine*, **11**, 201-206, 2000
21. Ersoz, E., Evaluation of stresses caused by dentin pin with finite elements stress analysis method, Journal of Oral Rehabilitation, 27, 769-773, 2000
22. Gher, Jr.M.E., Dunlap, RM, Anderson, Mh, Kuhl, *Journal of the American Dental Association*, 114, 174-177, 1987
23. Glazer, B., Restoration of endodontically treated teeth with carbon fibre posts-a prospective study, *Journal of the Canadian Dental Association*, **66**, 613-618, 2000
24. Guazzato, M., Albakry, M., Ringer, S.P., and Swain, M.V., Strength, fracture toughness and microstructure of a selection of all-ceramic materials. Part II. Zirconia-based dental ceramics. *Dental Materials*, 20, 449-456, 2004
25. Gungor, M.A., Artung, G., Sonugelen, M., and Toparli, M., The evolution of the removal forces on the conus crowned telescopic prostheses with the finite element analysis, *Journal of Oral Rehabilitation*, **29**, 1069-1075, 2002
26. Hew, Y.S., Purton, D.G. and Love, R.M., Evaluation of pre-fabricated root canal posts, *Journal of Oral Rehabilitation*, **28**, 207-211, 2001

27. Himmlova, L., Dostalova, T., Kacovsky, A., and Konvickova, S., Influence of implant length and diameter on stress distribution: A finite element analysis, *Journal of Prosthetic Dentistry*, **91**, 20-25, 2004
28. Holmes, D.C., Diaz-Arnold, A.M. and Leary, J.M., Influence of post dimension on stress distribution in dentin, *Journal of Prosthetic Dentistry*, **75**, 140-147, 1996
29. Ho, D., Stress analysis of an endodontically treated tooth by photoelastic methods, *B.Sc. Thesis*, Department of Mechanical Engineering, University of Manitoba, 2002
30. Ho, M.H., Lee, S. Chen, H. and Lee, M., Three-dimensional finite element analysis of the effects of posts on stress distribution in dentin, *Journal of Prosthetic Dentistry*, **72**, 367-372, 1994
31. Hood, J.A.A., Farah, J.W. and Craig, R.G., Modification of stresses in alveolar bone induced by a tilted molar, *Journal of Prosthetic Dentistry*, **34**, 415-421, 1975
32. Huysmans, M.C.D.N.J.M. and Van der Varst, P.G.T., Finite element analysis of quasistantic and fatigue failure of post and cores, *Journal of Dentistry*, **21**, 57-64, 1993
33. Huysmans, M.C.D.N.J.M., Peters, M.C.R.B., Plasschaert, A.J.M. and Van der Varst, P.G.T., Failure characteristics of endodontically treated promolars restored with a post and direct restorative materials, *International Endodontic Journal*, **25**, 121-129, 1992
34. Huysmans, M.C.D.N.J.M., Van der Varst, P.G.T., Schafer, R., Peters, M.C.R.B. and Soltesz, U., Fatigue behaviour of direct post-and-core restored premolars, *Journal of Dental Research*, **71,** 1145-1150, 1992

35. Huysmans, M.C.D.N.J.M., Peters, M.C.R.B., Van der Varst, P.G.T.and Plasschaert, A.J.M., Failure behavior of fatigue-tested posts and cores, *International Endodontic Journal*, **26**, 294-300, 1993
36. Joshi, S., Mukherjee, A., Kheur, M. and Mehta, A., Mechanical performance of endodontically treated teeth, *Finite Elements in Analysis and Design*, **37**, 587-601, 2001
37. Kato, H, Matsumura, H., Tanaka, T. and Atsuta, M., Bond strength and durability of porcelain bonding systems, *Journal of Prosthetic Dentistry*, **75**, 163-168, 1996
38. Ko, C.C., Chu, C.S., Chung, K.H. and Lee, M.C., Effects of posts on dentin stress distribution in pulpless teeth, *Journal of Prosthetic Dentistry*, **68**, 421-427, 1992
39. Lee, H.E., Lin, C.L., Wang, C.H., Cheng, C.H., and Chang, C.H., Stresses at the cervical lesion of maxillary premolar-a finite element investigation, *Journal of Dentistry*, **30**, 283-290, 2002
40. Lin, C.L., Chang, C.H., Wang, C.H., Ko, C.C., and Lee, H.E., Numerical investigation of the factors affecting interfacial stresses in an MOD restored tooth by auto-meshed finite element method, *Journal of Oral Rehabilitation*, **28**, 517-525, 2001
41. Liu, G.R., and Quek, S.S., The Finite Element Method a practical course, 2003
42. Loney, R.W., Kotowicz, W.E. and McDowell, G.C., Three dimensional stress analysis of the ferrule effect in cast post and cores, *Journal of Prosthetic Dentistry*, **63**, 506-512, 1990

43. Macho, G.A. and Spears, I.R., Effects of loading on the biomechanical behavior of molars of Homo, Pan, and Pongo, *American Journal of Physical Anthropology*, **109**, 211-227, 1999
44. Magne, P., Versluis, A. and Douglas, W.H., Rationalization of incisor shape: Experimental-numerical analysis, *Journal of Prosthetic Dentistry*, **81**, 345-355, 1999
45. Mahler, D. B. and Peyton, F. A., Photoelasticity as a research technique for analysing stresses in dental structures, *Journal of Dental Research*, **4**, 831-838, 1955
46. Mausner, I.K., Goldstein, G.R. and Georgescu, M., Effect of two dentinal desensitizing agents on retention of complete cast coping using four cements, *Journal of Prosthetic Dentistry*, **75**, 129-134, 1996
47. Mentink, A.G.B., Creugers, N.H.J. and Hoppenbrouwers, P.M.M., Qualitative assessment of stress distribution during insertion of endodontic posts in photoelastic material, *Journal of Dentistry*, **26**, 125-131, 1998
48. Musikant, B.L. and Deutsch, A.S., A new prefabricated post and core system, *Journal of Prosthetic Dentistry*, **52**, 631-634, 1984
49. Musikant, B.L. Cohen, B. I., and Deutsch, A.S., Fallacious Concepts of Post and Cores, *Dentistry Today*, October, 1997
50. Nergiz, I., Schmage, P., Ozcan, M. and Platzer, U., Effect of length and diameter of tapered posts on the retention, *Journal of Oral Rehabilitation*, **29**, 28-34, 2002
51. Nissan, J., Gross, M., Shifman, A., and Assif, D., Stress levels for well-fitting implant superstructures as a function of tightening force levels, *Journal of Prosthetic Dentistry*, **86**, 20-23, 2001

52. Nissan, J., Dmitry, Y., and Assif D., The use of reinforced composite resin cement as compensation for reduced post length, *Journal of Prosthetic Dentistry*, **86**, 304-308, 2001
53. Nissan, J., Barnea, E., Krauze, E., and Assif, D., Impression technique for partially edentulous patients, *The Journal of Prosthetic Dentistry*, **88**, 103-104, 2002
54. O'Mahony, A.M., Williams, J.L., Katz, J.O. and Spencer, P., Anisotropic properties of cancellous bone from a human edentulous mandible, *Clinical Oral Implants Research*, **11**, 415-421, 2000
55. Peters, M.C., Poort, H.W. and Farah, J.W. Stress analysis of a tooth restored with a post and core, *Journal Dental Research*, **62** 760-767, 1983
56. Pierrisnard, L., Bohin, F., Renault, P., and Barquins, M., Corono-radicular reconstruction of pulpless teeth: A mechanical study using finite element analysis, *The Journal of Prosthetic Dentistry*, **88**, 442-448, 2002
57. Pilo, R., Cardash, H.S., Levin, E., and Assif, D., Effect of core stiffness on the in vitro fracture of crowned, endodontically treated teeth, *Journal of Prosthetic Dentistry*, **88**, 302-306, 2002
58. Rees, J.S. and Jacobsen, P.H., The effect of interfacial failure around a class V composite restoration analysed by the finite element method, *Journal of Oral Rehabilitation*, **27**, 111-116, 2000
59. Robinson, John, Book: FEM in the Design Process, 1990
60. Rolf, K.C., Parker, M.W. and Pelleu, G.B., Stress analysis of five prefabricated endodontic dowel designs: a photoelastic study, *Operative Dentistry*, **17**, 86-92, 1992

61. Rosentritt, M., Furer, C., Behr, M., Lang, R. and Handel, G., Comparison of in vitro fracture strength of metallic and tooth-coloured posts and cores, *Journal of Oral Rehabilitation*, **27**, 595-601, 2000

62. Ragain, J.C., Yaman, P. and Craig, R.G., Photoelastic stress analysis of self-threading pins, *Operative Dentistry*, **18**, 218-223, 1993

63. Rizkalla, A.S., Jones, D.W., Mechanical properties of commercial high strength ceramic core materials, Dental materials, 20, 207-212, 2004

64. Rubin, C., Krishnamurthy, N., Capilouto, E. and Yi, H., Stress analysis of the human tooth using a three-dimensional finite element model, *Journal Dental Research*, **62**, 82-86, 1983

65. Silver-Thorn, M.B. and Joyce, T.P., Finite element analysis of anterior tooth root stresses developed during endodontic treatment, *Journal of Biomechanical Engineering*, **121**, 108-115, 1999

66. Standlee, J.P. and Caputo, A.A., The retentive and stress distributing properties of split threaded endodontic dowels, *Journal of Prosthetic Dentistry*, **68**, 436-442, 1992

67. Staninec, M., Marshall, G., Hilton, J., Pashley, D., Gansky, S., Marshall, S., and Kinney, J., Ultimate tensile strength of dentin: Evidence for a damage mechanics approach to dentin failure, *Journal of Biomedical Materials Research (Applied Biomaterial)* **63**, 342–345, 2002

68. Stockton, L.W., Factors affecting retention of post systems-a literature review of prosthetic dentistry, *Journal of Prosthetic Dentistry*, **81**, 380-385, 1999

69. Stockton, L.W., Williams, P.T. and Clarke, C.T., Post retention and post/core shear bond strength of four post systems, *Operative Dentistry*, **25**, 441-447, 2000

70. Stockton L.W., Williams, P.T., Retention and shear bond strength of two post systems, *Operative Dentistry*, **24**, 210-216, 1999

71. Stegaroiu, R., Yamada, H., Kusakari, H. and Miyakawa, O., Retention and failure mode after cyclic loading in two post and core systems, *The Journal of Prosthetic Dentistry*, **72**, 506-511, 1996

72. Thorsteinsson, T.S., Yaman, P.and Craig, R.G., Stress analyses of four prefabricated posts, *Journal of Prosthetic Dentistry*, **67**, 30-33, 1992

73. Toparli, M., Gokay, N. and Aksoy, T. Analysis of a restored maxillary second premolar tooth by using three-dimensional finite element method, *Journal of Oral Rehabilitation*, **26**, 157-164, 1999

74. Toparli, M., Gokay, N. and Aksoy, T. An investigation of the stress values on a tooth restored by amalgam, *Journal of Oral Rehabilitation*, **26**, 259-263, 1999

75. Toparli, M., Gokay, N., and Aksoy, T., An investigation of temperature and stress distribution on a restored maxillary second premolar tooth using a three-dimensional finite element method, *Journal of Oral Rehabilitation*, **27**, 1077-1081, 2000

76. Toparli, M., Stress analysis in a post-restored tooth utilizing the finite element method, *Journal of Oral Rehabilitation*, **30**, 470-476, 2003

77. Watson, T.F., Pagliari, D., Sidhu, S.K., Naasan, M.A., Confocal microscopic observation of structural changes in glass-ionomer cements and tooth interfaces, *Biomaterials*, **19**, 581-588, 1998

78. Wheeler, R.C., *An atlas of tooth form*, Philadelphia WB Saunders, 1984.

79. Wheeler, R.C., *A manual: Tooth Form Drawing and Carving*, Philadelphia W.B. Saunders Company

80. Willems, G., Lambrechts, P., Braem, M., Celis, J.P. and Vanherle, G., A classification of dental composites according to their morphological and mechanical characteristics, *Dental Materials*, **8**, 310-319, 1992

81. Williams, K.R., Edmunson, J.T., Finite element analysis of restored teeth, *Dental Materials*, **3**, 200-206, 1987

82. Yaman, S.D., Alacam, T. and Yaman, Y., Analysis of stress distribution in a vertically condensed maxillary central incisor root canal, *Journal of Endodontics*, **24,** 107-111, 1998

83. Yaman, S.D., Karacer, O., and Sahin, M., Stress distribution of post–core applications in maxillary central incisors, *Journal of Biomaterials Applications*, **18**, 163-177, 2004

84. Yang, H.S., Lang, L.A.L., Molina, A. and Felton, D.A., The effects of dowel design and load direction on dowel-and-core restorations, *The Journal of Prosthetic Dentistry*, **85**, 558-67, 2001

85. Yang, H.S., Lang, L.A., Guckes, A.D., and Felton, D.A. The effect of thermal change on various dowel-and-core restorative materials, *Journal of Prosthetic Dentistry*, **86**, 74-80, 2001

86. Zienkiewicz, O. C., The Finite Element Method in Engineering Science, McGraw-Hill Publ., London, 1971, 1977, 520 pp., ISBN 07-094138-6, 0-07-084072-5

Appendix A Command Line Input

The simulations in this study are operated with command line input script. There are many advantages using a command line input script as compared to a database file. A database file in ANSYS (ANSYS, Inc.) is usually a huge file, which contains the model's information and the results. A command input script is usually a small text file and very convenient to carry. A command input script can be edited to meet the requirements with any text editor. Using command line input script can speed up the input of information, and can be run at any time by choosing Utility Menu->File->Read Input from. A sample example command input file shown below demonstrates the procedure of analysis. Comments are made after comment character (!). The comments are in bold text size.

```
/title, Ceramic post, Axial load, Good contact, Mesh9, Solid92
! Define a title, indicate post type, loading direction, contact condition, mesh type, and element type
/AUX15
! Start the IGES file transfer processor
IOPTN,IGES,NODEFEAT
! Control option related to importing a model; set default values for all import options
!*
IOPTN,MERGE,YES
! Entity merge option, yes means automatic merge is performed
IOPTN,SOLID,YES
! Solid is created automatically
IOPTN,SMALL,YES
! Small area is deleted
IOPTN,GTOLER, DEFA
! Use system default merge tolerance
```

IGESIN,'ancrown',' ',' '
! Transfers a IGES data from a file to ANSYS
VPLOT
! Display the selected volume
!*
IOPTN,IGES,NODEFEAT
! IGES import option, no defeature
!*
IOPTN,MERGE,YES
IOPTN,SOLID,YES
IOPTN,SMALL,YES
IOPTN,GTOLER, DEFA
IGESIN,'ancore',' ',' '
! Import core
VPLOT
!*
IOPTN,IGES,NODEFEAT
!*
IOPTN,MERGE,YES
IOPTN,SOLID,YES
IOPTN,SMALL,YES
IOPTN,GTOLER, DEFA
IGESIN,'anpost',' ',' '
! Import post
VPLOT
!*
IOPTN,IGES,NODEFEAT
!*
IOPTN,MERGE,YES
IOPTN,SOLID,YES
IOPTN,SMALL,YES
IOPTN,GTOLER, DEFA
IGESIN,'andentin',' ',' '
! Import dentin
VPLOT
!*
IOPTN,IGES,NODEFEAT
!*
IOPTN,MERGE,YES
IOPTN,SOLID,YES
IOPTN,SMALL,YES

IOPTN,GTOLER, DEFA
IGESIN,'angp',' ',' '
! Import Gutta Percha
VPLOT
!*
IOPTN,IGES,NODEFEAT
!*
IOPTN,MERGE,YES
IOPTN,SOLID,YES
IOPTN,SMALL,YES
IOPTN,GTOLER, DEFA
IGESIN,'anpdl',' ',' '
! import PDL
VPLOT
!*
IOPTN,IGES,NODEFEAT
!*
IOPTN,MERGE,YES
IOPTN,SOLID,YES
IOPTN,SMALL,YES
IOPTN,GTOLER, DEFA
IGESIN,'anbone',' ',' '
! Import bone
VPLOT
!*
FINISH
! Finish importing IGES data
/PREP7
! Start PREP7 processor
FLST,2,7,6,ORDE,2
! Picking seven volumes
FITEM,2,1
! Identifies items chosen by a picking operation
FITEM,2,-7
VGLUE,P51X
! Generates new volumes by “gluing” volumes
!*
MPTEMP,,,,,,,,
! Input material properties
MPTEMP,1,0
! Define a temperature table

MPDATA,EX,1,,69e3
! material property, elastic module, material no. 1
MPDATA,PRXY,1,,.28
! material property, Poison ratio, material no. 1
MPTEMP,,,,,,,
MPTEMP,1,0
MPDATA,EX,2,,16.6e3
MPDATA,PRXY,2,,.24
! material property data for material no.2
MPTEMP,,,,,,,
MPTEMP,1,0
MPDATA,EX,3,,69e3
MPDATA,PRXY,3,,.3
! Input material property data for material no.3
MPTEMP,,,,,,,
MPTEMP,1,0
MPDATA,EX,4,,18.6e3
MPDATA,PRXY,4,,.3
MPTEMP,,,,,,,
MPTEMP,1,0
MPDATA,EX,5,,68.9
MPDATA,PRXY,5,,.4
MPTEMP,,,,,,,
MPTEMP,1,0
MPDATA,EX,6,,.96
MPDATA,PRXY,6,,.4
MPTEMP,,,,,,,
MPTEMP,1,0
MPDATA,EX,7,,13.7e3
MPDATA,PRXY,7,,.3
! Input material property data for material no.7
!*
ET,1,SOLID92
! Select a local element type, SOLID92, from element library
!*
CM,_Y,VOLU
! Start to assign material properties to different volumes
VSEL, , , , 1
! Select volume no.1
CM,_Y1,VOLU
CMSEL,S,_Y

!*
CMSEL,S,_Y1
VATT, 1, , 1, 0
! Assign material property no. 1 to volume no.1
CMSEL,S,_Y
CMDELE,_Y
CMDELE,_Y1
!*
CM,_Y,VOLU
VSEL, , , , 2
CM,_Y1,VOLU
CMSEL,S,_Y
!*
CMSEL,S,_Y1
VATT, 2, , 1, 0
! Assign material property no.2 to volume no.2
CMSEL,S,_Y
CMDELE,_Y
CMDELE,_Y1
!*
CM,_Y,VOLU
VSEL, , , , 9
! Select volume no. 9
CM,_Y1,VOLU
CMSEL,S,_Y
!*
CMSEL,S,_Y1
VATT, 3, , 1, 0
! Assign material property no.3 to volume no.9
CMSEL,S,_Y
CMDELE,_Y
CMDELE,_Y1
!*
CM,_Y,VOLU
VSEL, , , , 11
CM,_Y1,VOLU
CMSEL,S,_Y
!*
CMSEL,S,_Y1
VATT, 4, , 1, 0
CMSEL,S,_Y

```
CMDELE,_Y
CMDELE,_Y1
!*
CM,_Y,VOLU
VSEL, , , ,      10
CM,_Y1,VOLU
CMSEL,S,_Y
!*
CMSEL,S,_Y1
VATT,       5, ,   1,       0
CMSEL,S,_Y
CMDELE,_Y
CMDELE,_Y1
!*
CM,_Y,VOLU
VSEL, , , ,      8
CM,_Y1,VOLU
CMSEL,S,_Y
!*
CMSEL,S,_Y1
VATT,       6, ,   1,       0
CMSEL,S,_Y
CMDELE,_Y
CMDELE,_Y1
!*
CM,_Y,VOLU
VSEL, , , ,      7
CM,_Y1,VOLU
CMSEL,S,_Y
!*
CMSEL,S,_Y1
VATT,       7, ,   1,       0
CMSEL,S,_Y
CMDELE,_Y
CMDELE,_Y1
!*
! Assign material properties to different volumes
SMRT,9
! Specify meshing parameters for automatic element sizing
MSHAPE,1,3D
! 3D volume mesh with tetrahedral-shaped elements
```

MSHKEY,0
! Using free mesh
!*
FLST,5,7,6,ORDE,4
FITEM,5,1
FITEM,5,-2
FITEM,5,7
FITEM,5,-11
CM,_Y,VOLU
VSEL, , , ,P51X
CM,_Y1,VOLU
CHKMSH,'VOLU'
! Invokes a predefined ANSYS macro that checks areas and volumes to find out if they were previously meshed
CMSEL,S,_Y
!*
VMESH,_Y1
! Generates nodes and elements
!*
CMDELE,_Y
CMDELE,_Y1
CMDELE,_Y2
!*
FLST,2,2,5,ORDE,2
FITEM,2,35
FITEM,2,-36
!*
/GO
DA,P51X,ALL,
FLST,2,1,1,ORDE,1
FITEM,2,7
!*
/GO
F,P51X,FY,-100
! Specify force loads at nodes; the magnitude is 100N along the Y-axis
/UI,MESH,OFF
FINISH
! Finish assigning the material properties, loading, and element type.
/SOLU
/STATUS,SOLU
SOLVE

! Starts the solution of one load step of a solution sequence based on the current analysis type and option settings
/CPLANE,1
! Cutting plane defined to use the working plane
/TYPE,1,5
! Use the capped hidden display
/replot
! Display the half of the tooth
FINISH
/POST1
! Start POST1 post-processor
/EFACE,1
AVPRIN,0, ,
!*
PLNSOL,S,EQV,0,1
! Displays the results as continuous contours
VSEL,S, , , 11
ALLSEL,BELOW,VOLU
/REPLOT
!*